NTNU – Trondheim
Norwegian University of
Science and Technology

Using Harmonic Impedance to Investigate the Stability in a High Voltage Direct Current System

A Sensitivity Analysis with Focus on the Control System

Sigmund Bødal

Master of Science in Electric Power Engineering
Submission date: June 2013
Supervisor: Marta Molinas, ELKRAFT
Co-supervisor: Øyvind Rui, Statnett

Norwegian University of Science and Technology
Department of Electric Power Engineering

Problem Description

The transmission system is under continually change and development. In the recent past numerous High Voltage Direct Current (HVDC) lines have been developed for interconnection of power systems, and many more are under construction. It is likely to believe that the future transmission system will be dominated by, and dependent on, HVDC lines and Flexible Alternating Current Transmission System (FACTS) devices for optimal operating conditions. Implementations of these technologies involve large amounts of power electronics. In addition to making the power system larger and more reliable, HVDC interconnections and FACTS devices make the stability problems more complex and increase the consequences of instability.

With a growing complexity of the transmission system, new methods are developed for more convenient system analysis. In this report, a concept for utilizing harmonic impedance to carry out stability analysis of a complex power system will be examined. The concept, developed by Jian Sun, involves partitioning a system into source and load subsystems represented as harmonic impedances. After establishment of the two subsystems, stability analysis can take place by investigating satisfaction of the Nyquist stability criterion.

The system to investigate is a HVDC link based on Modular Multilevel Converters, the latest generation of HVDC converter technology, and a MATLAB/Simulink model has been developed for simulation purposes. To establish the harmonic impedance of the subsystems, frequency response analysis will be utilized, instead of analytical expressions. As the Nyquist stability criterion is based on graphical interpretation, it should be well suited for determining stability conditions in a system described by experimentally obtained dynamical characteristics.

Concerning the stability investigations, the importance of the control system will be the main subject. As the HVDC link model has a very complex control system, the intention of this work will be to find out to what extent the control systems influence the stability, and if the most stable tuning of the control system regulators can be achieved by using the proposed method.

Preface

During the work with this project report I have gained a lot of knowledge of the Modular Multilevel Converter and its control system. The topic has been quite challenging, as my knowledge in system control and power system stability was rather sparse before starting the project.

I would like to thank Øyvind Rui in Statnett for providing me with this interesting subject, and for guidance throughout the work. I will also like to thank my supervisor Marta Molinas and the PhD student Santiago Sanchez, for leading me through uncharted waters and helping me with the task. Finally, I would like to thank the PhD student Gilbert Bergna for letting me use his MATLAB/Simulink model as basis for my work, and the consequently aid and assistance.

Sigmund Bødal

Trondheim, June 2013

Summary

In this report, a method for determining the stability in a High Voltage Direct Current (HVDC) system by using harmonic impedance is explained and applied. This method turns out to be a powerful tool for performing sensitivity analysis of the control system, but applications for other parts of the power system should not be excluded.

A model of a HVDC link has been developed in MATLAB/Simulink, which constitutes the basis for simulations. As the HVDC model is based on Modular Multilevel Converters (MMC), the latest generation of converter technology, the control system is quite complex and sophisticated.

The chosen approach has been to determine the stability by investigating satisfaction of the Nyquist stability criterion. The HVDC system was then partitioned into a source and load subsystem, each represented as a harmonic impedance. Frequency response analysis was applied to obtain the harmonic impedance of the two subsystems.

The frequency response analysis involves two slightly different methods; current injection for the source subsystem and voltage injection for the load subsystem. The current injection method proved to be very sensitive for changes in simulation parameters and regulator settings at frequencies up to 100 Hz, and the accuracy in this frequency range is uncertain. On the other hand, the voltage injection method was found to be almost immune to any parameter value changes, as the harmonic impedance ended up as the same for all simulations.

The impedance magnitude for both subsystems was found to be the same at frequencies above 100 Hz. As both subsystems are identical, except from the control systems in the converters, this means that the two methods for frequency response analysis are accurate at high frequencies. It also means that the converters' influence on the harmonic impedance, and therefore also the stability, are less significant above this frequency.

From the sensitivity analysis, it has been discovered that the initial state of the system is actually vulnerable, as the curve in the Nyquist plot approaches the instability point at high frequencies. This means that instability is likely to occur if perturbations at the correct frequencies are present. The sensitivity analysis for the rectifier shows that the initial tuning of the control system is actually the most stable of the ones that are simulated. By changing the regulator parameter values in any direction, the Nyquist plots indicates increased probability for instability to occur. For the inverter, which proved to be almost immune to changes in the regulator parameter values, no changes concerning instability were observed during the sensitivity analysis.

As many values close to the instability point in the Nyquist plot represents frequencies that exceeds the frequency range where the converters are significant, the power system itself must be redesigned to guarantee stable operating conditions.

Sammendrag

I denne rapporten forklares og anvendes en metode for å fastslå stabiliteten i et høyspent likestrømssystem (HVDC-system). Denne metoden viser seg å være et kraftfullt verktøy for å utføre sensitivitetsanalyser av reguleringssystemet, men anvendelse i andre deler av kraftsystemet bør ikke utelukkes.

En modell av en HVDC-forbindelse har blitt utviklet i MATLAB/Simulink, og denne modellen utgjør grunnlaget for simuleringer. På grunn av at HVDC-modellen er basert på modulære multinivåomformere, som er den siste generasjonen av omformerteknologi, er reguleringssystemet ganske komplekst og sofistikert.

Den valgte fremgangsmåten har vært å fastslå stabiliteten ved å undersøke at Nyquists stabilitetskriterium er oppfylt. HVDC-systemet ble derfor delt opp i et kilde- og last-delsystem, der hvert delsystem er representert som en harmonisk impedans. Frekvensresponsanalyse ble anvendt for å finne den harmoniske impedansen i de to delsystemene.

Frekvensresponsanalysen involverer to forskjellige metoder; strøminjeksjon for kilde-delsystemet og spenningsinjeksjon for last-delsystemet. Metoden med strøminjeksjon viste seg å være veldig følsom for forandringer i simuleringsparametere og innstillinger for regulatorene ved frekvenser opp til 100 Hz, og nøyaktigheten i dette frekvensområdet er usikker. Metoden med spenningsinjeksjon viste seg derimot å være nesten immun mot endringer i parameterverdier, siden den harmoniske impedansen endte opp til å bli den samme for alle simuleringene.

Absoluttverdien av impedansen i begge delsystemene ble funnet til å være lik ved frekvenser over 100 Hz. Siden begge delsystemene er symmetriske, bortsett fra reguleringssystemene til omformerne, betyr dette at de to metodene for frekvensresponsanalyse er nøyaktige ved høye frekvenser. Det betyr også at omformernes innvirkning på den harmoniske impedansen, og derfor også på stabiliteten, er mindre betydningsfull over denne frekvensen.

Det har blitt oppdaget at den opprinnelige tilstanden til systemet faktisk er sårbart, siden kurven i Nyquistplottet nærmer seg ustabilitetspunktet ved høye frekvenser. Dette betyr at ustabilitet kan oppstå hvis forstyrrelser er tilstede på de spesifikke frekvensene. Sensitivitetsanalysen av likeretteren viser at de opprinnelige innstillingene til reguleringssystemet faktisk er de mest stabile av de som er simulert. Ved å endre regulatorparameterverdiene indikerer Nyquistplottene at sannsynligheten for at ustabilitet skal inntreffe øker. For vekselretteren, som viste seg å være nesten immun mot endringer i regulatorparameterverdier, har ingen endringer i ustabilitetsforholdene blitt observert under sensitivitetsanalysen.

Siden mange verdier nær ustabilitetspunktet i Nyquistplottet representerer frekvenser utenfor det betydningsfulle frekvensområdet til omformerne, må kraftsystemet i seg selv endres for at stabil operasjon skal kunne garanteres.

Contents

List of Abbreviations

AC	Alternating Current
AGC	Automatic Generation Control
BJT	Bipolar Junction Transistor
CTL	Cascaded Two-Level
DC	Direct Current
DFT	Discrete Fourier Transform
emf	Electromotive Force
FACTS	Flexible AC Transmission System
FFT	Fast Fourier Transform
HVDC	High Voltage Direct Current
IGBT	Insulated Gate Bipolar Transistor
LCC	Line Commutated Converter
MMC	Modular Multilevel Converter
MMS	Module Management System
MOSFET	Metal-Oxide-Semiconductor Field Effect Transistor
OPWM	Optimized Pulse Width Modulation
PLL	Phase-Locking Loop
PSS	Power System Stabilizer
pu	Per Unit
PWM	Pulse Width Modulation
rms	Root Mean Square
SVC	Static VAr Compensator
VSC	Voltage Source Converter

Chapter 1 Introduction

1.1. Background

With a fast development of High Voltage Direct Current (HVDC) technology and Flexible Alternating Current Transmission System (FACTS) devices, system control is important to keep the operation stable and within constraints. Interconnections result in increased reliability, but also make the stability problems more complex and increase the consequences of instability [1]. The rate of new HVDC links being built each year is tremendous, and FACTS devices are more and more used to increase the capacity of existing transmission lines. As electric energy production based on fossil fuel is being phased out, renewable sources are being utilized and new production sites are developed. This development demands a stable and robust grid, capable of large changes in power production. Particularly wind farms developed offshore require transmission systems capable of large power transfer at peak power production.

The massive amount of easily controllable hydro power production gives Norway the position as a balancing nation for its neighbours. With the already established interconnections, in addition to the planned links to England and Germany, the power system is becoming more flexible and receptive for stochastic energy production. By also taking energy storage systems into consideration, the future system for power supply can be highly flexible, reliable and steady across national and continental borders. This probable development makes great demands for stable interconnections. As the Modular Multilevel Converter (MMC) has several advantages compared to its predecessors, its entry to the market may contribute to solving many challenges regarding energy transmission.

As new interconnections are developed, the previous premises for stable system operation are changed. A tripping of a transmission line caused by instable operation may have consequences for the operation of large parts of the power system.

The increasing complexity of the power system makes the traditional methods of stability analysis based on analytical expressions challenging, and development of new methods are desirable. A method developed by [27] propose the use of a system's harmonic impedance to determine the stability by investigating satisfaction of the Nyquist stability criterion. By using frequency response analysis to obtain the harmonic impedance, the stability in large and complex transmission systems dominated by power electronics should easily be analysed with this method.

The motive for this report is to determine if the method proposed by [27] is suitable for finding the most stable tuning of a HVDC converter's control system, in addition to highlight the control systems' influence on the stability. As the chosen system to investigate is based on MMC technology, the control system is very complex and sophisticated. Since no

acknowledged tuning procedure is currently developed for the applied control strategy, the proposed method involving harmonic impedance may be a tool for such a purpose.

1.2. The case

The case to be investigated is a HVDC transmission system based on MMCs, connected between two stiff AC grids, as seen in Figure 1.1. The system is symmetrical regarding the AC sides, and the converters operate as rectifier and inverter at the sending end and receiving end respectively. For the system to be represented as a Thevenin equivalent, it is decided to split it in two subsystems at the dotted line. These two subsystems can then be referred to as source and load, both represented as harmonic impedances. A MATLAB/Simulink model of the system has been developed, and all the simulations performed in this work are based on this model.

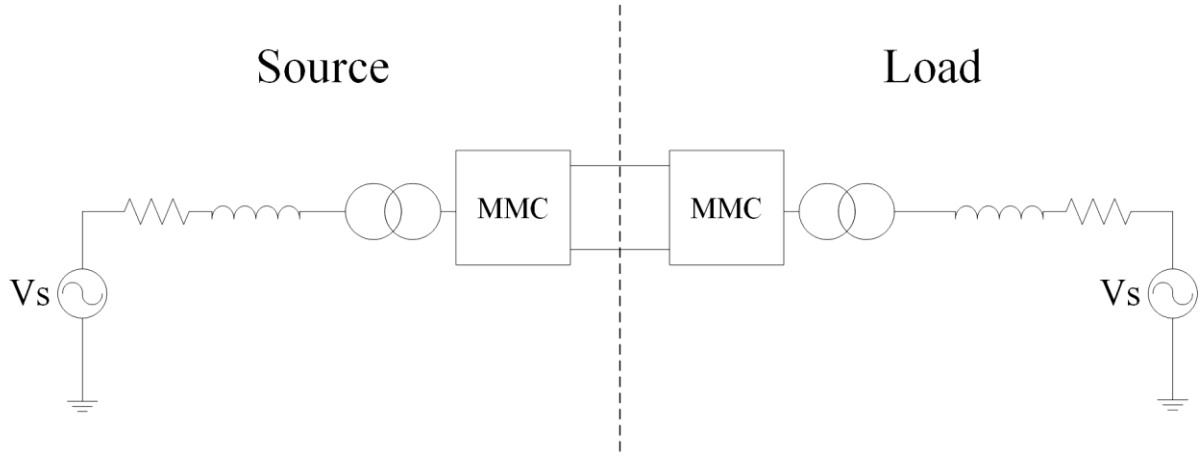

Figure 1.1: The system to investigate

1.3. Outline

Chapter 2 gives an introduction to the development of HVDC technology and explains briefly the different converter technologies. In addition, the methods used for stability analysis that are applied later in the report are explained in this chapter.

In Chapter 3, a short overview of different stability categories for a power system is given. Although this report does not deal with all the different stability problems, they are given an introduction to illustrate the extent of the stability subject.

The power system, including the converter stations, is presented in Chapter 4. In this chapter the different component values are listed, and the purpose of the central components are mentioned.

Chapter 5 explains the control system for the converters. First, a general overview of the control strategy is given, before the detailed mathematical deduction follows.

The simulation results are presented and analysed in Chapter 6. This chapter explains both the applied simulation strategy and the results from the sensitivity analysis.

The Discussion takes place in Chapter 7, where the method and simulation results will be further discussed and analysed, before the conclusion and suggested further work finishes the report.

As this work in many ways is a continuation of the specialization project [30], parts of theory and background from this thesis is included.

Chapter 2 Background and Theory

2.1. HVDC technology

The use of HVDC technology for power transmission began in the 1950s, and since then the technology has been developed into a very effective way of transmitting electrical energy. The development of different technologies used in HVDC applications is given a brief overview in the following sections.

2.1.1. The Line Commutated Converter

In the 1970s the first thyristor based Line Commutated Converter (LCC) HVDC system was commissioned and put into operation. Today the LCC technology is the preferred choice for transmission of large amounts of power over long distances. The largest converter station is under construction in India, and will have capacity of 8000 MW when operational in 2015 [2]. The voltage level of this system will be ± 800 kV, which is the highest commercially available DC voltage today. In addition to high power ratings, the main advantage with LCCs is low losses in the converter stations, usually 0,7 % per converter [3]. Some disadvantages with the LCC are the need of an AC source at each terminal for commutation, and also AC filters for compensation of reactive power and harmonic currents.

2.1.2. The Voltage Source Converter

The first VSC based HVDC transmission line was a 3 MW test installation in Sweden, which was operational in 1997 [4]. With introduction of VSC HVDC systems, the Insulated Gate Bipolar Transistor (IGBT) made its entrance to this market. The first generations of VSCs were based on two- and three-level converter design, and had high losses compared to LCCs.

For now, the latest generation of two-level converters have losses close to 1,7 % per converter by utilizing Optimized Pulse Width Modulation (OPWM), indicated in Figure 2.1 [5]. The highest rated advantage of the VSC is probably its ability to independently control both active and reactive power flow by controlling the amplitude and phase angle of the AC voltage. This fact implies that the need for reactive compensation is removed, and the reduced generation of harmonics leads to fewer filters and more compact terminals. In addition, the VSC enables connection to weak networks, and also the capability of black starts [4].

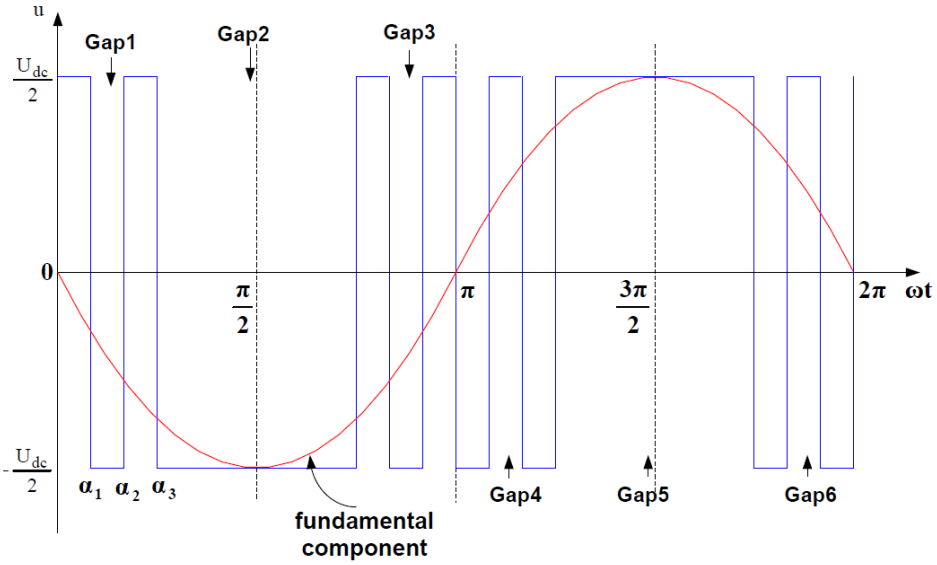

Figure 2.1: Two-level bipolar OPWM voltage output [5]

2.1.3. The Modular Multilevel Converter

The MMC is a further development of the VSC, and is the latest generation of HVDC converter technology, commercially operational since 2010 [6]. MMC includes many fairly similar designs, but most used is the Cascaded Two-Level (CTL) design. The DC poles on the CTL design are connected to a multivalve, often referred to as an arm. There is an arm for both positive and negative pole, which together make a phase unit, also called a leg. In a converter there are then three legs, or six arms. The arms are composed of many submodules in series, and each submodule is a two-level converter. The arrangement of the basic components in the MMC can be seen in Figure 2.2.

The submodule itself consists of two IGBTs, two diodes and a capacitor, as seen in Figure 2.3. In fact, the submodule can be simplified to a capacitor which is inserted, bypassed or blocked [4]:

- In inserted mode the IGBT in series with the capacitor is turned on, and the other one off. The output voltage of the submodule equals the capacitor voltage and the capacitor charges if arm current is positive, and discharges otherwise.
- In bypassed mode the capacitor is disconnected by the series connected IGBT, and the other IGBT makes a short circuit between input and output terminal. The output voltage is then zero, while the capacitor voltage remains constant.
- By turning both IGBTs off, the submodule is blocked. The current is then passing only the freewheeling diodes, and the capacitor will charge at positive arm current and ideally not discharge.

The required number of submodules in each multivalve is determined by the voltage in the DC link, and the withstand voltage of each submodule.

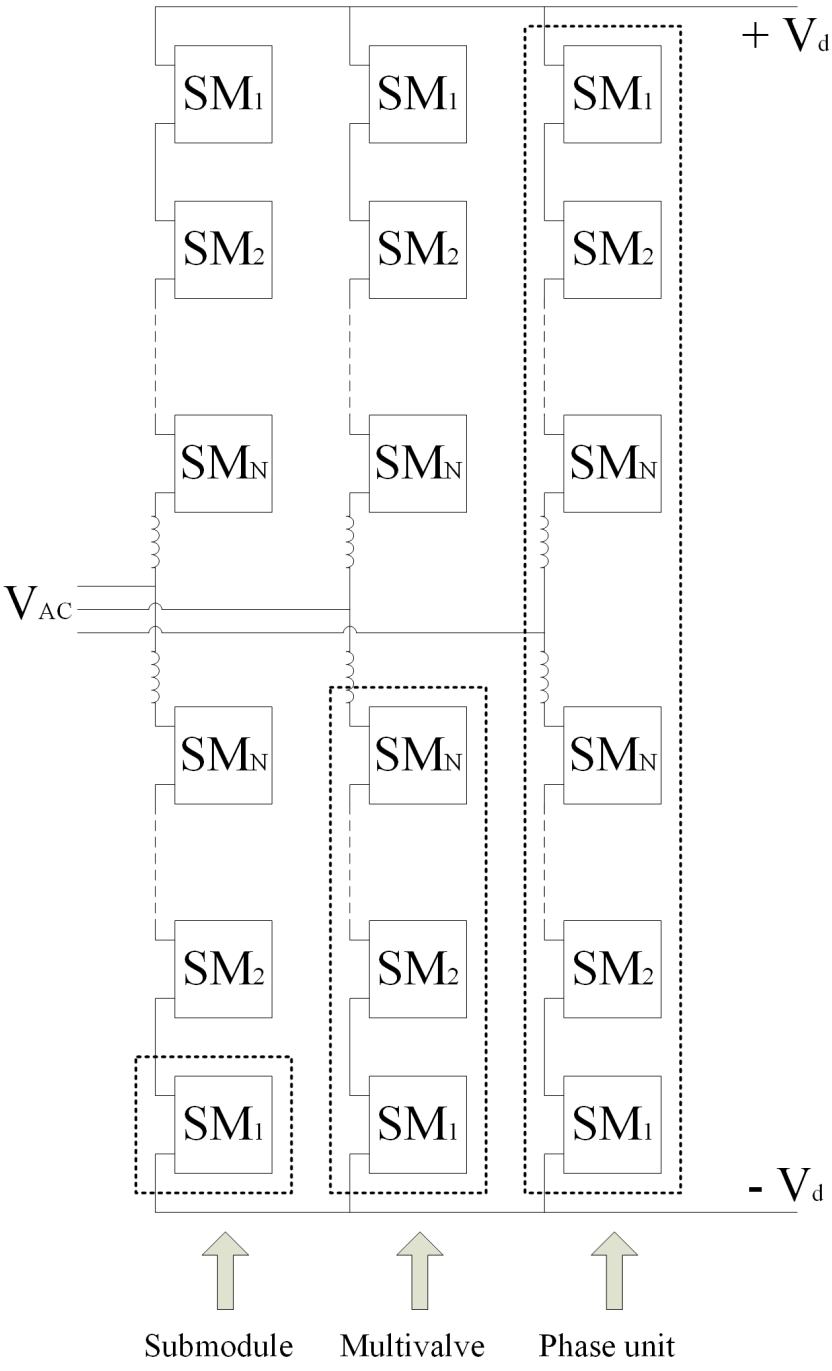

Figure 2.2: Block diagram of an MMC with submodules

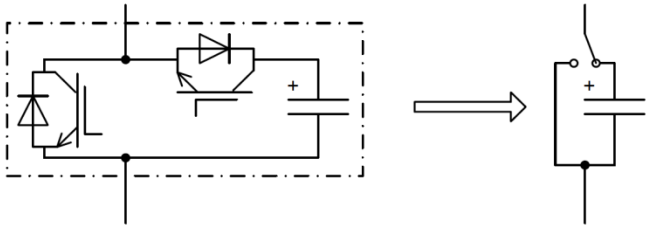

Figure 2.3: Submodule arrangement [5]

Compared to the LCC, and also the early generations of VSC, the MMC has the following advantages [7]:

- Low generation of harmonics
- Low high frequency noise
- Low switching losses

The low switching losses is due to low switching frequency in each submodule, and low dv/dt in each voltage step. In the CTL design only one submodule is usually switched at a time, but a large amount of submodules lead to an effective switching frequency way above LCCs and early generation VSCs. For now the MMC is capable of power transfer up to 1200 MW at ± 500 kV DC, with losses typically around 1,0 % per converter [8].

During one fundamental period each submodule capacitor in a multivalve can be both charged and discharged, depending on its mode. This allows separate and selective control of the submodules, and each phase unit can be viewed as a controllable voltage source. The total voltage in a phase unit equals the voltage in the DC line, and the output voltage of the inverter can be controlled in a sinusoidal looking way by carefully adjusting the modes of the submodules. [5]

A typical output voltage of the MMC is shown in Figure 2.4. The number of voltage steps between the DC poles depends on the switching strategy, and can be as many as the number of submodules in a phase unit, plus one.

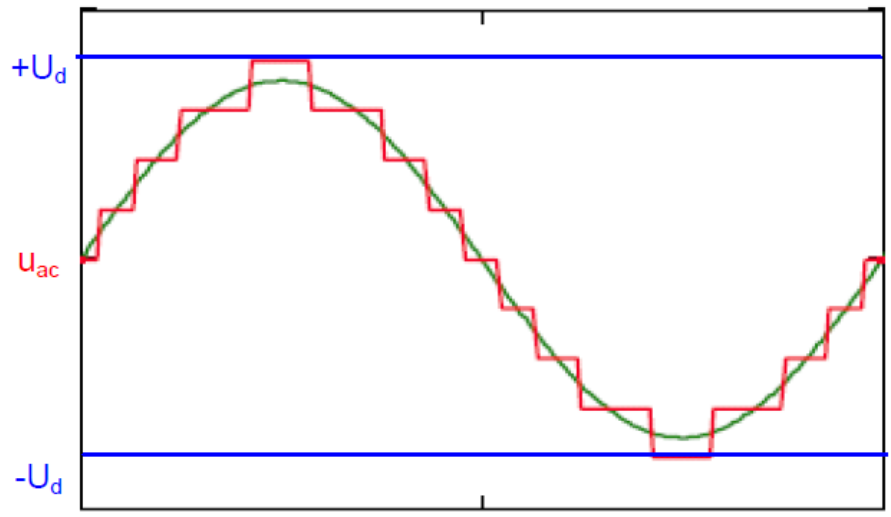

Figure 2.4: MMC voltage output [5]

A quite sophisticated system is needed to monitor and balance the voltage level in each submodule, and calculate a state that delivers a correct output voltage level. To achieve this, a current control system in cooperation with a pulse pattern generator calculates the submodule state every few microseconds. These signals are received by a Module Management System (MMS) that communicates with each submodule, and receives the actual state and voltage from these. The command signal for switching each submodule is then based on the actual voltage

in the submodule, and the desired output voltage. To obtain electric isolation, the communication between the MMS and the submodules are transmitted via fibre optics. [5]

2.1.4. The IGBT

The IGBT is a further development of the Bipolar Junction Transistor (BJT) and the Metal-Oxide-Semiconductor Field Effect Transistor (MOSFET), and has the property of low on-state voltage combined with large blocking voltage rating [9]. Unlike the thyristor the IGBT can be controlled both to turn on and off, and is therefore used in VSCs. By investigating the I-V characteristics of an IGBT, shown in Figure 2.5, it can be seen that the collector current can be controlled by the gate-emitter voltage signal. However, for HVDC applications only the on and off states are used.

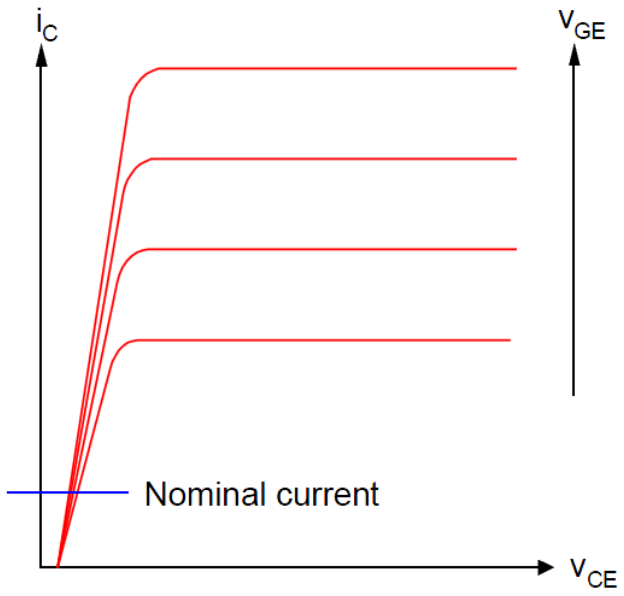

Figure 2.5: I-V characteristic of an IGBT [10]

In section 2.1.3 it was stated that a submodule consisted of two IGBTs. That is actually a simplification, as the fact is that each switch shown in Figure 2.3 consists of a stack composed of several IGBTs. The reason for series connecting IGBTs in stacks is to ensure correct withstand voltage for each submodule. The IGBTs are fitted into press packs, where several chips are installed in parallel, and the amount of chips determine the current capability.

2.2. Fourier transform

Fourier transform can be used for analysing the frequency spectrum in a signal. As a physical interpretation we can have a signal consisting of sinusoidal oscillations in infinitely many frequencies. By applying Fourier transform to this signal, we can make a spectral representation of the signals magnitude for each frequency. Fourier transform is then advantageous in the case of finding harmonic impedance by injection of voltage or current.

Discrete Fourier Transform (DFT) and Fast Fourier Transform (FFT) is elaborated in [13]. The most important parts are reproduced in the following sections.

2.2.1. Discrete Fourier Transform

When using Fourier transform we have to assume that the function $f(x)$, that is to be transformed, is given over an interval. For the case in this report the function $f(x)$ is given in terms of values at finitely many points, and we are interested in using Fourier analysis. As we are dealing with sampled values rather than with functions, Fourier transform is replaced by DFT.

If we let $f(x)$ to be periodic over a period of 2π, and assume that we have N measurements of $f(x)$ over the interval from 0 to 2π at regularly spaced points

$$x_k = \frac{2\pi k}{N} \tag{2.1}$$

where $k = 0,1, \dots, N-1$. The function $f(x)$ is sampled at these points. We will now determine a complex trigonometric polynomial

$$q(x) = \sum_{n=0}^{N-1} c_n \cdot e^{inx_k} \tag{2.2}$$

This polynomial interpolates $f(x)$ at the nodes in (2.1), such that $q(x_k) = f(x_k)$. f_k then denotes $f(x_k)$:

$$f_k = f(x_k) = q(x_k) = \sum_{n=0}^{N-1} c_n \cdot e^{inx_k} \tag{2.3}$$

The coefficients $c_0, \dots, c_{N-1}$ must be determined such that (2.3) holds.

After some derivation, it can be shown that the DFT of the signal $\mathbf{f} = [f_0 \dots f_{N-1}]^{\boldsymbol{T}}$ is the vector $\hat{\mathbf{f}} = [\hat{f}_0 \dots \hat{f}_{N-1}]$ with components:

$$\hat{f}_n = Nc_n = \sum_{k=0}^{N-1} f_k \cdot e^{-inx_k} \tag{2.4}$$

Where $f_k = f(x_k)$ and $n = 0, \dots, N-1$. This is then the frequency spectrum of the signal and can be written in vector notation $\hat{\mathbf{f}} = \mathbf{F}_N\mathbf{f}$, where $\mathbf{F}_N$ is the $N \times N$ Fourier matrix.

2.2.2. Fast Fourier Transform

To avoid aliasing when using Fourier transform, in the calculations the n's should be much smaller than $N/2$. When applying DFT, N is usually large, and (2.4) requires $O(N)$ operations for any particular n, which leads to $O(N^2)$ operations in total. For a large number of sampling points, say 1000, this gives a million operations to solve.

The amount of work can be reduced by FFT. This method will only need $O(N)\log_2 N$ operations compared to the $O(N^2)$ needed for DFT. Codes for FFT are implemented in programs such as MATLAB and Maple, and is convenient to use.

2.3. Stability analysis

There exist many methods for investigating the stability in a system. As this work deals with harmonic impedance, it is decided to apply the Nyquist stability criterion for determining the stability.

The most important advantage of the Nyquist stability criterion is the fact that it is based on graphical interpretation. This leads to possibilities for determining stability conditions also in systems described by experimentally obtained dynamical characteristics instead of analytical expressions. [17]

2.3.1. Harmonic impedance

Harmonic impedance is an important parameter characterizing the frequency response of a power system. It is mainly used for designing harmonic filters, checking harmonic emission limits and predicting the system's resonance. [11]

The harmonic impedance in a system can be obtained by frequency response analysis. In this report the harmonic impedance is obtained by sweeping the system with injected currents and voltages in a defined frequency interval. The responding behaviour of the system makes it possible to calculate the impedance. One advantage of this method is that the impedance of large and complex systems can be obtained during different operational conditions, in a quite simple manner.

The details about voltage and current injection are explained in the following sections. When the harmonic impedance is obtained by usage of this method, the stability of the system can be investigated by creating a Nyquist plot.

2.3.1.1. Voltage injection

Voltage injection is applied if the system to investigate is represented as a Thevenin equivalent, and is done by adding a perturbation voltage source in series with the fundamental voltage source, as indicated in Figure 2.6. The perturbation voltage is injected at the same time as the system is supplied with voltage at fundamental frequency. The perturbation voltage, termed V_p, has a frequency inside the defined interval where the impedance should be obtained, usually up to half the switching frequency of the converters. By running several simulations in series, where the perturbation frequency is changed for each run, the impedance can be calculated for the defined frequency interval. The load impedance at one defined frequency ω is then

$$Z(\omega) = \frac{V_p(\omega)}{I_p(\omega)} \tag{2.5}$$

where Z, V_p and I_p are complex values. It should be noted that the total current in the system consists of both a fundamental component and a perturbation component, in addition to other possible harmonic components and distortions. The perturbation component I_p is obtained by applying Fourier transform to the current signal.

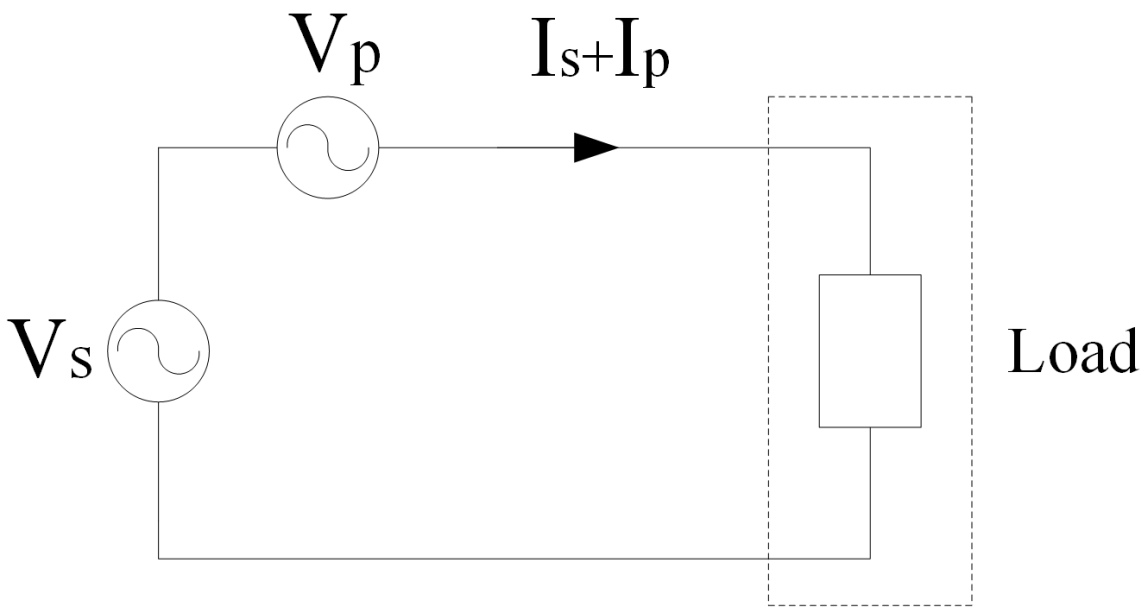

Figure 2.6: Voltage injection in a power system

2.3.1.2. Current injection

Current injection is applied if a system is represented as a Norton equivalent, and is done in nearly the same way as voltage injection. Now a perturbation current source, I_p, is placed in parallel with the fundamental current source, as seen in Figure 2.7. The load impedance is obtained by applying (2.5). It is now the voltage over the load that consists of several components at different frequencies, and the perturbation component V_p is extracted from the load voltage by applying Fourier transform.

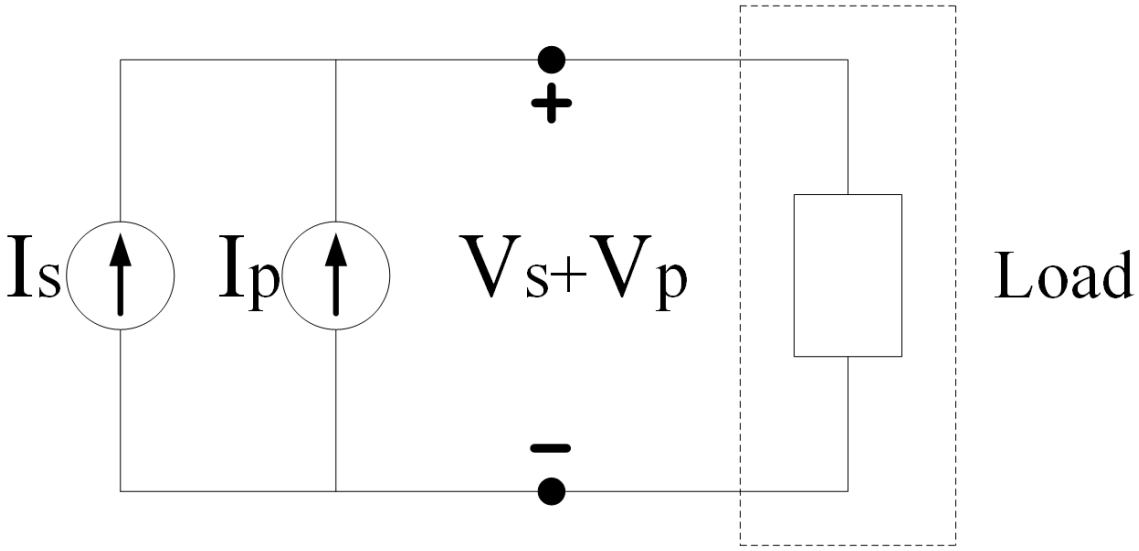

Figure 2.7: Current injection in a power system

2.3.1.3. Bode plot

The Bode diagram is used as a graphic representation of the frequency response in a system, in this case the harmonic impedance. It is composed of two diagrams showing the magnitude, or gain, and the phase angle as a function of frequency. The abscissa axis is common for both diagrams and indicates the quantity in a logarithmic scale; both Hz and rad/s are usual units. In the magnitude (or gain) diagram, the decibel scale is used to indicate the absolute value of the function. The transformation from a linear quantity to decibel is defined as

$$|Z|\,[dB] = 20 \cdot \log_{10}|Z| \tag{2.6}$$

where Z originally is given in ohm.

In the phase diagram the phase angle of the function is given in either degrees or radians, and an example of the complete Bode diagram is presented in Figure 2.8.

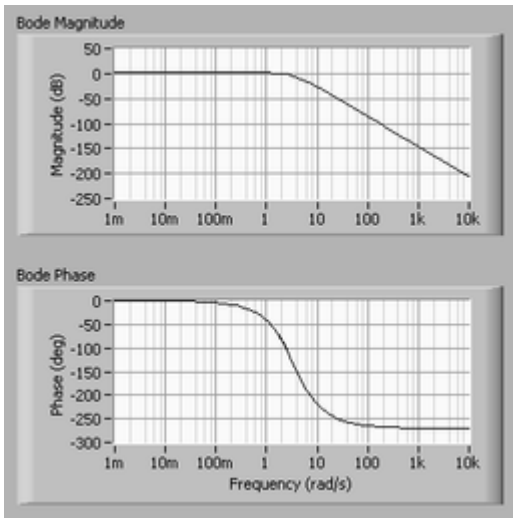

Figure 2.8: The Bode plot showing magnitude and phase [12]

2.3.2. Stability margins

Once the harmonic impedance of a system is obtained and presented in a Bode plot, it is possible to investigate the stability margins. The stability in a system should be described in a more informative way than yes/no, and both Bode and Nyquist plots can be used to determine the stability in a system by indicating the phase margin ψ, and the gain margin ΔK.

Figure 2.9 indicates how phase margin and gain margin can be found in a Bode plot.

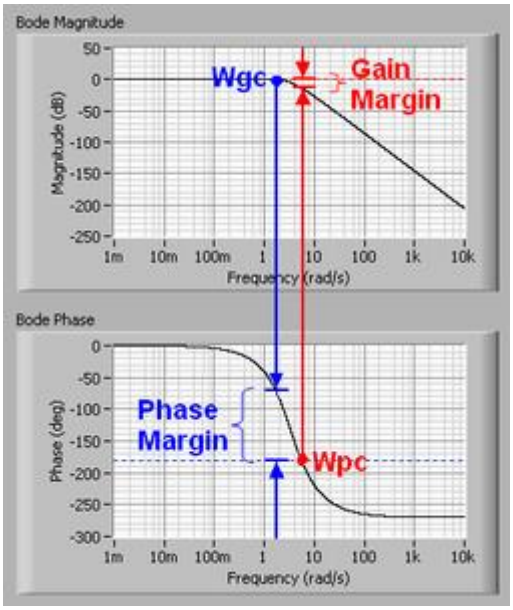

Figure 2.9: Stability margins in a Bode diagram [16]

The gain margin is defined as the difference in magnitude between the curve and the zero line, at the frequency where the phase angle crosses -180º. In the same way, the phase margin is defined as the difference in phase between the curve and the -180º line, at the frequency where the magnitude crosses 0 dB. If we define the function in the Bode plot to be $f(\omega)$, the stability margins is defined in the following way:

$$\psi = \angle f(\omega_{gc}) - (-180°) \tag{2.7}$$

$$\Delta K = \frac{1}{|f(\omega_{pc})|} \tag{2.8}$$

ω_{gc} denotes the frequency where the magnitude crosses the 0 dB line, and ω_{pc} the frequency where the phase crosses the -180º line. The conditions for stability can then be expressed as

$$\psi > 0 \tag{2.9}$$

$$\Delta K > 0\ [dB] \tag{2.10}$$

The phase margin is an expression for the extra negative phase shifting tolerated at $|f(\omega)| = 0$ [dB], while gain margin is a measure for the gain increase tolerated at $\omega = \omega_{180}$, before instability occur. [17]

As both phase shift and gain may change during operation because of parameter changes or other circumstances, stability margins are often specified as minimum values. [17]

2.3.3. The Nyquist stability criterion

Nyquist analysis can be used for investigating stability when the harmonic impedance of the system has been obtained from frequency response analysis. For a system to remain stable it will have to satisfy the Nyquist stability criterion, explained in the following section. The Nyquist analysis can be performed by creating a Nyquist plot that easily shows possible instability concerns in the system.

A power system can be simplified into a Thevenin equivalent circuit shown in Figure 2.10, where the source is represented as the ideal voltage source V_S and the source output impedance Z_S. The load is represented as the impedance Z_L, and the load voltage V_L can be expressed as

$$V_L = V_S \cdot \frac{Z_L}{Z_L + Z_S} = V_S \cdot \frac{1}{1 + \frac{Z_S}{Z_L}} \tag{2.11}$$

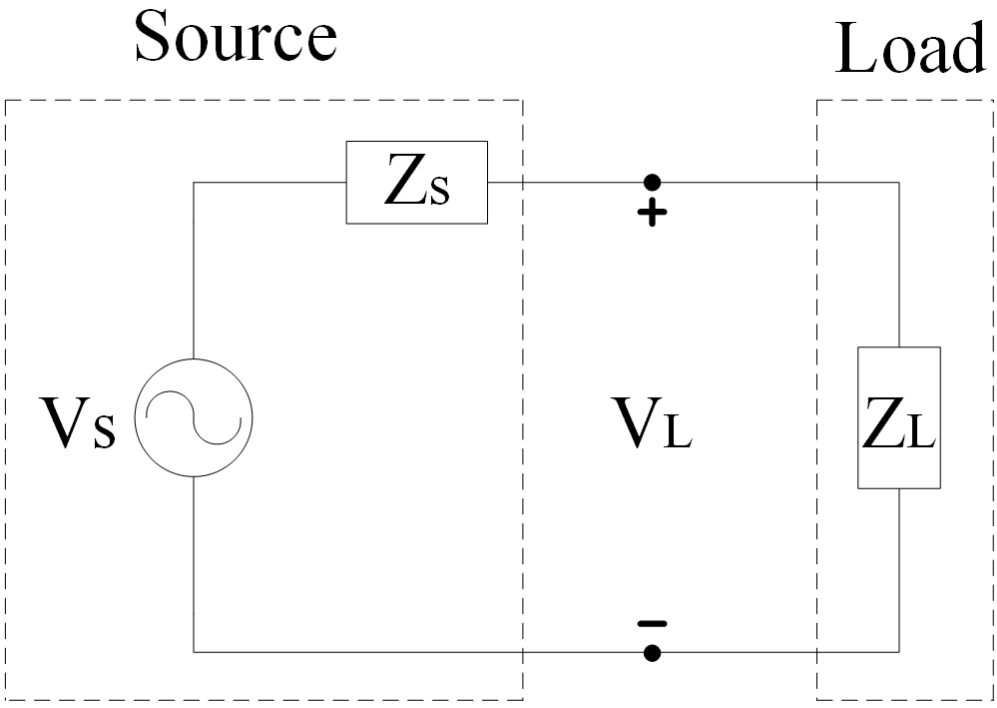

Figure 2.10: Thevenin representation of a simplified system

Assuming the source itself is stable, for the system to satisfy the Nyquist stability criterion it is required that the interconnected systems transfer function is stable:

$$\frac{1}{1 + \frac{Z_S}{Z_L}} \tag{2.12}$$

It should be clear that (2.12) resembles the transfer function of a feedback control loop, where the loop gain is Z_S/Z_L. This system is then stable if, and only if

$$\frac{Z_S}{Z_L} \neq (-1,0) \tag{2.13}$$

and the Nyquist stability criterion is then satisfied. [14]

For the case with a system simplified as a Norton equivalent, as indicated in Figure 2.11, the load current can be expressed as

$$I_L = I_S \cdot \frac{Z_S}{Z_S + Z_L} = I_S \cdot \frac{1}{1 + \frac{Z_L}{Z_S}} \tag{2.14}$$

It is worth noting that the stability criterion has now has slightly changed. The system is now stable if, and only if

$$\frac{Z_L}{Z_S} \neq (-1,0) \tag{2.15}$$

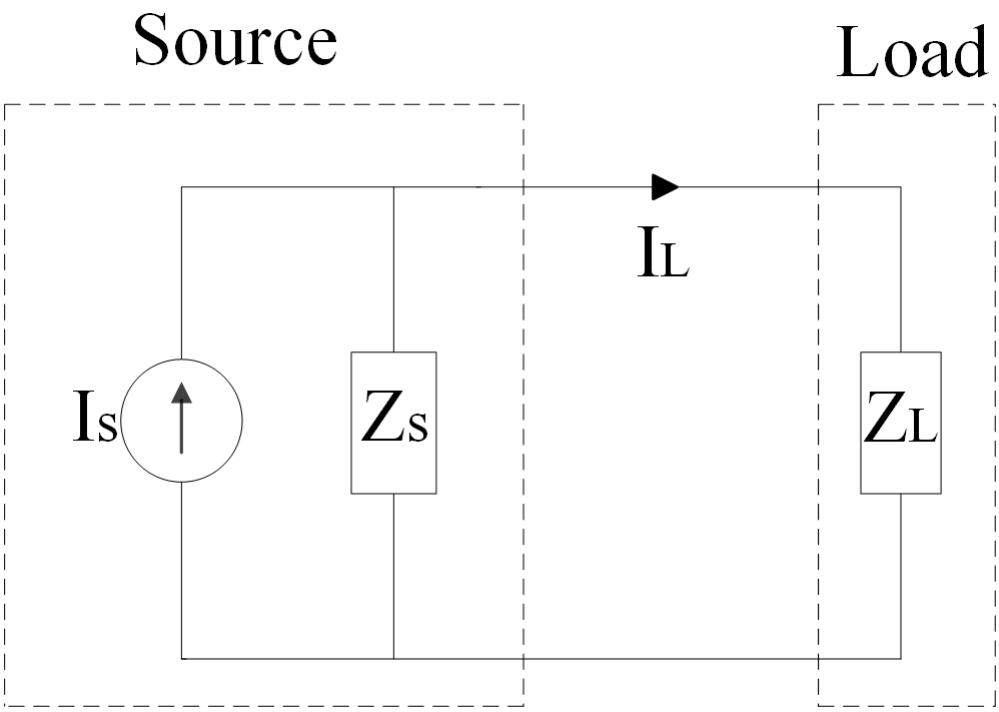

Figure 2.11: Norton representation of a simplified system

2.3.4. The Nyquist plot

A Nyquist plot can be used as a graphical solution for the Nyquist stability criterion, containing information about both magnitude and phase angle, as Figure 2.12 shows. Although this figure shows plotting of the impedance, concerning the Nyquist stability criterion the idea is to plot the ratio between source and load impedance. Then it is easy to see if the instability point, located at the coordinates (-1,0), are encircled or touched, and thus if instability may occur.

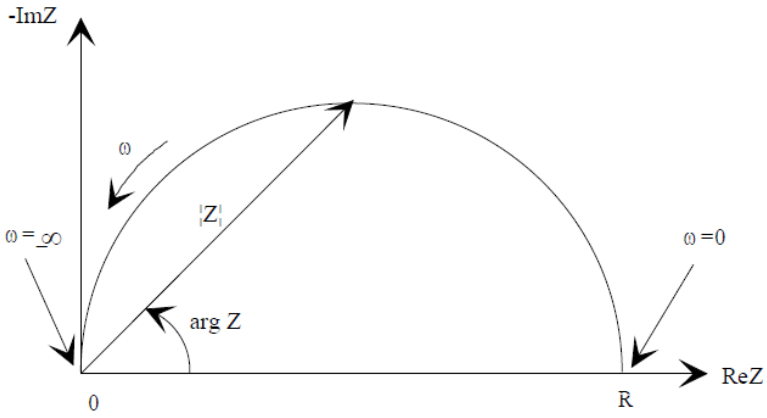

Figure 2.12: The Nyquist plot [15]

The fact that the Nyquist plot does not give any information about where each frequency is represented, and thus which of them that might cause instability, is a drawback. To obtain such information the background data for the plot has to be further investigated.

Chapter 3 Power System Stability

For a power system to operate under desired conditions it needs to be in a stable state. That is, it needs to have the property of remaining in a state of operating equilibrium during normal conditions, and it has to regain an accepted state of equilibrium after a disturbance has occurred [1].

Operational stability can be divided into different categories [18]:

- Rotor angle stability
- Frequency stability
- Voltage stability

In addition, a fourth category should be added which deals with electrical resonance stability, which is the main focus in this report. However, all the different stability categories has to be considered for stability investigations of a large power system, and the other categories are therefore given a brief explanation.

3.1. Rotor angle stability

According to [1], rotor angle stability is defined as the ability of interconnected synchronous machines in a power system to remain in synchronism. A synchronous machine that operates with unstable rotor angle will experience electromechanical oscillations, causing unstable power output as the rotor oscillates.

As power electronic converters have no mechanically rotating parts, the problem of oscillating rotor is non-existent. Nevertheless, the VSC/MMC has many of the same properties as a synchronous machine, and the inverter needs to operate in synchronism with the receiving grid regarding angular stability.

To ensure angular synchronism between a synchronous machine and the receiving grid, a Power System Stabilizer (PSS) is implemented in the control system.

3.2. Frequency stability

When large loads are either suddenly connected or disconnected, there will be a deviation between delivered and consumed power. The power system will react to the unbalanced power conditions by changing the system frequency. The change in frequency is due to extraction or storage of kinetic energy in the rotating mass in the generating units.

The frequency change in the system will continue until the power generation is in equilibrium with the power demand. This is controlled by a system called Automatic Generation Control (AGC). AGC is a fairly complex system operated by the transmission system operator, and

involves primary, secondary and tertiary control. The differences between these controls are mainly the extent of potential power correction and respond time. A power electronic converter itself can hardly contribute to frequency stability in a power system dominated by synchronous machines as generating units. The power electronic converters are rather locked to the grid frequency by using Phase-Locking Loops (PLL) which is implemented in the control systems.

The challenge of meeting the demand for immediate increase of power is solved by having a spinning reserve in the system. Spinning reserve can be explained as having several generating units, evenly distributed in the grid, running at synchronous speed at low power output. At increasing power demand, the power output of the spinning reserve is quickly increased to meet the demand for power.

The fact that Norway has an energy production based on hydro power, which is highly controllable with low respond time, results in a very stable and reliable power supply.

3.3. Voltage stability

Voltage stability is a power system's ability to maintain steady and acceptable voltage at all buses in the system, both during normal operation and after occurrence of disturbances. Voltage instability occurs if the system is exposed to a disturbance which causes an ongoing and uncontrollable drop in voltage. [1]

As the main factor causing voltage instability is the inability of providing reactive power [1], large transformer stations are often equipped with Static VAr Compensators (SVC) or other FACTS devices. The intention of such devices is to control the bus voltage by providing the necessary amount of reactive power. As FACTS devices are dominated by power electronics, the power output is accurate and the response time is low. These properties allows for both transient and continuous power compensation.

3.4. Electrical resonance stability

The main intention of this report is to investigate the system for voltage and current instability caused by interaction between the HVDC link and the connected grid. If the system is simplified to a Thevenin equivalent, with source and load impedance, series resonance is a phenomenon that may cause stability problems. Series resonance occurs at a specific frequency where the inductive reactance equals the capacitive reactance. The resonance frequency can be found by applying the equation

$$f_r = \frac{1}{2 \cdot \pi \cdot \sqrt{L \cdot C}} \tag{3.1}$$

Even small signals may cause problems in a system if they appear at the exact frequency of the resonance, and large oscillations are expected to arise.

Regarding the Nyquist stability criterion, the frequency causing series resonance is not the main concern. Now the frequency causing the ratio between source and load impedance to be -1 is

the one to worry about. When this occur the load voltage, or current, will theoretically approach infinity.

Even though a system has a resonance point, or do not satisfy the Nyquist stability criterion, it is not a matter of course that it will get instable during operation. For instability to occur, a signal at the resonance frequency has to be present in the system. This perturbation can take place either as harmonic or transient currents generated in converters or nearby equipment. As potentially harmful harmonics normally are removed by filters, temporary perturbations are most likely to cause problems as these are not always taken into consideration when designing the system.

Chapter 4 The Power System

4.1. System description

The power system used for simulations and analysis is a HVDC link connected between two stiff AC grids. As earlier mentioned the converters are the latest generation of VSC, called MMC. A short explanation of the system components and their mode of operation is given in this chapter. In addition, the pu system and the values of the components in the power system are presented.

4.2. System parameters

The pu values for the system are listed in Table 4.1. The conversion of pu values from the AC side to the DC side is based on [20].

Table 4.1: Per unit values for the power system

Symbol	Description	Computation	Value
$S_{AC\ base}$	AC power		30 MVA
$V_{AC\ base}$	AC voltage rms		13,8 kV
$I_{AC\ base}$	AC line current	$\frac{S_{base}}{\sqrt{3} \cdot V_{AC\ base}}$	1255 A
$Z_{AC\ base}$	AC impedance	$\frac{V_{AC\ base}}{\sqrt{3} \cdot I_{AC\ base}}$	6,35 Ω
$V_{d,q\ base}$	dq voltage	$\frac{\sqrt{2}}{\sqrt{3}} \cdot V_{AC\ base}$	11,27 kV
$I_{d,q\ base}$	dq current	$\sqrt{2} \cdot I_{AC\ base}$	1775 A
$S_{d,q\ base}$	dq power	$\frac{2}{3} \cdot S_{AC\ base}$	20 MVA
$I_{DC\ base}$	DC line current	$\frac{3 \cdot \sqrt{2}}{4} \cdot I_{AC\ base}$	1331 A
$V_{DC\ base}$	DC voltage	$2 \cdot V_{d,q\ base}$	22,54 KV
$Z_{DC\ base}$	DC impedance	$\frac{V_{DC\ base}}{I_{DC\ base}}$	16,93 Ω
$S_{DC\ base}$	DC power	$V_{DC\ base} \cdot I_{DC\ base}$	30 MVA

All relevant parameters and component values for the power system are listed in Table 4.2. The power system is not designed by the writer himself, but is based on a HVDC system modelled by Gilbert Bergna, coauthor of [24] [25] [26].

Table 4.2: Power system parameters and component values

Symbol	Description	Physical value	Per unit value
R_a	Arm resistance	0,1 Ω	0,016
L_a	Arm inductance	3 mH	0,15
$R_{DC\ cable}$	DC cable resistance	1,0425 Ω/km	
$L_{DC\ cable}$	DC cable inductance	11,925 mH/km	
$C_{DC\ cable}$	DC cable capacitance	17,325 µF/km	
$L_{DC\ cable}$	DC cable length	1 km	
R_g	Grid resistance	1 mΩ	0,16 m
L_g	Grid inductance	2 mH	0,10
C_{sm}	Submodule capacitance	5 mF	
N_{ns}	Submodules per arm	5	
f_{grid}	Nominal AC grid frequency	50 Hz	
f_s	Effective switching frequency	2 kHz	
L_t	Transformer inductance	6 mH	0,30

4.3. System components

In addition to explain the components' modes of operation, formulas for calculating the component values are given. As designing a HVDC system is a fairly complicated affair, complex techniques are used to find the optimal component values. The given formulas may therefore give other values then the ones listed in Table 4.2.

4.3.1. Multivalves

The multivalves, or arms, are in general composed of IGBTs, capacitors and valve reactors. The most important requirements the multivalves have to fulfill are the following [5]:

- Adjust an even DC voltage from each of the three phase units in order to minimize circulating currents between them.
- Provide a sinusoidal voltage at the AC terminals or sinusoidal AC current waveforms by adjusting the ratio of the upper and lower multivalves of a phase unit.
- Minimize the DC component in the AC terminal currents due to transformer requirements.
- Balancing the capacitor voltage in the individual submodules, and keep them within a defined range.
- Control the power transfer between the AC and DC sides.

The multivalve capacitors, placed inside the submodules, serve as energy storage during switching. Therefore the capacitance will directly influence the DC voltage ripple, and also the

dynamic performance of the converter. These capacitors will also to an extent be able to filter high frequency harmonics. [5]

The phase unit capacitance can be calculated as

$$C_T = \frac{m_a \cdot I}{2 \cdot \omega \cdot \Delta V} \tag{5.1}$$

where m_a is the modulation index, I is the converter current, and ΔV is the DC ripple voltage which generally can be set to 10 % [21]. When the phase unit capacitance is found, the submodule capacitance can be calculated as

$$C_{SM} = 2 \cdot N_{MV} \cdot C_T \tag{5.2}$$

where N_{MV} denotes the number of submodules per multivalve.

The valve reactor is placed in series with the submodules, one in each multivalve. Its functions are in general [5]:

- Limit the circulating currents between the three phase units, and enable to control them.
- Limit the short circuit current.
- Contribute to the interface impedance between the converter and the AC network.

According to [22], the short circuit voltage of the valve reactor can be assumed to be 15 %. The reactance is then calculated as

$$X_f = 0{,}15 \cdot \frac{V^2}{S} \tag{5.3}$$

The resistance in the valve reactor can be assumed as 1 % of the reactance, and can therefore be calculated as

$$R_f = 0{,}01 \cdot X_f \tag{5.4}$$

4.3.2. Interface transformer

The interface transformer is connected directly before the converter, and the purpose is in general to perform the following tasks [5]:

- Adapt a standard AC system voltage to a value matching the converter AC output voltage and allow optimal utilization of VSC valve ratings.
- Prevent zero sequence currents from flowing between the AC system and the converter DC side.
- Provide a galvanic isolation between the DC and the AC systems.
- Provide isolation for the DC side zero sequence voltage.
- Facilitate the variation of the converter side AC voltage for optimal utilization of the converter depending on the reactive and active power exchange.

In the HVDC model, the interface transformer is modeled as a series connected inductances in each phase on the AC side. Thus, there is no voltage transformation in the system, and the reference voltage is the same for the whole AC grid at both sending and receiving end. The resistance in the transformer can in many cases be neglected, and the short circuit voltage is usually 10 %. (5.4) can be used for calculating the reactance.

$$X_t = 0{,}10 \cdot \frac{V^2}{S} \tag{5.4}$$

The transformer reactance in the HVDC link model is 0,3 pu, which is a rather high value.

4.3.3. DC cable

The two converters are connected together with cables for both poles, modelled as pi section lines with resistive, capacitive and inductive elements. As the system is to be divided in the middle as two subsystem, it is decided to use two series connected pi sections per pole. The complete DC cable configuration illustrated in Figure 4.1, where the dots mark the connection points for the converters.

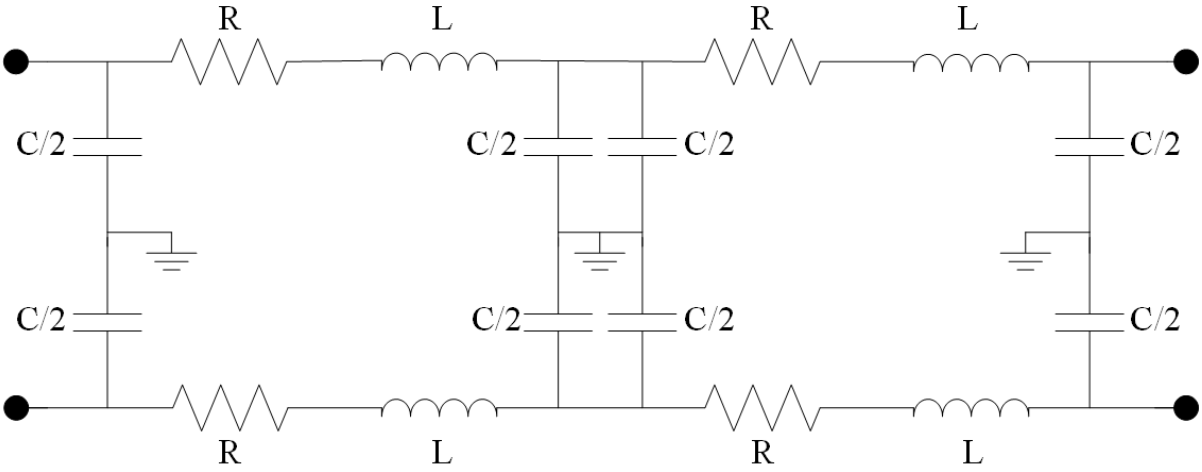

Figure 4.1: DC cable configuration

4.3.4. AC grid

As indicated in Figure 1.1, the AC grid is modelled as series connected resistive and inductive elements for each phase. The AC sides for both source and load are symmetric, and contain both the grid and the interface transformer.

Chapter 5 The Control System

5.1. General control strategy

The converters in the HVDC system operate as rectifier and inverter, at the source and load respectively. Depending on the desired load flow conditions, the control strategies for the two converters are different regarding the parameters to control.

The basic intention of the control system is to operate with the wanted active and reactive power flow. As the VSC/MMC has the ability of independent P and Q control, it can operate in all the four quadrants of the P-Q diagram.

The power transferred between two nodes in an AC grid is given by

$$P = \frac{V_1 \cdot V_2 \cdot \sin\theta}{X} \tag{5.1}$$

$$Q = \frac{{V_1}^2 - V_1 \cdot V_2 \cdot \cos\theta}{X} \tag{5.2}$$

where V_1 and V_2 are the node voltage magnitude, θ is the voltage angle difference and X is the reactance between the nodes. This implies that the active power transfer is strongly dependent on the voltage angle difference, while the reactive power is more related to the voltage magnitude difference. These relationships are then utilized at the converters AC sides to control the power flow between the interconnected AC grids.

Each of the converters in the system has two degrees of freedom, one for reactive power and one for either active power or DC voltage control [23]. The reactive power in one converter can be controlled independently of the other one, while the active power transfer must be balanced. This implies that the active power at receiving end is equal to the active power at sending end, when neglecting losses in the system. Balanced power conditions are achieved by having one converter controlling DC voltage, and the other converter controlling active power. The essential control structure of a MMC HVDC system is indicated in Figure 5.1.

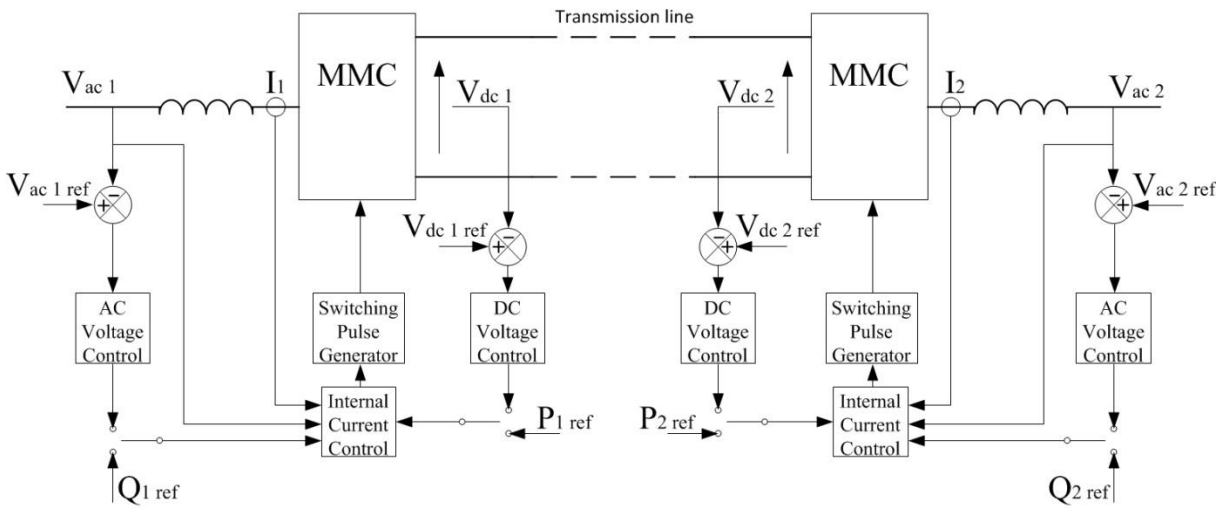

Figure 5.1: Fundamental control structure of a VSC HVDC system

However, as the MMC contains a large amounts of capacitors with stored energy, the task of balancing the capacitor energies while performing a stable power transfer between the DC side and the AC side is rather complex [24]. Due to this issue, the MMC requires a more sophisticated control system than earlier generations of VSCs.

For the system investigated in this report, two different control systems are implemented. This is due to the fact that the MMC operates with two ideally independent currents; the load current and the differential current. The load current is used to control active power or the total stored energy in the MMC, which is proportional to the DC voltage, as one degree of freedom. The other degree of freedom is used for reactive power or AC voltage control. When it comes to the differential current, which is a circulating current inside the converter, it is utilized for balancing and equally distribute the total energy between each multivalve, or to eliminate ripple. [25]

The theories used for controlling the load current and the differential current are parts of ongoing research, and is more explicitly elaborated in section 5.3 and 5.4. As a basis, the classical theory for vector control is explained in the following section.

5.2. Vector control

In a three phase system, the voltage and current is normally represented in the stationary *abc* coordinate system. When applying vector control, these quantities are transformed into the rotating *dq* reference frame in two steps.

First, the three phase stationary *abc* quantities are transformed into two phase stationary $\alpha\beta$ quantities as indicated in Figure 5.2. The transformation can easily be executed by applying Clarke transformation presented in (5.3), where the zero-sequence component γ is included for inverse transformation purposes.

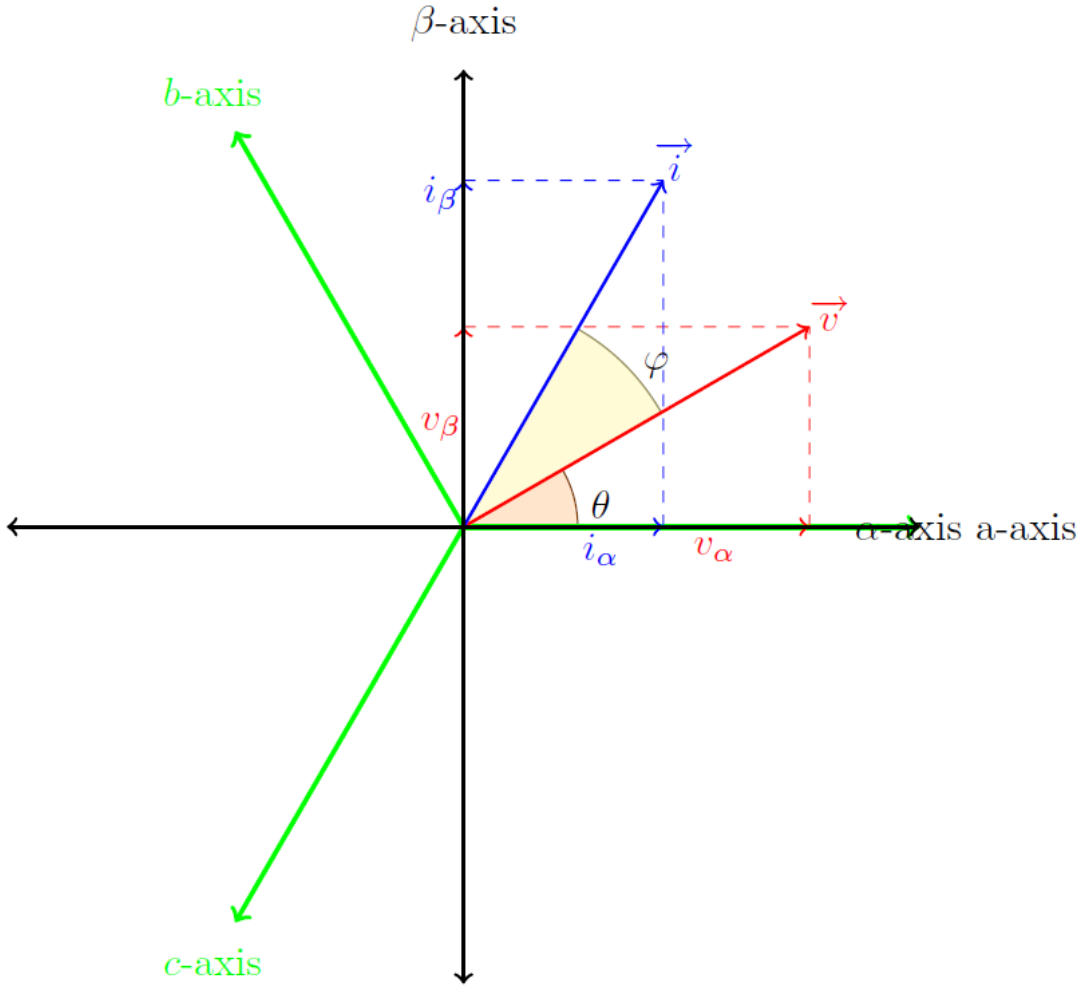

Figure 5.2. The stationary $\alpha\beta$ system [19]

$$\begin{bmatrix} v_\alpha \\ v_\beta \\ v_\gamma \end{bmatrix} = \frac{2}{3} \begin{bmatrix} 1 & -\frac{1}{2} & -\frac{1}{2} \\ 0 & \frac{\sqrt{3}}{2} & -\frac{\sqrt{3}}{2} \\ \frac{1}{2} & \frac{1}{2} & \frac{1}{2} \end{bmatrix} \begin{bmatrix} v_a \\ v_b \\ v_c \end{bmatrix} \tag{5.3}$$

The second step involves transformation from the stationary $\alpha\beta$ quantities to rotating dq quantities, indicated in Figure 5.3. The transformation can be executed by applying (5.4). As the dq reference frame rotates synchronously aligned with the voltage and current vectors, the resulting dq components act like static values.

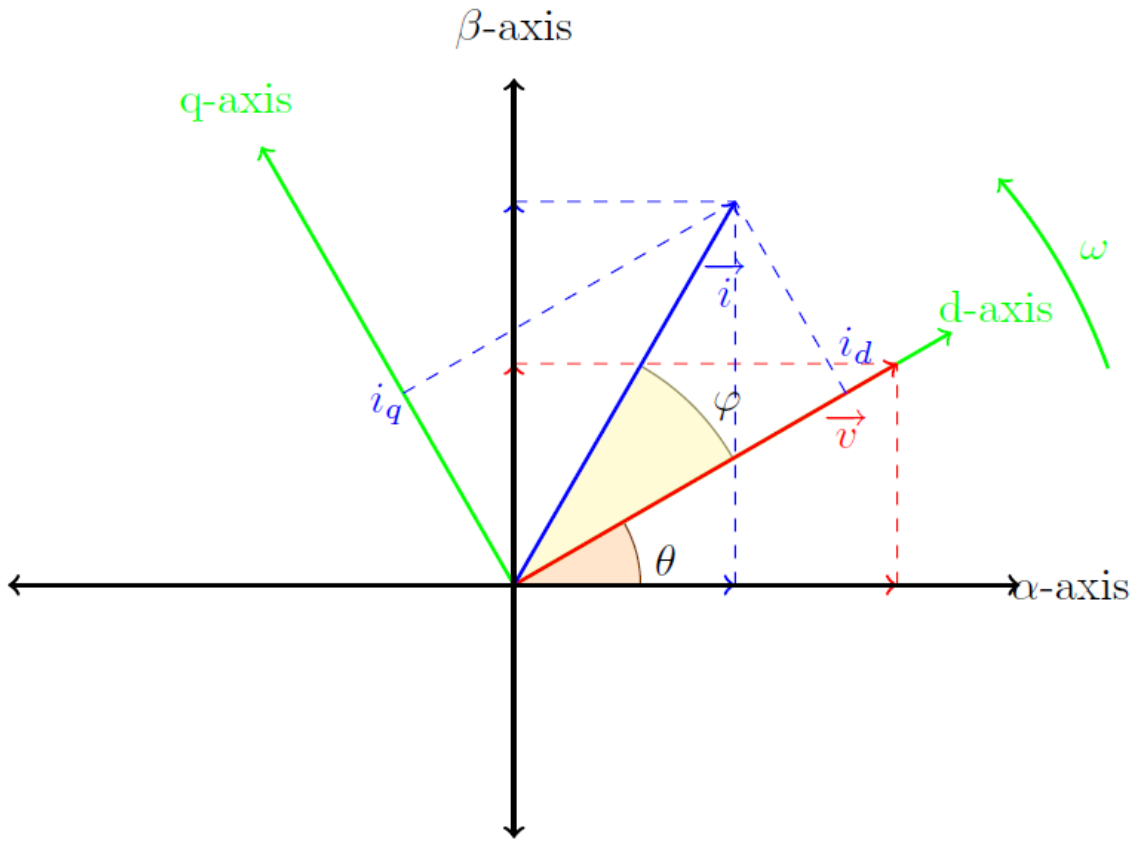

Figure 5.3: The rotating *dq* reference frame [19]

$$\begin{bmatrix} v_d \\ v_q \end{bmatrix} = \begin{bmatrix} \cos\theta & \sin\theta \\ -\sin\theta & \cos\theta \end{bmatrix} \begin{bmatrix} v_\alpha \\ v_\beta \end{bmatrix} \tag{5.4}$$

The procedure can be inversed when transforming *dq* quantities to *abc* quantities, and is also applicable to currents.

In vector control, the voltage space vector is aligned with the d-axis, leading to zero voltage in the q-axis. The following equations can then be elaborated, meaning that the currents in the *dq* reference frame can be used for independent control of active and reactive power.

$$P = \frac{3}{2} \cdot v_d \cdot i_d \tag{5.5}$$

$$Q = -\frac{3}{2} \cdot v_d \cdot i_q \tag{5.6}$$

5.3. Load current control

The load current control system is developed with focus on withstanding voltage dips caused by unbalanced faults. Unbalanced faults are characterized by appearance of negative-sequence components in the grid voltage, and rise of double-frequency oscillations in the system, reflected as ripple in the DC link voltage and output power [29]. During such operating conditions, generation of correct reference currents is important, and symmetrical components are therefore applied. The control strategy is thoroughly explained in [28], and the most important parts are reproduced below.

For a three-phase converter, the instantaneous active and reactive power at the grid terminals are given as

$$p = \boldsymbol{v} \circ \boldsymbol{i} = v_a \cdot i_a + v_b \cdot i_b + v_c \cdot i_c \tag{5.7}$$

$$q = \boldsymbol{v}_\perp \circ \boldsymbol{i} = \frac{1}{\sqrt{3}}[(v_a - v_{b)} \cdot i_c + (v_b - v_{c)} \cdot i_a + (v_c - v_{a)} \cdot i_b] \tag{5.8}$$

where $\boldsymbol{v} = [v_a \quad v_b \quad v_c]^T$, and $\boldsymbol{i} = [i_a \quad i_b \quad i_c]^T$. The bold characters represent vectors, "$\circ$" means the dot product and "$\perp$" represent a vector derived from matrix transformation.

$\boldsymbol{v}_\perp$ is given as

$$\boldsymbol{v}_\perp = \frac{1}{\sqrt{3}} \cdot \begin{bmatrix} 0 & 1 & -1 \\ -1 & 0 & 1 \\ 1 & -1 & 0 \end{bmatrix} \cdot \boldsymbol{v}$$

Symmetric–sequence transformation is used to decompose unbalanced multiphase quantities, and instantaneous quantities for unbalanced *abc* voltages are represented as:

$$\boldsymbol{v} = \boldsymbol{v}^+ + \boldsymbol{v}^- + \boldsymbol{v}^0 \tag{5.9}$$

where $\boldsymbol{v}^{+,-,0} = \left[v_a^{+,-,0} \quad v_b^{+,-,0} \quad v_c^{+,-,0}\right]^T$, and "+,-,0" denote the positive, negative and zero sequence, respectively. The same concept applies to the currents:

$$\boldsymbol{i} = \boldsymbol{i}^+ + \boldsymbol{i}^- + \boldsymbol{i}^0 \tag{5.10}$$

The instantaneous power can therefore be written as

$$p = \boldsymbol{v} \circ \boldsymbol{i} = (\boldsymbol{v}^+ + \boldsymbol{v}^- + \boldsymbol{v}^0) \circ (\boldsymbol{i}^+ + \boldsymbol{i}^- + \boldsymbol{i}^0) \tag{5.11}$$

$$q = \boldsymbol{v}_\perp \circ \boldsymbol{i} = (\boldsymbol{v}_\perp^+ + \boldsymbol{v}_\perp^- + \boldsymbol{v}_\perp^0) \circ (\boldsymbol{i}^+ + \boldsymbol{i}^- + \boldsymbol{i}^0) \tag{5.12}$$

With respect to the definitions of symmetric-sequence vector in (5.9), corresponding orthogonal vectors in (5.12) can be derived by using the matrix transformation in (5.8). It should be noted that $\boldsymbol{v}_\perp^+$ lags $\boldsymbol{v}^+$ by 90º, $\boldsymbol{v}_\perp^-$ leads $\boldsymbol{v}^-$ by 90º, and $\boldsymbol{v}_\perp^0$ is always zero. The dot product of $\boldsymbol{i}^0$ and positive-sequence or negative-sequence voltage vectors are also zero, and the power equations can be simplified:

$$p = \boldsymbol{v} \circ \boldsymbol{i} = (\boldsymbol{v}^{+} + \boldsymbol{v}^{-}) \circ (\boldsymbol{i}^{+} + \boldsymbol{i}^{-}) + \boldsymbol{v}^{0} \circ \boldsymbol{i}^{0} \tag{5.13}$$

$$q = \boldsymbol{v}_{\perp} \circ \boldsymbol{i} = (\boldsymbol{v}_{\perp}^{+} + \boldsymbol{v}_{\perp}^{-}) \circ (\boldsymbol{i}^{+} + \boldsymbol{i}^{-}) \tag{5.14}$$

To do separate analysis of the contributions of currents to independent active and reactive power control, the sequence currents $\boldsymbol{i}^{+,-}$ can be decoupled into two orthogonal quantities. The decomposition of the current vectors is presented in Figure 5.4, where "*p*" and "*q*" in subscripts denote active and reactive power, respectively.

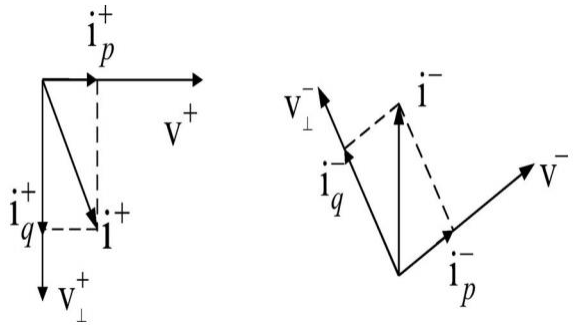

Figure 5.4: Decomposition of voltage and current vectors [28]

Reactive power control mode:

First, for reactive power control, only $\boldsymbol{i}_{\boldsymbol{q}}^{+}$ and $\boldsymbol{i}_{\boldsymbol{q}}^{-}$ are present, which are defined in phase with $\boldsymbol{v}_{\perp}^{+}$ and $\boldsymbol{v}_{\perp}^{-}$ in order to generate reactive power only. The instantaneous power equations can then be rewritten:

$$p = \underbrace{\boldsymbol{v}^{+} \circ \boldsymbol{i}_{q}^{-} + \boldsymbol{v}^{-} \circ \boldsymbol{i}_{\boldsymbol{q}}^{+}}_{\tilde{p}2\omega} \tag{5.15}$$

$$q = \underbrace{\boldsymbol{v}_{\perp}^{+} \circ \boldsymbol{i}_{q}^{+}}_{Q^{+}} + \underbrace{\boldsymbol{v}_{\perp}^{-} \circ \boldsymbol{i}_{q}^{-}}_{Q^{-}} + \underbrace{\boldsymbol{v}_{\perp}^{-} \circ \boldsymbol{i}_{q}^{+} + \boldsymbol{v}_{\perp}^{+} \circ \boldsymbol{i}_{q}^{-}}_{\tilde{q}2\omega} \tag{5.16}$$

where Q^{+} and Q^{-} denote the constant reactive power introduced by positive and negative sequences, $\tilde{p}2\omega$ represents oscillating active power, and $\tilde{q}2\omega$ the oscillating reactive power. The two terms of $\tilde{p}2\omega$ are in-phase quantities oscillating at the double fundamental frequency, which also holds for $\tilde{q}2\omega$. As the oscillating powers may cause voltage problems, output distortion, control instability, power loss and operating current rise, it is desirable to eliminate or mitigate them. A trade-off between $\tilde{p}2\omega$ and $\tilde{q}2\omega$ is not necessarily easy, and strategies to achieve controllable oscillating active and reactive power are derived from two considerations.

Controllable oscillating reactive power:

For a desired level of reactive power injected into a grid, the first two terms of (5.16) must be

$$Q = \boldsymbol{v}_{\perp}^{+} \circ \boldsymbol{i}_{q}^{+} + \boldsymbol{v}_{\perp}^{-} \circ \boldsymbol{i}_{q}^{-} \tag{5.17}$$

The other terms representing $\tilde{q}2\omega$ are in-phase quantities, and can easily compensate each other. The following equation can be made:

$$\boldsymbol{v}_{\perp}^{+} \circ \boldsymbol{i}_{q}^{-} = -k_q \cdot \boldsymbol{v}_{\perp}^{-} \circ \boldsymbol{i}_{q}^{+} \tag{5.18}$$

Here k_q is a scalar coefficient in the region $0 \leq k_q \leq 1$, used as a weighting factor for the elimination of $\tilde{q}2\omega$. Further it can be shown that the negative-sequence current can be derived from (5.18) as

$$\boldsymbol{i}_{q}^{-} = \frac{-k_q \cdot \boldsymbol{v}_{\perp}^{+} \circ \boldsymbol{i}_{q}^{+}}{\|\boldsymbol{v}_{\perp}^{+}\|^{\mathbf{2}}} \cdot \boldsymbol{v}_{\perp}^{-} \tag{5.19}$$

where $\|\boldsymbol{v}_{\perp}^{+}\|^{\mathbf{2}} = \|\boldsymbol{v}^{+}\|^{\mathbf{2}} = \boldsymbol{v}^{+} \circ \boldsymbol{v}^{+}$, and the operator "‖ ‖" means the norm of a vector. By substituting (5.19) into (5.17), and using $\left\|\boldsymbol{v}_{\perp}^{+,-}\right\|^{\mathbf{2}} = \|\boldsymbol{v}^{+,-}\|^{\mathbf{2}}$, the following equation is obtained:

$$Q \cdot \|\boldsymbol{v}^{+}\|^{2} = (\|\boldsymbol{v}^{+}\|^{\mathbf{2}} - k_q \cdot \|\boldsymbol{v}^{-}\|^{\mathbf{2}}) \cdot (\boldsymbol{v}_{\perp}^{+} \circ \boldsymbol{i}_{q}^{+}) \tag{5.20}$$

Based on (5.19) and (5.20), the currents for reactive power control can be expressed as

$$\boldsymbol{i}_{q}^{+} = \frac{Q}{\|\boldsymbol{v}^{+}\|^{2} - k_q \cdot \|\boldsymbol{v}^{-}\|^{\mathbf{2}}} \cdot \boldsymbol{v}_{\perp}^{+} \tag{5.21}$$

$$\boldsymbol{i}_{q}^{-} = \frac{-k_q \cdot Q}{\|\boldsymbol{v}^{+}\|^{2} - k_q \cdot \|\boldsymbol{v}^{-}\|^{\mathbf{2}}} \cdot \boldsymbol{v}_{\perp}^{-} \tag{5.22}$$

Then the total current reference $\boldsymbol{i}_{q}^{*}$ is the sum of $\boldsymbol{i}_{q}^{+}$ and $\boldsymbol{i}_{q}^{-}$:

$$\boldsymbol{i}_{q}^{*} = \frac{Q}{\|\boldsymbol{v}^{+}\|^{2} - k_q \cdot \|\boldsymbol{v}^{-}\|^{\mathbf{2}}} \cdot (\boldsymbol{v}_{\perp}^{+} - k_q \cdot \boldsymbol{v}_{\perp}^{-}) \tag{5.23}$$

Controllable oscillating active power:

Now the goal is to control the oscillating active power $\tilde{p}2\omega$, expressed in (5.15). The negative-sequence currents have to meet

$$\boldsymbol{v}^{+} \circ \boldsymbol{i}_{q}^{-} = -k_q \cdot \boldsymbol{v}^{-} \circ \boldsymbol{i}_{q}^{+} \tag{5.24}$$

where k_q now is a weighting factor for elimination of oscillating active power, still representing the reactive power control mode. As $\boldsymbol{v}^{+} \circ \boldsymbol{i}^{-} = \boldsymbol{v}_{\perp}^{+} \circ \boldsymbol{i}_{\perp}^{-}$, the left side of (5.24) can be rewritten as

$$\boldsymbol{v}^{+} \circ \boldsymbol{i}_{q}^{-} = \boldsymbol{v}_{\perp}^{+} \circ \boldsymbol{i}_{q\perp}^{-} = -k_q \cdot \boldsymbol{v}^{-} \circ \boldsymbol{i}_{q}^{+} \tag{5.25}$$

where $\boldsymbol{i}_{q\perp}^{-}$ is the orthogonal vector of $\boldsymbol{i}_{q}^{-}$, and can be expressed as

$$\boldsymbol{i}_{q\perp}^{-} = \frac{-k_q \cdot \boldsymbol{v}_{\perp}^{+} \circ \boldsymbol{i}_q^{+}}{\|\boldsymbol{v}^{+}\|^2} \cdot \boldsymbol{v}^{-} \tag{5.26}$$

The negative-sequence current for reactive power control can then be directly derived from (5.26):

$$\boldsymbol{i}_{q}^{-} = \frac{k_q \cdot \boldsymbol{v}_{\perp}^{+} \circ \boldsymbol{i}_q^{+}}{\|\boldsymbol{v}^{+}\|^2} \cdot \boldsymbol{v}^{-} \tag{5.27}$$

By solving (5.27) and (5.17), the positive-sequence and negative-sequence current can be derived:

$$\boldsymbol{i}_{q}^{+} = \frac{Q}{\|\boldsymbol{v}^{+}\|^2 + k_q \cdot \|\boldsymbol{v}^{-}\|^2} \cdot \boldsymbol{v}_{\perp}^{+} \tag{5.28}$$

$$\boldsymbol{i}_{q}^{-} = \frac{k_q \cdot Q}{\|\boldsymbol{v}^{+}\|^2 + k_q \cdot \|\boldsymbol{v}^{-}\|^2} \cdot \boldsymbol{v}_{\perp}^{-} \tag{5.29}$$

The total current reference can again be expressed as a sum of the positive-sequence and negative-sequence currents:

$$\boldsymbol{i}_{q}^{*} = \frac{Q}{\|\boldsymbol{v}^{+}\|^2 + k_q \cdot \|\boldsymbol{v}^{-}\|^2} \cdot (\boldsymbol{v}_{\perp}^{+} + k_q \cdot \boldsymbol{v}_{\perp}^{-}) \tag{5.30}$$

Merging strategies:

For controlling both oscillating active and reactive power, (5.23) and (5.30) can be put together in the following way, with k_q now being in the range $-1 \leq k_q \leq 1$:

$$\boldsymbol{i}_{q}^{*} = \frac{Q}{\|\boldsymbol{v}^{+}\|^2 + k_q \cdot \|\boldsymbol{v}^{-}\|^2} \cdot (\boldsymbol{v}_{\perp}^{+} + k_q \cdot \boldsymbol{v}_{\perp}^{-}) \tag{5.31}$$

By substituting (5.31) into (5.15) and (5.16), the following power equations are obtained:

$$p = \frac{Q \cdot (1 - k_q) \cdot (\boldsymbol{v}_{\perp}^{+} \circ \boldsymbol{v}^{-})}{\|\boldsymbol{v}^{+}\|^2 + k_q \cdot \|\boldsymbol{v}^{-}\|^2} \tag{5.32}$$

$$q = Q + \frac{Q \cdot (1 + k_q) \cdot (\boldsymbol{v}_{\perp}^{+} \circ \boldsymbol{v}_{\perp}^{-})}{\|\boldsymbol{v}^{+}\|^2 + k_q \cdot \|\boldsymbol{v}^{-}\|^2} \tag{5.33}$$

It can be seen that oscillating active and reactive power is controlled by the coefficient k_q.

Active power control mode:

In a similar way as presented earlier, at a given level of active power injected into a grid, the current reference can be expressed as

$$\boldsymbol{i}_p^* = \frac{P}{\|\boldsymbol{v}^+\|^2 + k_p \cdot \|\boldsymbol{v}^-\|^2} \cdot (\boldsymbol{v}_\perp^+ + k_p \cdot \boldsymbol{v}^-) \tag{5.34}$$

k_p here represents a coefficient similar to k_q in the range $-1 \leq k_p \leq 1$, and denotes a weighting factor for eliminating oscillating active and reactive power related to the active power control mode.

Schematics of the load current control system for the rectifier and inverter is attached in Appendix A and Appendix B, respectively. The load current control system for the rectifier has first a DC voltage regulator implemented in the *abc* reference frame, which minimizes the deviation between reference voltage and the measured voltage. A current regulator is then implemented in the *αβ* reference frame, where the input is the active power reference current given in (5.34) minus the measured current.

The load current control system for the inverter, which is controlling the DC current, is given an active power reference, so that no regulator is implemented in the *abc* reference frame. Similar to the rectifier, it has a current regulator implemented in the *αβ* reference frame.

The output signals from the load current control systems are fed into the switching pulse generators, the system responsible for switching the individual submodules.

5.4. Differential current control

The three phase units in each converter can be regarded as three DC voltage sources connected in parallel. As the voltages in the phase units are not exactly equal during operation, circulating currents arise. These circulating currents, subsequently referred to as differential currents, have to be controlled for balancing end equally distributing the total stored energy between the multivalves, or to reduce ripple. [5] [25]

To control the submodules in the MMCs, a control strategy based on mathematical optimization using Lagrange multipliers in *abc* frame is applied. This control strategy is explained in [25] and [26], and is implemented in the HVDC model. The mathematical deduction of this concept is outside the scope of this work, but is described in [26]. The most important parts are reproduced in this section.

In general, this control method is developed to minimize differential current oscillations $\Delta i_{diff\,k}$ or capacitive phase energy oscillations $\Delta w_{\Sigma k}$. At the same time, the energy distribution inside the MMC is to be controlled. That includes the capacitive phase average energy sum $\overline{w}_{\Sigma k}$ and difference $\overline{w}_{\Delta k}$. A schematic for the MMC topology with the parameters used for the mathematical deduction is presented in Figure 5.5.

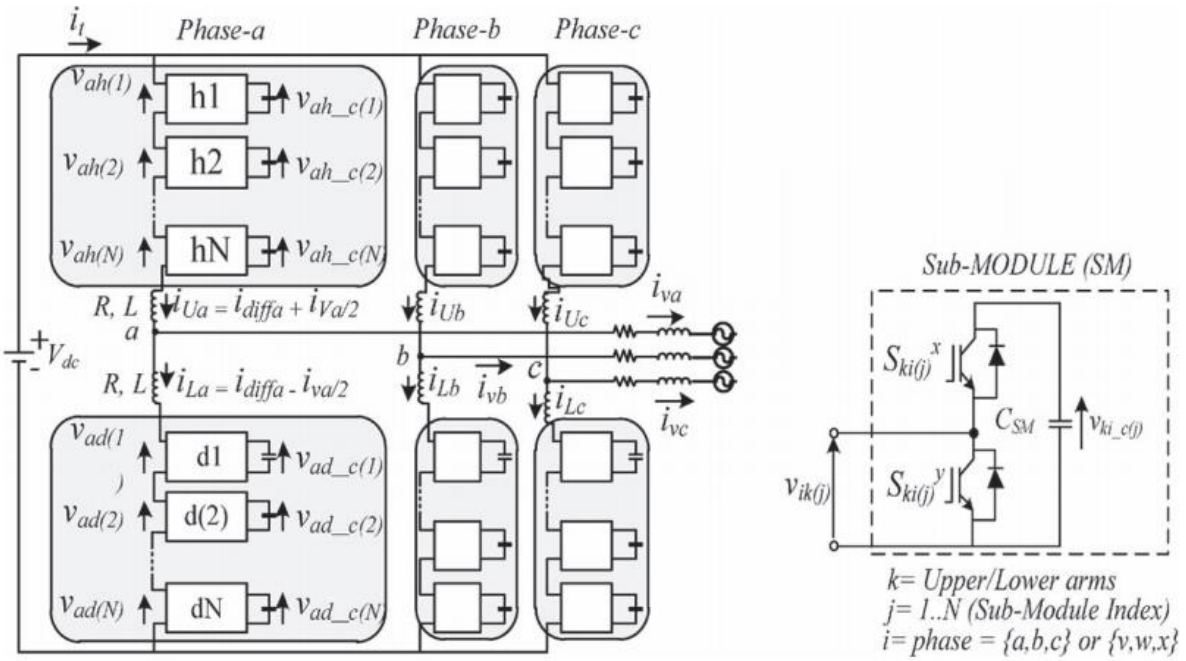

Figure 5.5: Topology of MMC and submodule [24]

The currents in the upper and lower arm can be written in the following way:

$$i_{U\,k} = i_{diff\,k} + \frac{i_{v\,k}}{2} \tag{5.35}$$

$$i_{L\,k} = i_{diff\,k} - \frac{i_{v\,k}}{2} \tag{5.36}$$

The dynamics of the sum and difference of the capacitive energy between the upper and lower arms are expressed as

$$\dot{w}_{\Sigma\,k} = \dot{w}^{\Sigma}_{cU\,k} + \dot{w}^{\Sigma}_{cL\,k} = -e_{vk} \cdot i_{vk} + \left(v_{DC} - 2 \cdot u_{diff\,k}\right) \cdot i_{diff\,k} \tag{5.37}$$

$$\dot{w}_{\Delta\,k} = \dot{w}^{\Delta}_{cU\,k} + \dot{w}^{\Delta}_{cL\,k} = \frac{i_{vk}}{2} \cdot \left(v_{DC} - 2 \cdot u_{diff\,k}\right) - 2 \cdot e_{vk} \cdot i_{diff\,k} \tag{5.38}$$

To simplify (5.37) and (5.38) and to avoid stability issues, the voltage difference $u_{diff\,k}$ should be approximately zero.

Constant differential current control:

In this section, the goal is to analytically calculate the differential current constant reference that makes it possible to control the average energy distribution. The approach will then be to minimize the instantaneous value of the DC power phase contribution oscillations $\Delta(v_{DC} \cdot i_{diff\,k})$. This will be done by creating an average objective function by minimizing the average of the variable squared value:

$$min \rightarrow \frac{1}{T}\int_{t0}^{t0+T} (v_{DC} \cdot i_{diff\,k})^2\, dt \tag{5.39}$$

As the goal is to control the average energy distribution inside the MMC, the optimization problem is subject to two averaged constraint equations

$$\frac{1}{T}\int_{t0}^{t0+T}(-e_{vk}\cdot i_{vk}+v_{DC}\cdot i_{diff\,k})\,dt=\overline{P_{\Sigma_k}^{ref}} \tag{5.40}$$

$$\frac{1}{T}\int_{t0}^{t0+T}(\frac{i_{vk}}{2}\cdot v_{DC}-2\cdot e_{vk}\cdot i_{diff\,k})\,dt=\overline{P_{\Delta_k}^{ref}} \tag{5.41}$$

where e_{vk} denotes the MMC load emf, (5.40) is the average value of the energy sum dynamics $\dot{w}_{\Sigma}(t)$, and (5.41) is the average value of the energy-difference dynamics $\dot{w}_{\Delta}(t)$. These two energy dynamics are required to be equal to the references expressed in (5.42) and (5.43).

$$\overline{P_{\Sigma_k}^{ref}}=\left[kp_{\Sigma}\left(W_{\Sigma}^{ref}-\overline{w_{\Sigma_k}}\right)+ki_{\Sigma}\int\left(W_{\Sigma}^{ref}-\overline{w_{\Sigma_k}}\right)dt\right] \tag{5.42}$$

$$\overline{P_{\Delta_k}^{ref}}=\left[kp_{\Delta}\left(W_{\Delta}^{ref}-\overline{w_{\Delta_k}}\right)+ki_{\Delta}\int\left(W_{\Delta}^{ref}-\overline{w_{\Delta_k}}\right)dt\right] \tag{5.43}$$

$\overline{w_{\Sigma_k}}$ and $\overline{w_{\Delta_k}}$ are the average values of the energy sum and difference as a function of time. The ideal value of the left side of (5.40) and (5.41) is zero, but as this would lead to the average value of $w_{\Sigma_k}(t)$ and $w_{\Delta_k}(t)$ to be any constant and not the desired constant, they are set as W_{Σ_k} and W_{Δ_k} which are calculated in (5.42) and (5.43).

The Lagrange equations for this case is written as

$$\begin{aligned}\mathcal{L}\left(i_{diff\,k},\lambda_{\Sigma},\lambda_{\Delta}\right)=&\frac{1}{T}\int_{t0}^{t0+T}v_{DC}\cdot i_{diff\,k}(t)^2\,dt\\&+\lambda_{\Sigma}(\overline{\dot{w}_{\Sigma_k}}(t)-\overline{P_{\Sigma_k}^{ref}}\\&+\lambda_{\Delta}(\overline{\dot{w}_{\Delta_k}}(t)-\overline{P_{\Delta_k}^{ref}}\end{aligned} \tag{5.44}$$

where $\overline{\dot{w}_{\Sigma_k}}(t)$ is given as the left side of (5.40) and $\overline{\dot{w}_{\Delta_k}}(t)$ is given by the left side of (5.41). In order to find the differential current, solving (5.45) is necessary.

$$\nabla_{(i_{diff\,k},\lambda_{\Sigma},\lambda_{\Delta})}\mathcal{L}\left(i_{diff\,k},\lambda_{\Sigma},\lambda_{\Sigma}\right)=0 \tag{5.45}$$

The first derivative is expressed as

$$\begin{aligned}\frac{\partial\mathcal{L}}{\partial i_{diff\,k}}=&\frac{1}{T}\int_{t0}^{t0+T}2\cdot v_{DC}^2\cdot i_{diff\,k}\,dt\\&+\lambda_{\Sigma}\frac{1}{T}\int_{t0}^{t0+T}v_{DC}dt\\&-2\cdot\lambda_{\Delta}\frac{1}{T}\int_{t0}^{t0+T}e_{vk}dt=0\end{aligned} \tag{5.46}$$

(5.46) can be rewritten as the following equation, by cancelling the integrating action:

$$\frac{\partial \mathcal{L}}{\partial i_{diff\,k}} = 2 \cdot v_{DC}^2 \cdot i_{diff\,k} + \lambda_{\Sigma} \cdot v_{DC} - 2 \cdot \lambda_{\Delta} \cdot e_{vk} = 0 \tag{5.47}$$

The solutions for the two other derivatives are expressed in (5.48) and (5.49).

$$\frac{\partial \mathcal{L}}{\partial \lambda_{\Sigma}} = \overline{\dot{w}_{\Sigma_k}}(t) - \overline{P_{\Sigma_k}^{ref}} = 0 \tag{5.48}$$

$$\frac{\partial \mathcal{L}}{\partial \lambda_{\Delta}} = \overline{\dot{w}_{\Delta_k}}(t) - \overline{P_{\Delta_k}^{ref}} = 0 \tag{5.49}$$

By replacing $\overline{\dot{w}_{\Sigma_k}}(t)$ and $\overline{\dot{w}_{\Delta_k}}(t)$ with the left side of (5.40) and (5.41), and solving the three dimensional equation system composed of (5.47), (5.48) and (5.49), the solution for the differential current reference can be obtained as

$$i_{diff\,k} = \left[\frac{\overline{P}_{\Sigma k}^{ref} + \overline{P}_{vk}}{v_{DC}^2}\right] \cdot v_{dc} + \left[\frac{-\overline{P}_{\Delta k}^{ref}}{2 \cdot v_{DC}^2 \cdot (e_{vk,\ p.u.}^{rms})^2}\right] \cdot e_{vk} \tag{5.50}$$

where the following notations are used:

$$\overline{P}_{vk} = \frac{1}{T}\int_{t0}^{t0+T} e_{vk} \cdot i_{vk}\, dt$$

$$(e_{vk,\ p.u.}^{rms})^2 = \frac{1}{T}\int_{t0}^{t0+T} \frac{e_{vk}^2}{v_{DC}^2}\, dt$$

(5.50) has a mathematical structure similar to the structures of instantaneous power theories-based currents definitions, in this case two conductances directly proportional to the two voltages e_{vk} and v_{DC}.

Constant energy sum:

Now we are interested in operating the converter with constant capacitive energy in each phase, as this will reduce the capacitor voltages oscillations. Therefore, the optimization problem will have the instantaneous energy sum dynamics $\dot{w}_{\Sigma k}$ as the objective function to be minimized:

$$min \rightarrow \frac{1}{T}\int_{t0}^{t0+T} (\dot{w}_{\Sigma k})^2\, dt \tag{5.51}$$

The constraints of the optimization problem are the same constraints as the ones from (5.40) and (5.41), and the Lagrange equation can be expressed as in (5.52).

$$\mathcal{L}\left(i_{diff\,k}, \lambda_{\Sigma}, \lambda_{\Delta}\right) = \frac{1}{T}\int_{t0}^{t0+T} (\dot{w}_{\Sigma k})^2\, dt + \lambda_{\Sigma}(\overline{\dot{w}_{\Sigma_k}}(t) - \overline{P_{\Sigma_k}^{ref}} + \lambda_{\Delta}(\overline{\dot{w}_{\Delta_k}}(t) - \overline{P_{\Delta_k}^{ref}} \tag{5.52}$$

In order to find the differential current control reference, the three partial derivatives, given in (5.45), of (5.52) must be solved. The first derivative results in:

$$\frac{\partial \mathcal{L}}{\partial i_{diff\,k}} = \frac{1}{T}\int_{t0}^{t0+T} 2 \cdot \left(-e_{vk} \cdot i_{vk} + v_{dc} \cdot i_{diff\,k}\right) \cdot v_{dc}\, dt + \lambda_{\Sigma}\frac{1}{T}\int_{t0}^{t0+T} v_{dc}\, dt - 2 \cdot \lambda_{\Delta}\frac{1}{T}\int_{t0}^{t0+T} e_{vk}\, dt = 0 \tag{5.53}$$

Cancelling the integral action gives the following equation:

$$\frac{\partial \mathcal{L}}{\partial i_{diff\,k}} = 2 \cdot (-e_{vk} \cdot i_{vk} + v_{dc} \cdot i_{diff\,k}) \cdot v_{dc} + \lambda_{\Sigma} \cdot v_{dc} - 2 \cdot \lambda_{\Delta} \cdot e_{vk} = 0 \tag{5.54}$$

As the same optimization constraints are used in this case, the solution of the other two derivatives are the same as (5.48) and (5.49). By solving the three dimensional system composed of (5.54), (5.48) and (5.49), the following equations is found for the differential current control reference:

$$i_{diff\,k} = \left[\frac{\overline{P}_{\Sigma k}^{ref}}{v_{dc}^2}\right] \cdot v_{dc} + \frac{P_{vk}}{v_{dc}} + \left[\frac{-\overline{P}_{\Delta k}^{ref}}{2 \cdot v_{dc}^2 \cdot (e_{vk,\ p.u.}^{rms})^2}\right] \cdot e_{vk} \tag{5.55}$$

Generalized equation:

By solving the following multi-objective optimization problem, it is possible to obtain a generalized differential current control equation that includes both results from (5.50) and (5.55):

$$min \rightarrow \frac{1}{T}\int_{t0}^{t0+T} \alpha \cdot (\dot{w}_{\Sigma k})^2 + (1-\alpha) \cdot (v_{dc} \cdot i_{diff\,k})^2\, dt \tag{5.56}$$

Here α is a weighting factor within the region [0, 1]. The two periphery circumstances are constant energy addition when $\alpha = 0$, and constant differential current when $\alpha = 1$. The resulting optimization problem, subject to constraints of (5.40) and (5.41), gives the following generalized equation:

$$i_{diff\,k} = \frac{\overline{P}_{\Sigma k}^{ref} + (1-\alpha)\cdot \overline{P}_{vk}}{v_{dc}^2} \cdot v_{dc} + \frac{\alpha \cdot P_{vk}}{v_{dc}} + \frac{-\overline{P}_{\Delta k}^{ref}}{2 \cdot v_{dc}^2 \cdot (e_{vk,\ p.u.}^{rms})^2} \cdot e_{vk} \tag{5.57}$$

A graphical representation of the energy based differential current control system is presented in Figure 5.6. The schematic includes both contribution from the load current control system and the differential current control system. Both output signals are fed into a system for controlling the individual submodules.

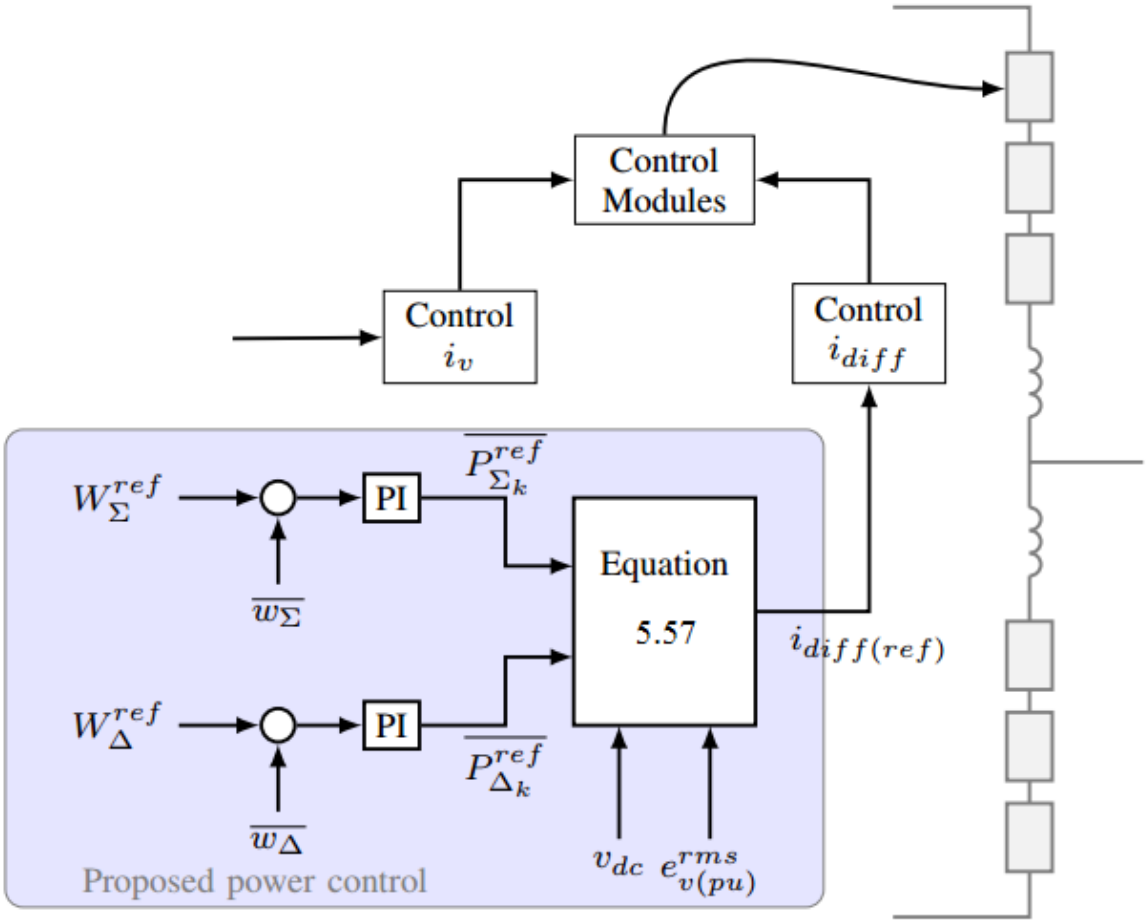

Figure 5.6: Schematic representation of the differential current control system [25]

Chapter 6 The Simulations

6.1. Simulation strategy

The main intention of this work is find out to what extent the control system affects the stability, and if the proposed method is suited for finding the tuning of the control system that gives the most stable operating conditions. The chosen approach is to use the Nyquist stability criterion to determine the stability conditions in the system. By performing a sensitivity analysis where the parameters for the PI regulators are gradually adjusted, one by one, it is assumed that the Nyquist plot will tell if the stability conditions are getting better or worse.

In this work the Nyquist plot is based on the harmonic impedance in the two subsystems, obtained from frequency sweeps. This implies that the frequency sweeping must be carried out for each single change in the control system parameters in order to create Nyquist plot for different operating conditions.

Stability investigations will be performed for one PI regulator at a time. The desired regulator parameter value will then be adjusted in a defined area, while reference values are used for the other regulators. When the best suited parameter values are found for each single regulator, it is assumed that the most stable tuning of the whole system will be composed of the most stable tuning of each single regulator.

Unfortunately, and after several attempts, the differential current control system turned out as so challenging to tune that simulations could be not be performed. As there exist none acknowledged tuning methods for this system, the trial and error method had to be used, leading to none satisfactory operating conditions. The contribution from the differential current control system is therefore set to zero, and the load current control system will be the main focus during the simulations.

The reference values for the control system parameters are listen Table 6.1, while the voltage and current reference values used during all simulations are listed in Table 6.2.

Table 6.1: Reference values for control system parameters

	K_p^*	T_i^*
Rectifier:		
Voltage regulator	$16{,}2598 \cdot 10^{-6}$	$16{,}6823 \cdot 10^{-6}$
Current regulator	2,3967	40,3453
Inverter:		
Current regulator	23,967	403,453

Table 6.2: Reference values for power system parameters

Symbol	Description	Physical value	Per unit value
V_{DC}	DC voltage	25 kV	1,11
V_s	AC voltage, line-line rms	13,8 kV	1,0
I_{DC}	DC current	270 A	0,2

6.1.1. Frequency sweep

The simulations are performed as explained in the following sections for obtaining the harmonic impedance. A frequency range from 1 to 1000 Hz is chosen, as this covers up to half the effective switching frequency for the converters. The sampling rate used for creating discrete signals is kept at 100 kHz.

The frequency steps are chosen in a logarithmic scale, shown in the frequency matrix below:

$$\mathbf{f}_{sweep} = [1,2,3,\dots,10,20,30,\dots,100,200,300,\dots,1000]$$

6.1.1.1. Source impedance

In order to obtain the harmonic impedance of the source subsystem, current injection is applied. During simulations the load subsystem is removed, and replaced by current sources. The perturbation current source is placed in parallel with the DC current source, which gives a constant DC current, while the rectifier is controlling the DC voltage. Multiple simulations are run in a series, where the perturbation current frequency is changed for each run. The setup with current injection in the source subsystem can be seen in Figure 6.1.

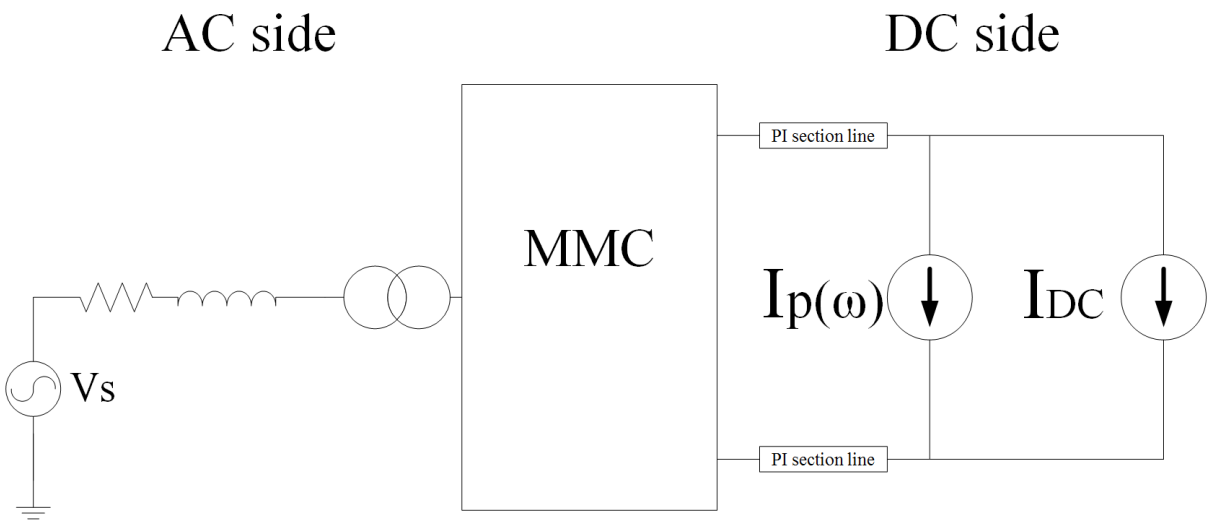

Figure 6.1: Current injection into source subsystem

After the simulations have been performed, the measurements of voltage and current for all frequency steps are analysed with DFT to extract the correct frequency components of the signals, and the impedance for each precise frequency is calculated. In this way the distortions in voltage and current are less likely to interfere with the injected signal, and the obtained harmonic impedance is expected to be more accurate.

6.1.1.2. Load impedance

The harmonic impedance of the load subsystem is obtained in a similar way as for the source, where the main difference is that voltage injection is used. Now the source subsystem is replaced by two voltage sources in series, one that supplies the DC voltage and one to inject the perturbation voltage. The inverter is now controlling the DC current, and the procedure for obtaining the harmonic impedance is the same as for the source, with multiple simulations and DFT analysis. The setup is shown in Figure 6.2.

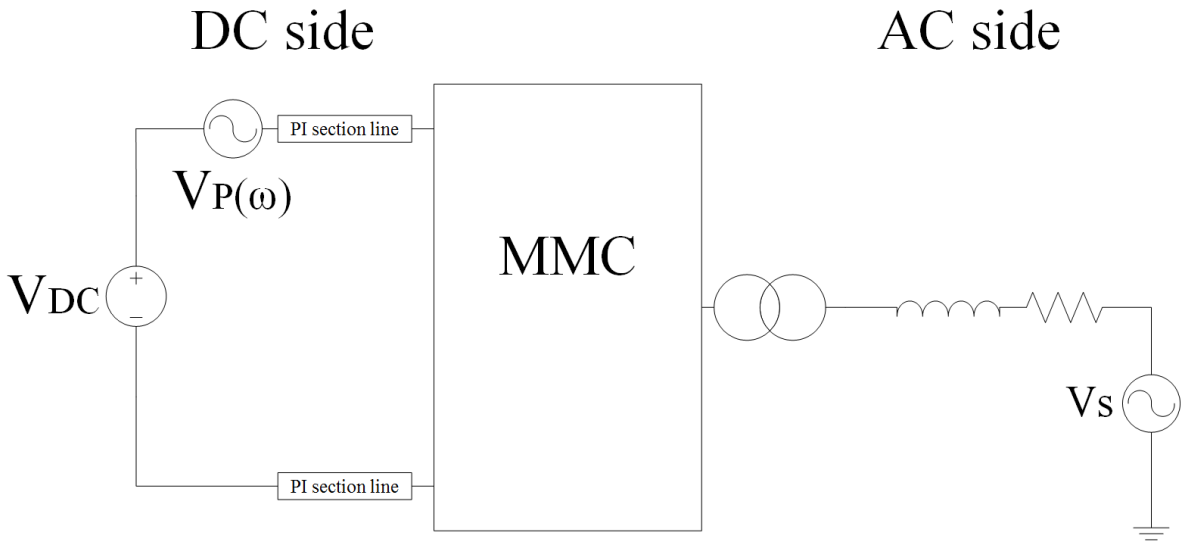

Figure 6.2: Voltage injection into load subsystem

6.1.2. Nyquist plot

When the harmonic impedance of both subsystems is obtained the Nyquist plot can be created. The plot is actually showing multiple points representing the ratio between the two subsystem impedances, for different frequencies. A consequence of this method is that all information about frequency disappear from the plot, and what is left is only a series of processed sampling points with real and imaginary components.

The resulting Nyquist plot will thus be a scatter plot, and not a continuous curve. For the Nyquist plot to appear as a curve, infinitely many sampling points is needed, which of course is a quite challenging achievement. Instead, a line can be drawn between the sampling points to make it appear as a continuous curve. However, such a representation of the data may add incorrectness to the plots, as the occurrence between the selected sampling points is unknown.

In fact, the Nyquist plot should contain values for both negative and positive frequencies in order to create a closed loop. Negative frequencies will give values that are the complex conjugated of those at positive frequencies. Only values for positive frequencies are included in this report to increase readability of the Nyquist plots.

6.2. Preliminary simulations

Before carrying out the sensitivity analysis, it is decided to investigate what simulation parameters that give the most accurate results. During the work with the specialization project [30], a test circuit was made to investigate the accuracy of the frequency sweep method. The results from the test circuit indicate that the method has very good accuracy for the magnitude, and only a few small deviations in the phase angle, compared to the analytical correct values. However, the test circuit was composed of passive RC elements fed from a 50 Hz source, containing no other harmonics or noise interfering with the injection signals.

When the frequency sweep was carried out on the HVDC model used in the specialization project [30], a lot of noise was observed in the resulting bode plots. Both magnitude and phase angle had spontaneous alterations, which also caused a lot of noise in the Nyquist plots. Therefore, it is decided to experiment with both the simulation time length and voltage/current injection amplitude to find the conditions that give the most accurate and credible results.

6.2.1. Simulation time length

To find out what simulation time length that gives the most accurate results, four different simulation time lengths between 0,5 and 2,0 seconds is tried for each single frequency step. For these simulations, the source subsystem with current injection is used, and the current injection amplitude is 1 % of the DC reference current.

In Figure 6.3 the difference in impedance magnitude due to different simulation time length is shown. It is clear that the simulation time has significant influence in the obtained harmonic impedance. In the region up to 200 Hz the difference between the results are in many cases over 20 dB. On the other hand, at frequencies above 300 Hz all the results correlate.

The deviation in phase angle is presented in Figure 6.4, and the results here are interesting, as they indicate large differences. It is not clear which simulation time that gives the most credible results in this case, as no one stands out as more likely than the other. It should be worth noting that weak results for the harmonic impedance will follow to the Nyquist analysis. Consequently, one cannot expect accurate and credible sensitivity analysis based on doubtful groundwork.

From an insufficient basis of assessment, it is decided to use a simulation time length of 1,0 second in all the following simulations.

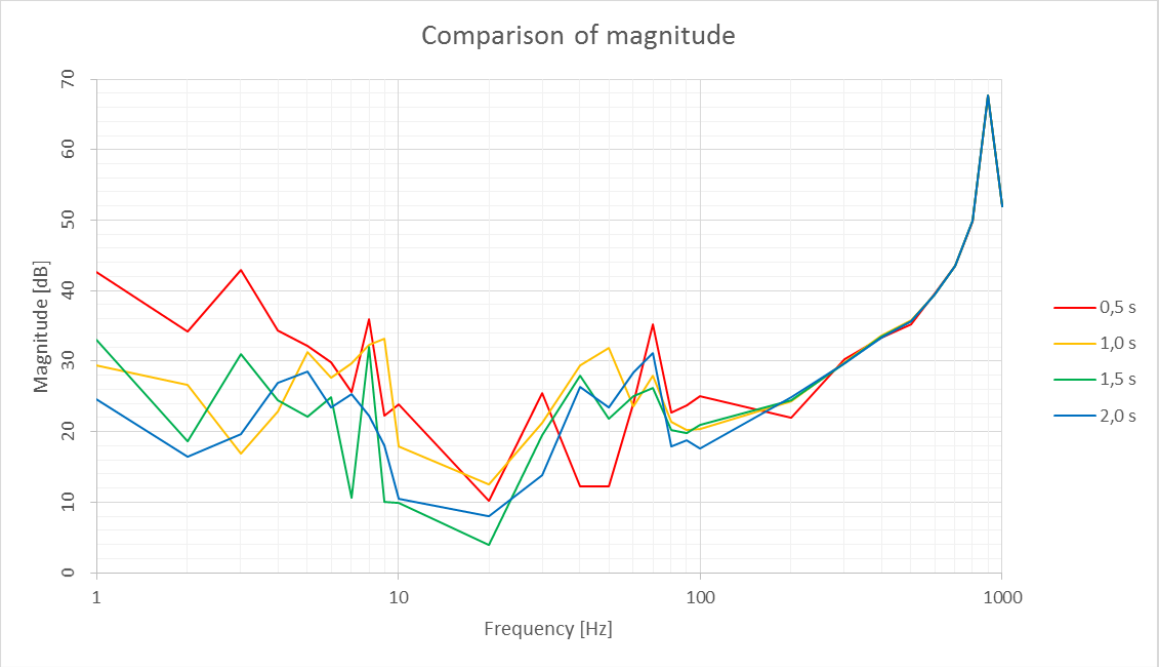

Figure 6.3: Influence on impedance magnitude from simulation time length

Figure 6.4: Influence on impedance phase angle from simulation time length

6.2.2. Injection current amplitude

For the current injection method, used to find the source subsystem harmonic impedance, it is tried four different injected current amplitudes. The amplitude is in the region of 1 % to 20 % of the DC reference current.

Figure 6.5 presents the different harmonic impedance magnitudes obtained with the different current injection amplitudes. The 1 % curve stands out with somewhat higher values compared to the other curves. At 40 Hz the largest deviation between the curves occur, here the difference between the 1 % curve and the 10 % curve is close to 40 dB. However, at frequencies above 100 Hz, the curves are almost identical.

In Figure 6.6, the difference in phase angle is shown. Particularly the region between 10 and 100 Hz is subject to a lot of noise. While several spikes occur for both 1 %, 5 % and 10 %, the 20 % curve is more predictable and has less spontaneous behavior. The harmonic impedance obtained with a current injection amplitude of 20 % of the DC line current seems most credible, and will be used for further simulations.

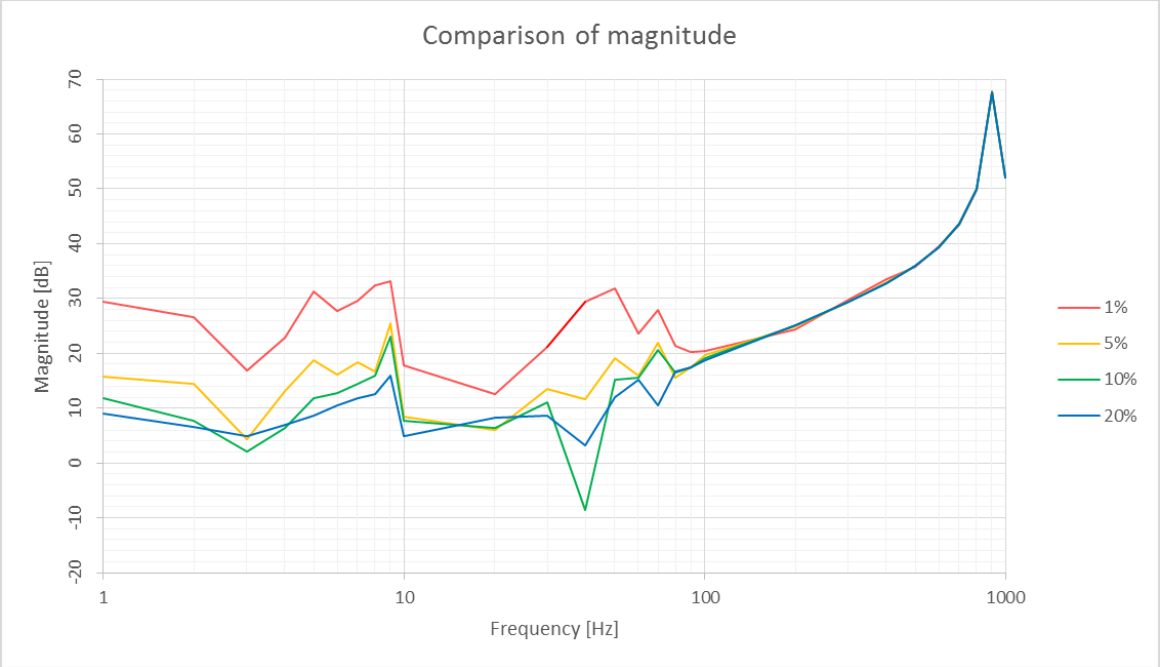

Figure 6.5: Influence on impedance magnitude from injection current amplitude

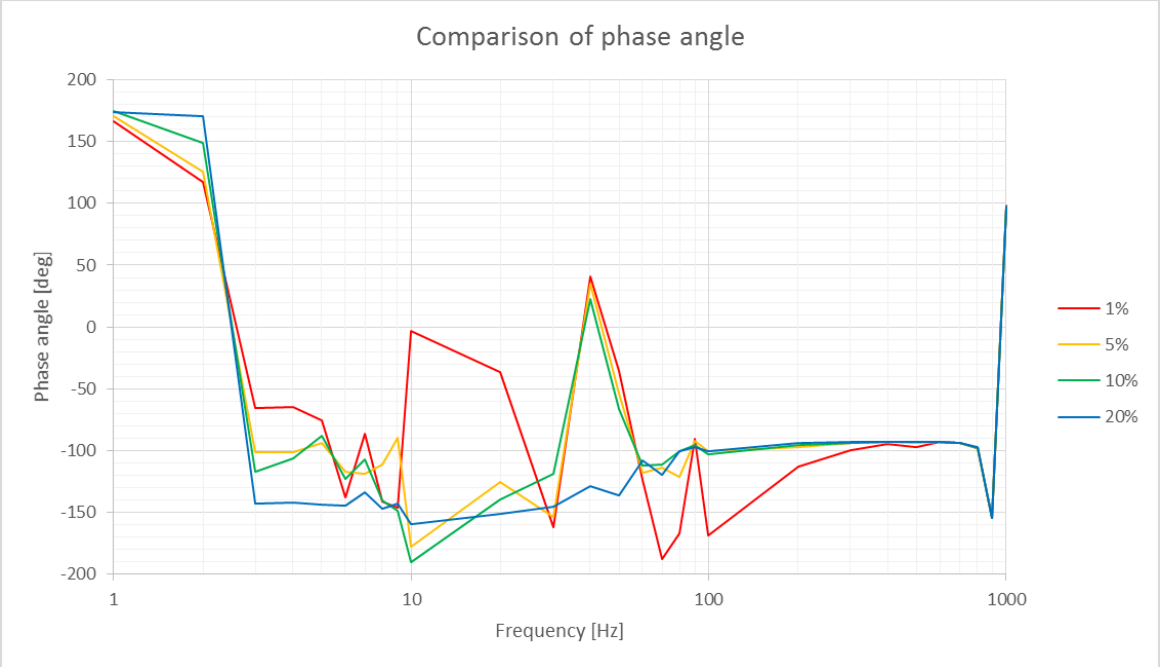

Figure 6.6: Influence on impedance phase angle from injection current amplitude

6.2.3. Injection voltage amplitude

The voltage injection method is used for finding the load subsystem harmonic impedance. Four different voltage injection amplitudes has been tried out, in the region 1 % to 20 % of the DC reference voltage. As both Figure 6.7 and Figure 6.8 indicates, the obtained harmonic impedance is approximately the same, and therefore independent of the injection voltage magnitude.

Compared to the method involving current injection, it is strange that voltage injection is not affected by the injection signals amplitude. Though, it might be that voltage injection gives more credible and accurate results than current injection. However, the two methods are not interchangeable, and both methods will have to be used for further work. For the coming simulations, the injection voltage amplitude will be kept at 20 % of the DC reference voltage.

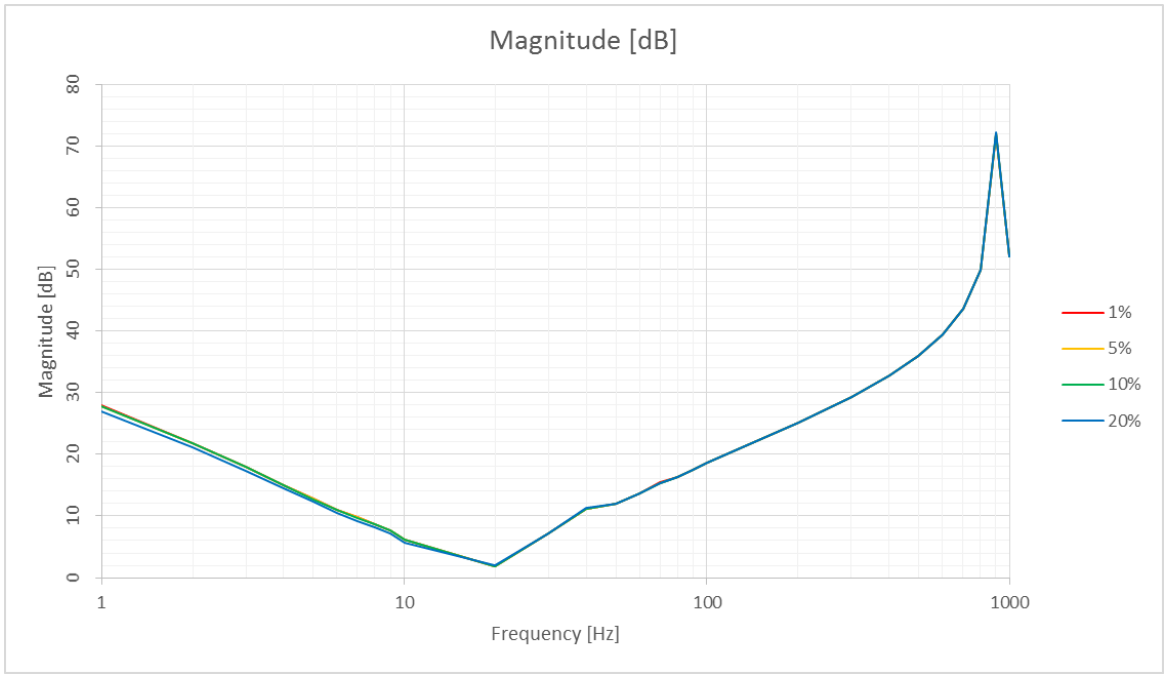

Figure 6.7: Influence on impedance magnitude from injection voltage magnitude

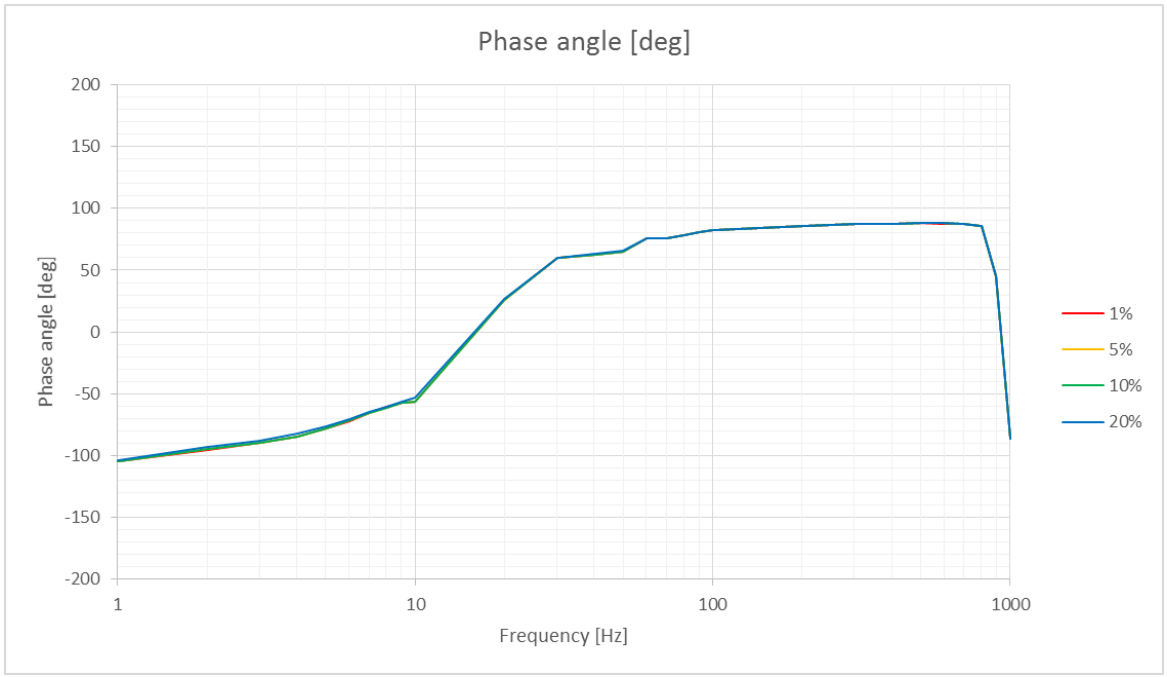

Figure 6.8: Influence on impedance phase angle from injection voltage amplitude

6.2.4. Initial system state

The system is first analyzed with reference values for the PI regulator parameters. The voltage and current spectrum in the DC line, with both subsystems operating together, is presented in Figure 6.9 and Figure 6.10, respectively. For the DC voltage, the most harmonics occur at frequencies around 60 and 70 Hz, with a magnitude close to 180 V. Compared to the DC voltage magnitude, these signals are quite small.

The DC current spectrum shows significant harmonic contents in frequencies around 10 to 20 Hz, and also 60 to 70 Hz. Compared to the nominal DC current of 270 A, the harmonic content is significant, with magnitude close to 18 ampere on several frequencies. The waveforms for both voltage and current is attached in Appendix C.

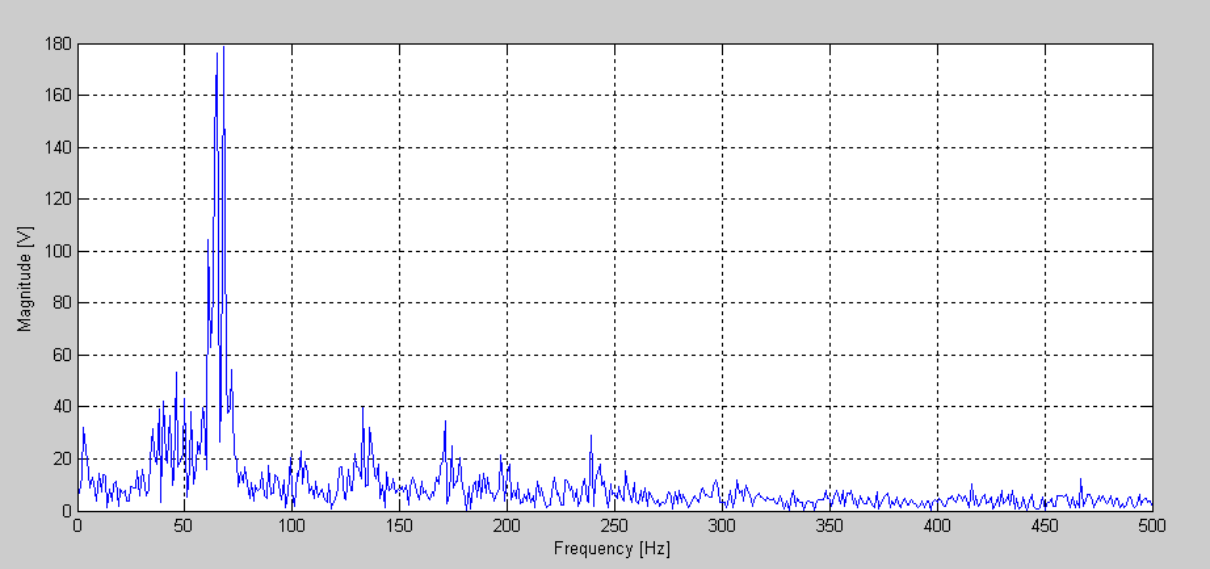

Figure 6.9: Harmonic spectrum for the DC voltage

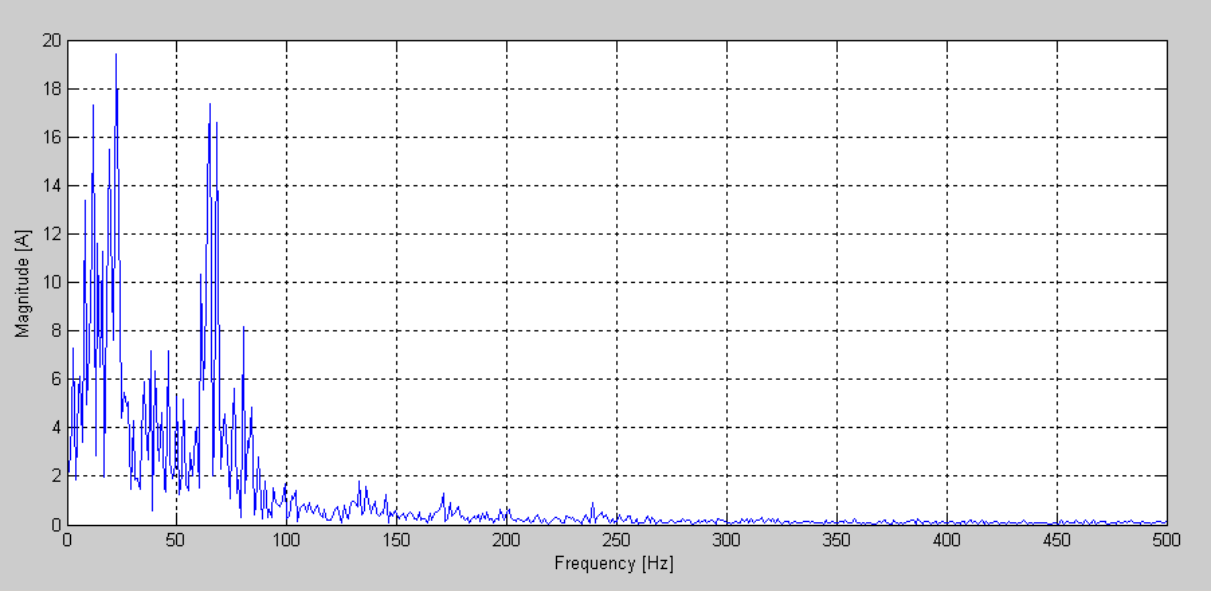

Figure 6.10: Harmonic spectrum for the DC current

The magnitude of the harmonic impedance for both source and load is displayed in Figure 6.11. An interesting observation is that the magnitude of both source and load seems to be equal above 100 Hz. This might be the point where the converters have less significance on the impedance, and the passive components begin to dominate.

In Figure 6.12, the phase angle for both source and load is shown. To increase readability, some values for the source have been relocated from the lower to upper area, and will therefore hold values above 180º. This is also done for phase angle plots further in this report.

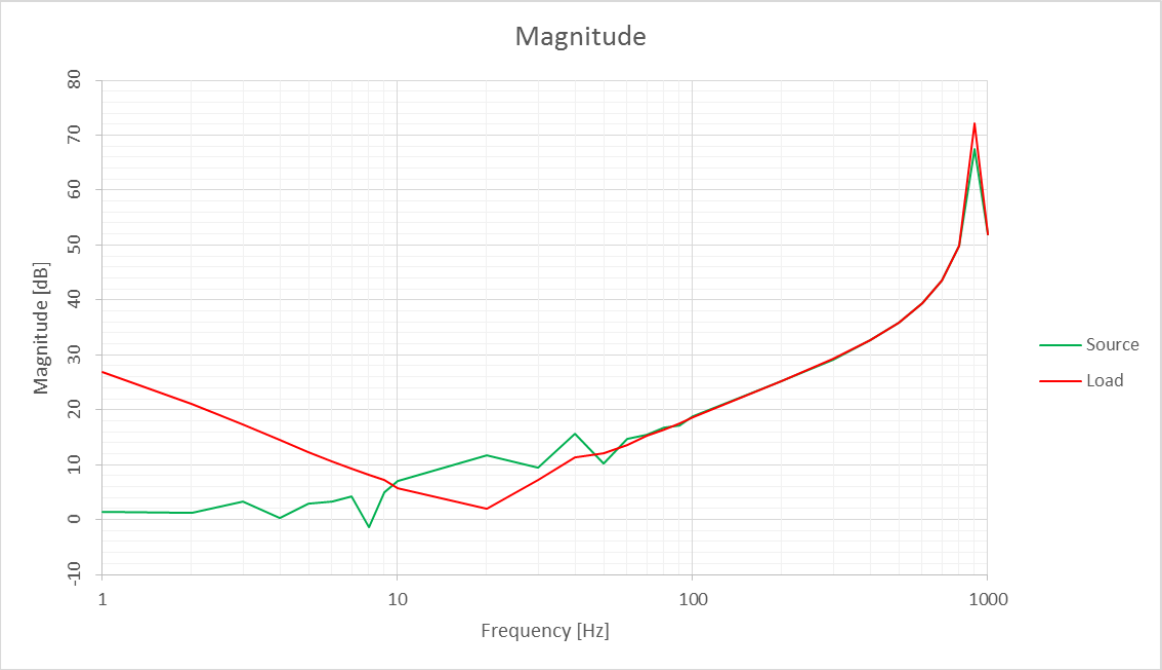

Figure 6.11: Magnitude of harmonic impedance for initial system state

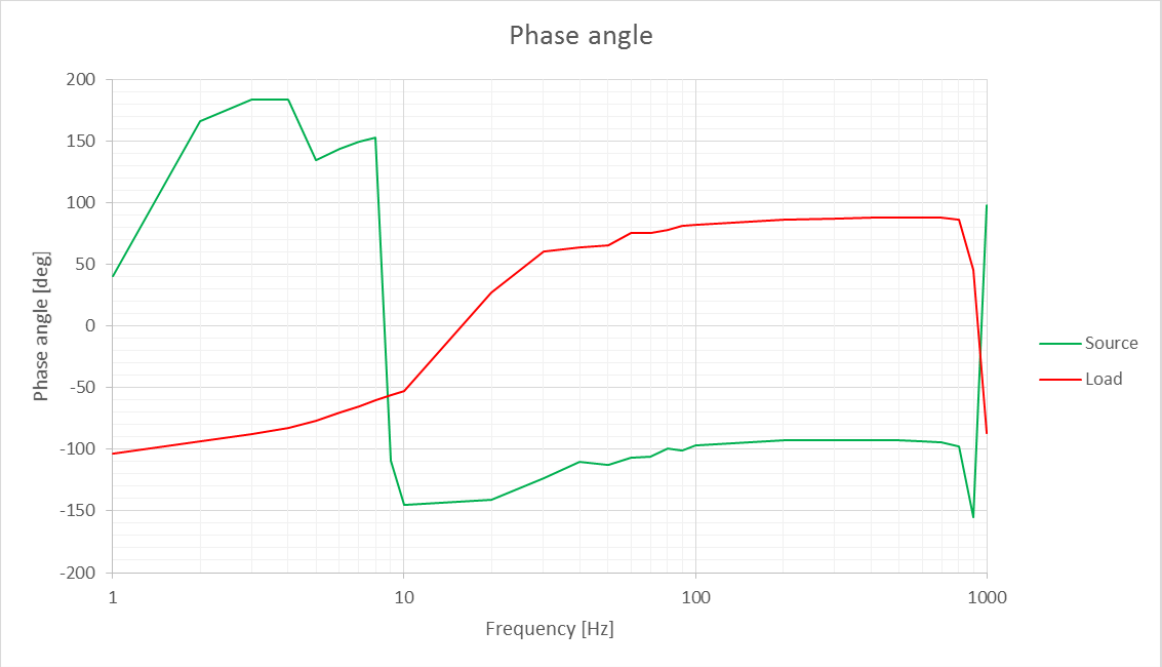

Figure 6.12: Phase angle of harmonic impedance for initial system state

A Nyquist plot for the initial system state is displayed in Figure 6.13. For this plot, and all the following, the horizontal axis holds real values, and the vertical axis holds the imaginary values. As earlier mentioned, only positive frequencies are represented.

The starting point, at 1 Hz, is close to origin, and as the frequency increases the curve approaches the point (-1,0) which may cause instability. This plot does not appear as nice and smooth as those created on the basis of analytical expressions, such as transfer functions. As the plot is created of a series of sampled values, noise and other distortions may have been absorbed during the processing, giving a disorderly appearance of the curve.

The Nyquist stability criterion states that a system may get instable if the curve encloses the coordinates (-1,0). In this case the curve is rather approaching these coordinates as the frequency increases. From the plot it is not possible to read out any details about frequency, but above 70 Hz the curve is mainly located close to instability point.

Figure 6.14 presents a section of the Nyquist plot around the instability point. Now the lines have been removed, and markers are representing the ratio between source and load impedance at specific frequencies. In this plot one can clearly see that the instability point itself is not touched, although several markers are surrounding it. The marker closest to the instability point represents 400 Hz, which according Figure 6.9 and Figure 6.10 is not significant in either the voltage or current spectrums.

The closer the markers are to the instability point, the higher the probability for occurrence of instability. If any markers takes place at the exact coordinates of the instability point, the load voltage will in theory approach infinity if a signal is present at that specific frequency.

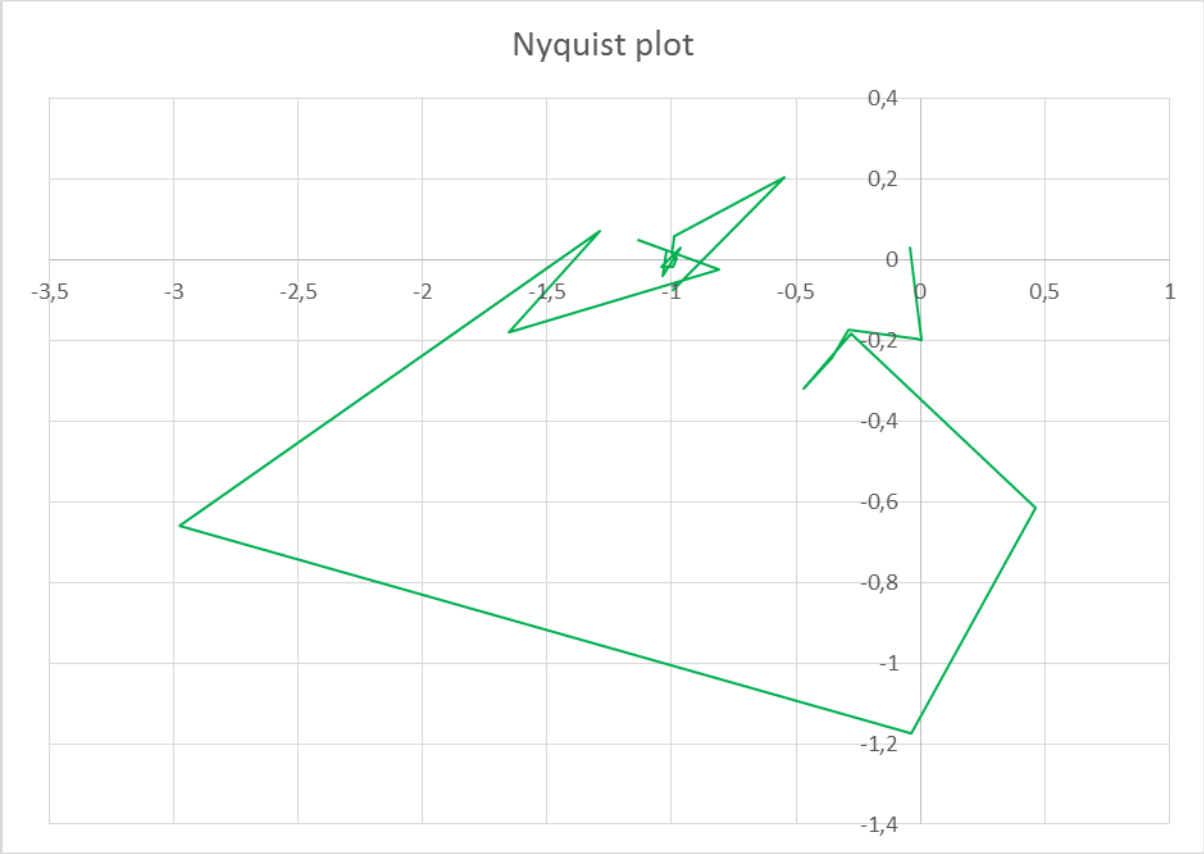

Figure 6.13: Nyquist plot for initial system state

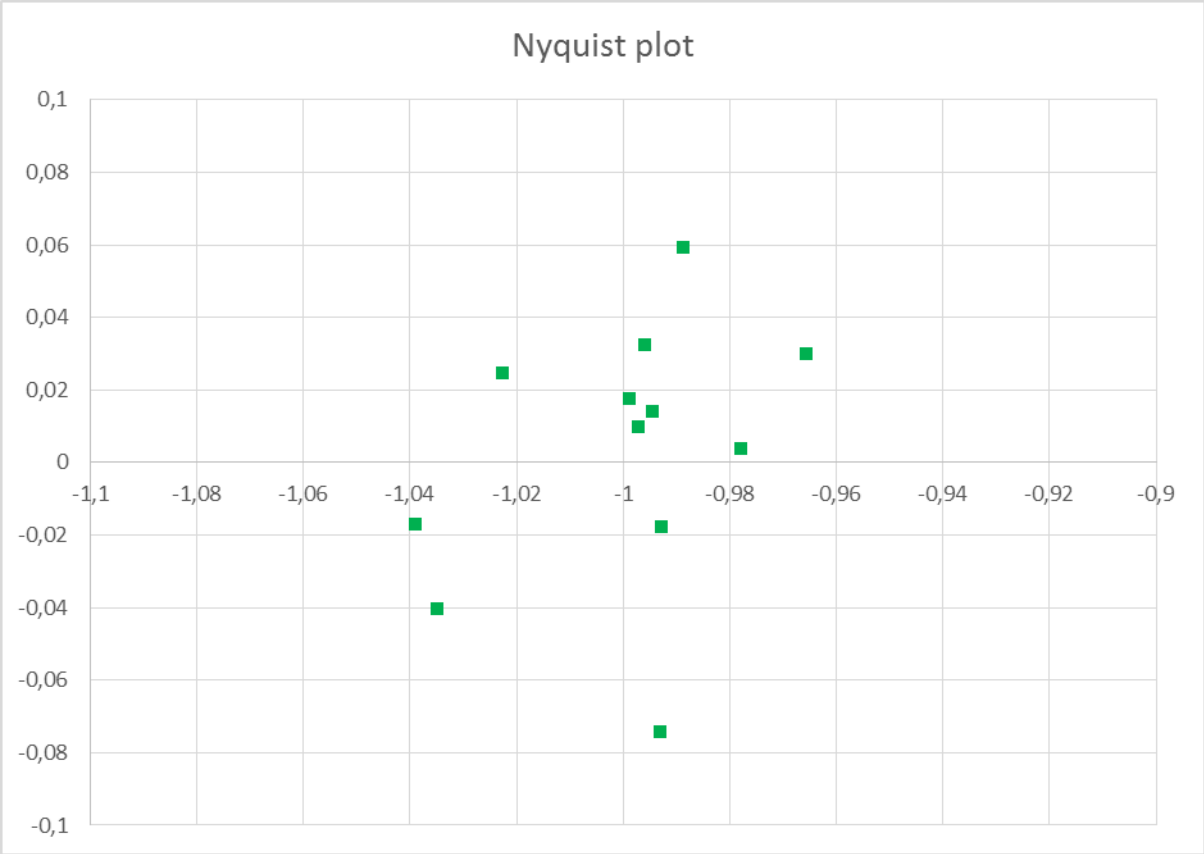

Figure 6.14: Nyquist plot for initial system state, highlighted around the instability point

6.3. Sensitivity results for rectifier

In this chapter, the rectifier control system's influence on the stability will be examined. The rectifier's load current control system has implemented both a voltage regulator and a current regulator. These regulators are of the type PI, thus there are parameters for proportional gain and integral time. There are then four parameters to investigate in the source subsystem load current control system.

6.3.1. Voltage regulator proportional gain

In this section the voltage regulator proportional gain's influence on the system stability will be analyzed. The gain is adjusted in turns, in the range between 0,5 and 2 times the reference value.

The proportional gain's influence on the magnitude of the harmonic impedance is demonstrated in Figure 6.15. It is clear that the gain affects the impedance, particularly at lower frequencies. From 100 Hz and above, the magnitude for all different gain parameters closes in on the same track. Again, this seems to be the point where the converter's influence on the impedance gets less significant. Below 100 Hz, it is difficult to see any patterns except that the difference between the curves is largest at low frequencies, and decreases with increasing frequency.

In Figure 6.16, the influence on phase angle is indicated. Particularly for the lowest frequencies, differences can be observed in the plot. As the frequency increases the differences get smaller, and the curves seems to be in accordance above 200 Hz. For some of the gain values, particularly $0{,}5 \cdot K_p^*$, the phase angle has a more spontaneous and fluctuating behavior compared to the reference curve.

The Nyquist plots for the five different gain values for the voltage regulator are shown in Figure 6.17. At first the plots may seem difficult to follow, and the differences observed in the bode plot seem to enhance when creating the Nyquist plots. What is clear, is that although the curves are dispersed, they all aim for the instability point as the frequency increases.

In Figure 6.18 the area around the instability point has been magnified. The lines have been removed, and markers are representing values at different frequencies. Again, markers close to the instability point indicate that instability is more likely to occur. It can be observed that markers representing $0{,}5 \cdot K_p^*$ and $2 \cdot K_p^*$ lie closer to the instability point than the reference. For the other gain values, the markers gather in the same area above the instability point.

The markers closest to the instability point represent 100 Hz for $0{,}5 \cdot K_p^*$, and 300 Hz for $2 \cdot K_p^*$. In general, on would want the markers close to the instability point to represent the frequencies where no signal is present. In most cases that will imply higher frequencies where harmonic voltages or currents are often small or non-existing.

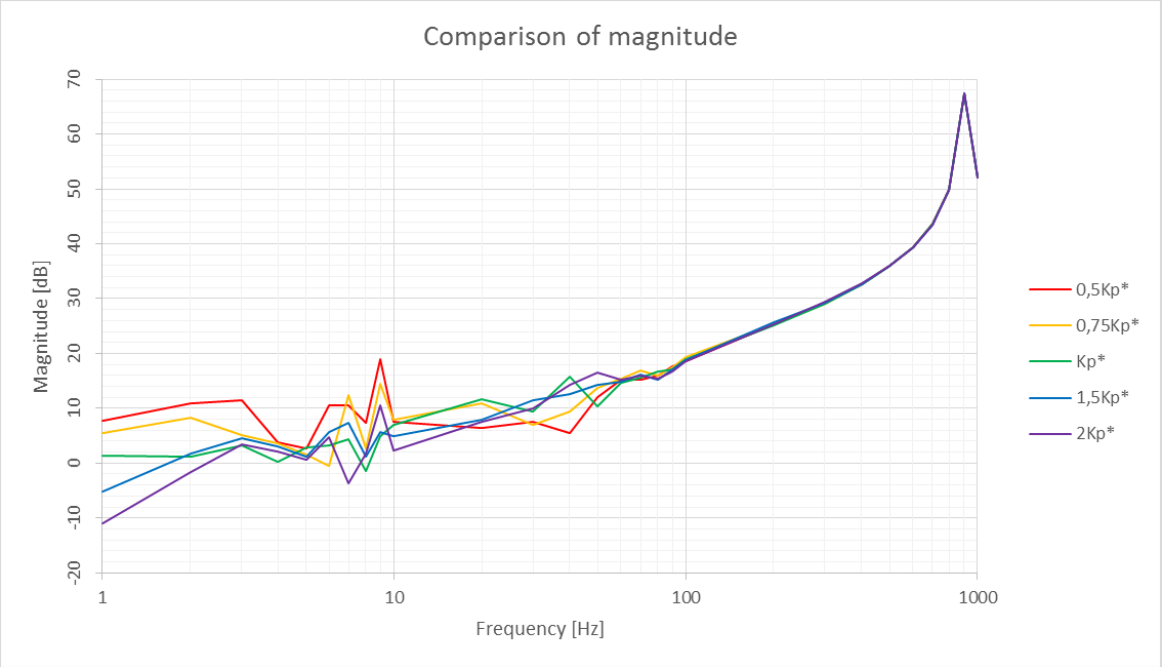

Figure 6.15: Influence on impedance magnitude from voltage regulator proportional gain

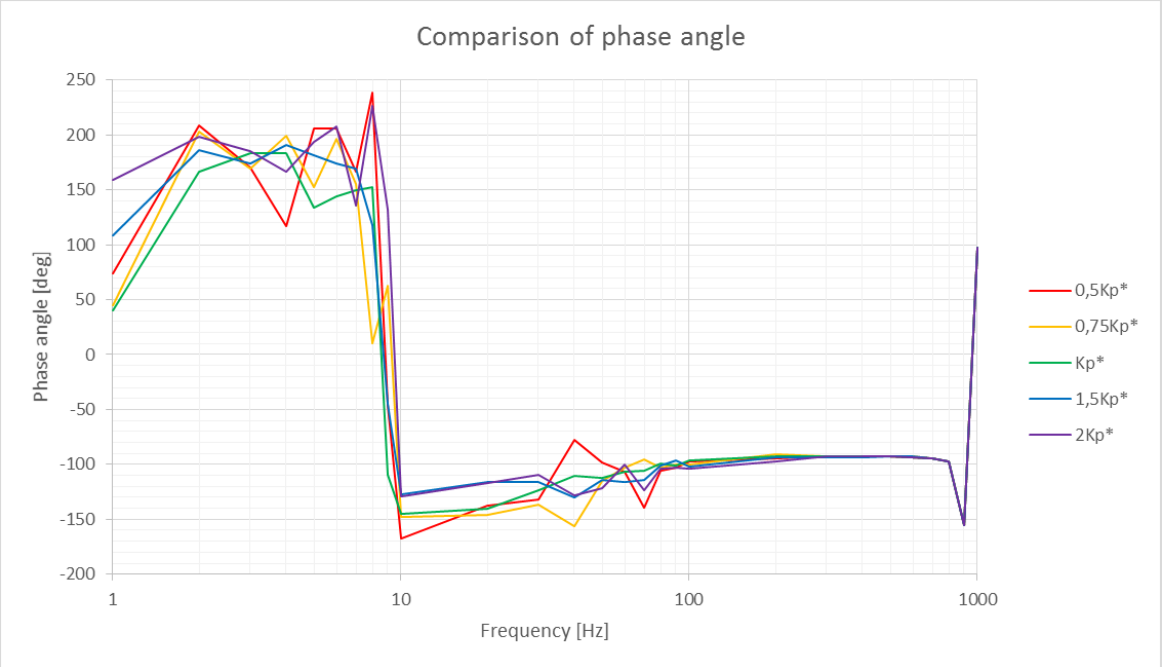

Figure 6.16: Influence on impedance phase angle from voltage regulator proportional gain

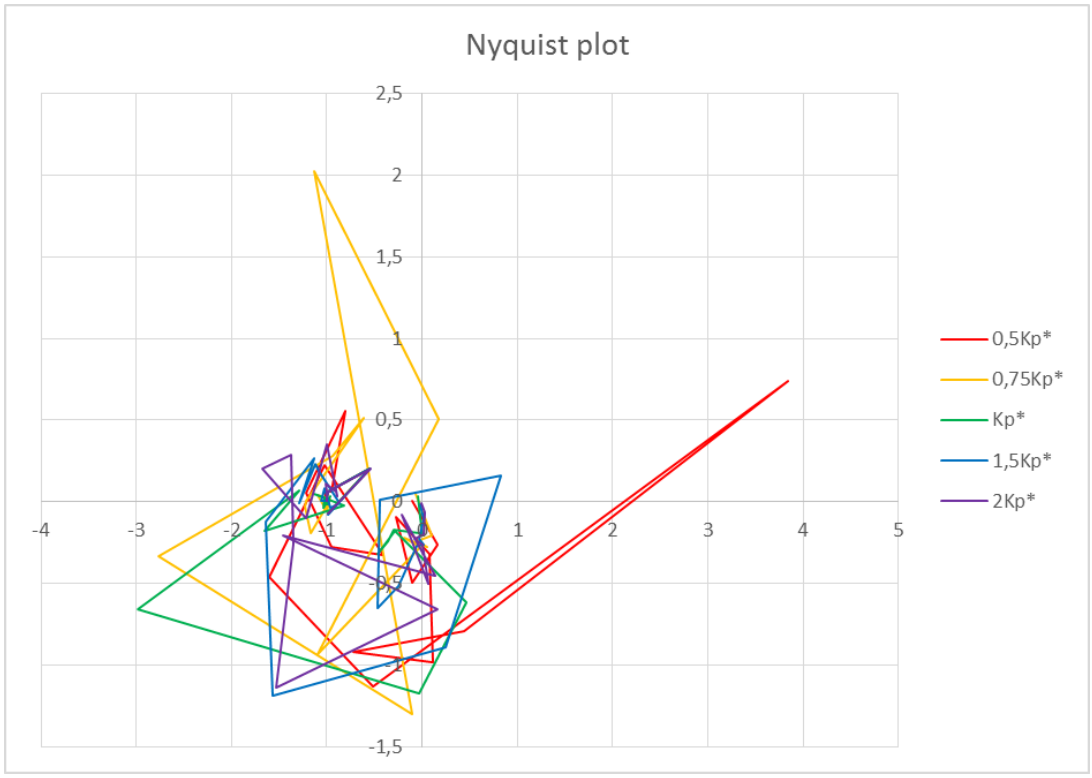

Figure 6.17: Influence on Nyquist plot from voltage regulator proportional gain

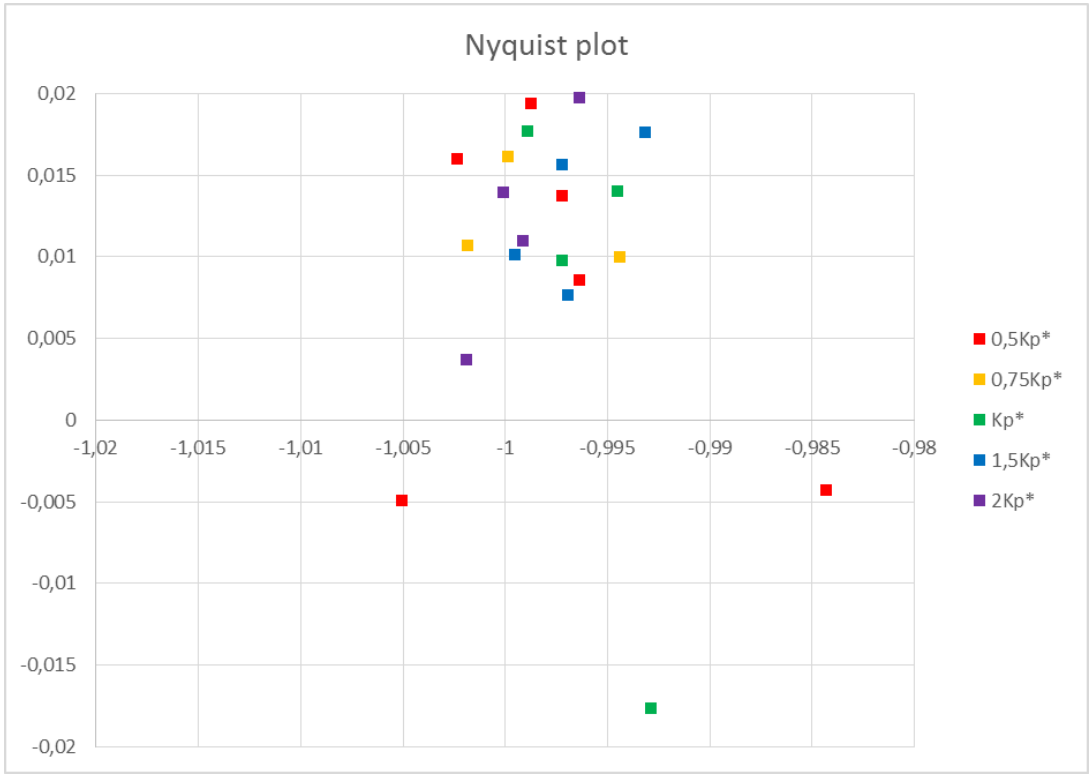

Figure 6.18: Influence on Nyquist plot from voltage regulator proportional gain, highlighted around the instability point

6.3.2. Voltage regulator integral time

Now the voltage regulator's integral time will be investigated. The integral time's influence on the impedance magnitude is presented in Figure 6.19, and at first glance the difference between the curves appear smaller compared to Figure 6.15. This means that changes in the proportional gain influence the impedance more than changes in the integral time. At most, the difference between the curves is around 10 dB. Statistical methods for calculating the deviation for each curve with regards to the reference curve might be applied for accurate analysis. Such methods will however be quite time consuming, and is regarded outside the scope of this work.

Also the phase angle, indicated in Figure 6.20, proves to be less affected by changes in integral time compared to proportional gain. Particularly for the lowest frequencies the curves appear to be more gathered, and the largest deviations occur between 5 and 10 Hz.

The Nyquist plots created by adjusting the integral time are shown in Figure 6.21. The curves appear to be more similar now, and they are easier to follow than on the previous plot showing the influence by proportional gain. Also in this plot all curves are approaching the instability point at high frequencies.

The zoomed Nyquist plot, presented in Figure 6.22, gives a clearer picture around the instability point. For this case no integral time values stands out as more likely to cause instability than any other, although the marker closest to the instability point represents two times the reference value, and a frequency of 400 Hz.

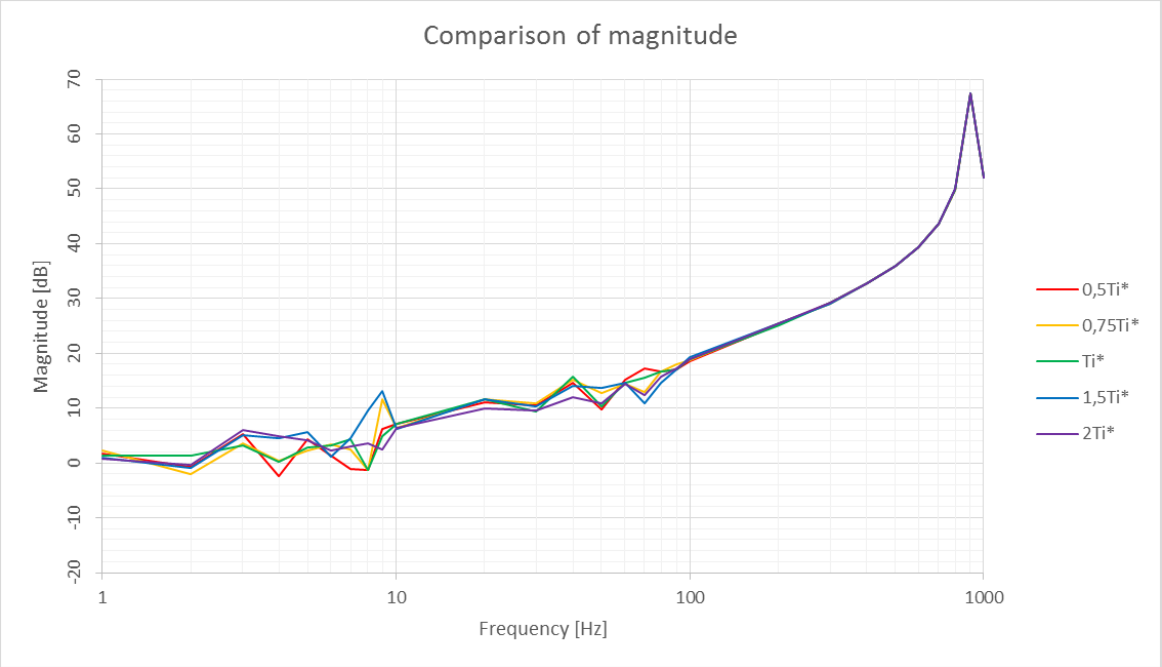

Figure 6.19: Influence on impedance magnitude from voltage regulator integral time

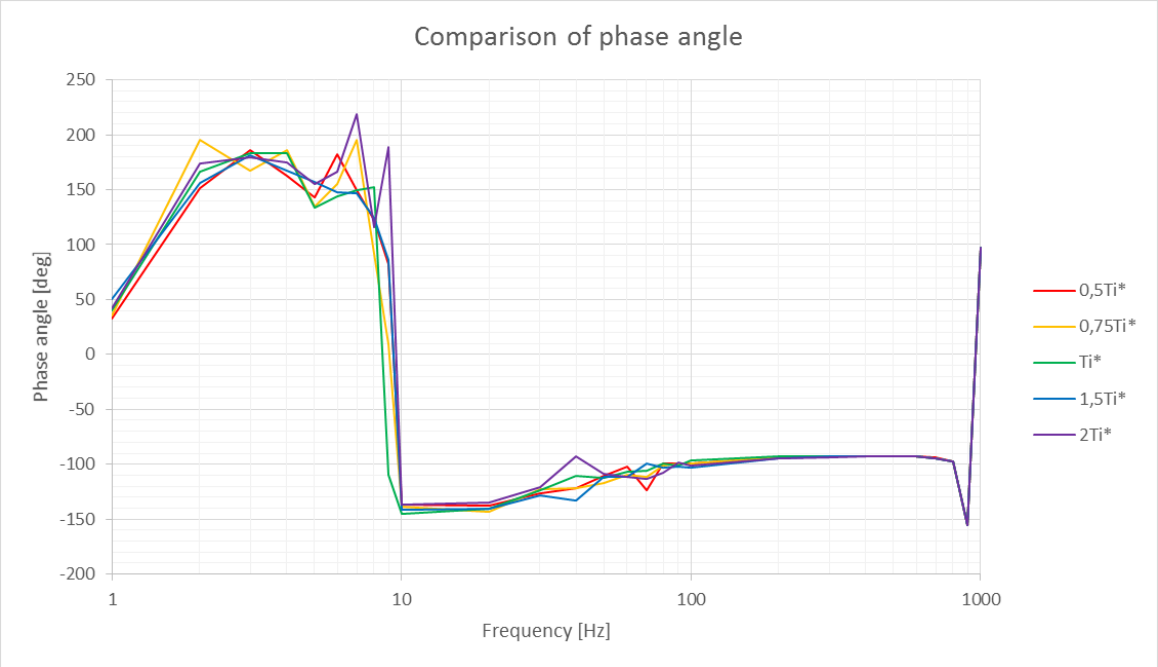

Figure 6.20: Influence on impedance phase angle from voltage regulator integral time

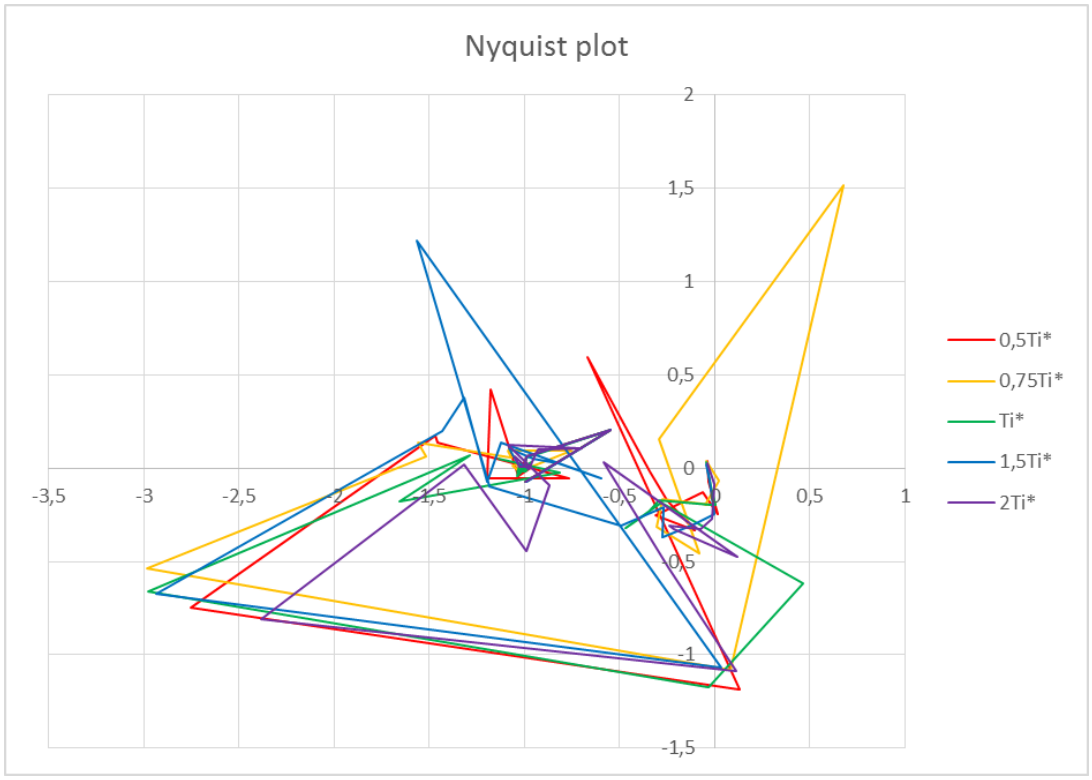

Figure 6.21: Influence on Nyquist plot from voltage regulator integral time

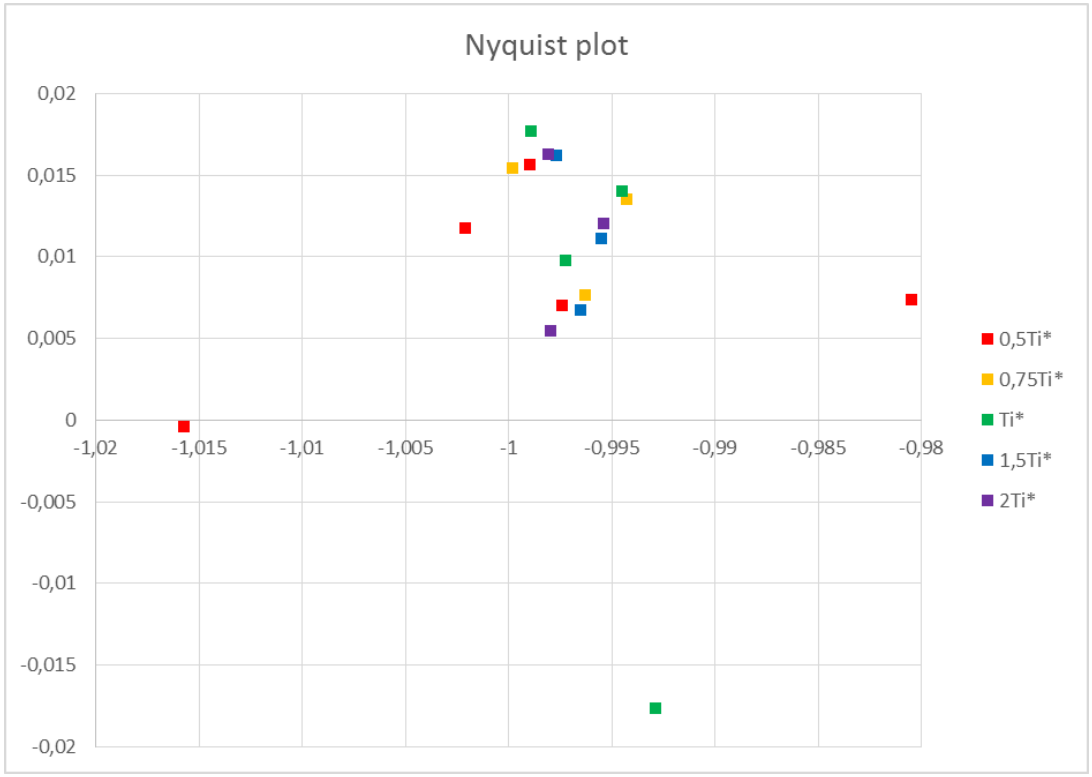

Figure 6.22: Influence on Nyquist plot from voltage regulator integral time, highlighted around the instability point

6.3.3. Current regulator proportional gain

In this section the current regulator in the rectifier will be subject to sensitivity analysis. The comparison of impedance magnitude for different values of gain is shown in Figure 6.23. As the gain is adjusted, it is clear that the impedance magnitude is affected, and again the largest differences occur on low frequencies. The same phenomena as seen before is also observable here, where the regulator's influence on the impedance ends around 100 Hz.

Also the phase angle of the impedance, presented in Figure 6.24, demonstrates a significant influence from the proportional gain on low frequencies. The difference on 1 Hz is so large that it is likely to believe is caused by noise. In this plot it can also be observed that differences in phase angle exist up to 300 Hz.

As large differences appeared in the bode plot, the Nyquist plot can be expected to show differences between curves, at least for low frequencies. The Nyquist plots for different values of gain is presented in Figure 6.25, and as expected some differences are seen, although they gather around the instability point as the frequency increase.

Around the instability point, demonstrated in Figure 6.26, it can be observed that $0{,}75 \cdot K_p^*$ and $2 \cdot K_p^*$ have corresponding values close to the instability point. This might indicate increased probability for instability with these parameters.

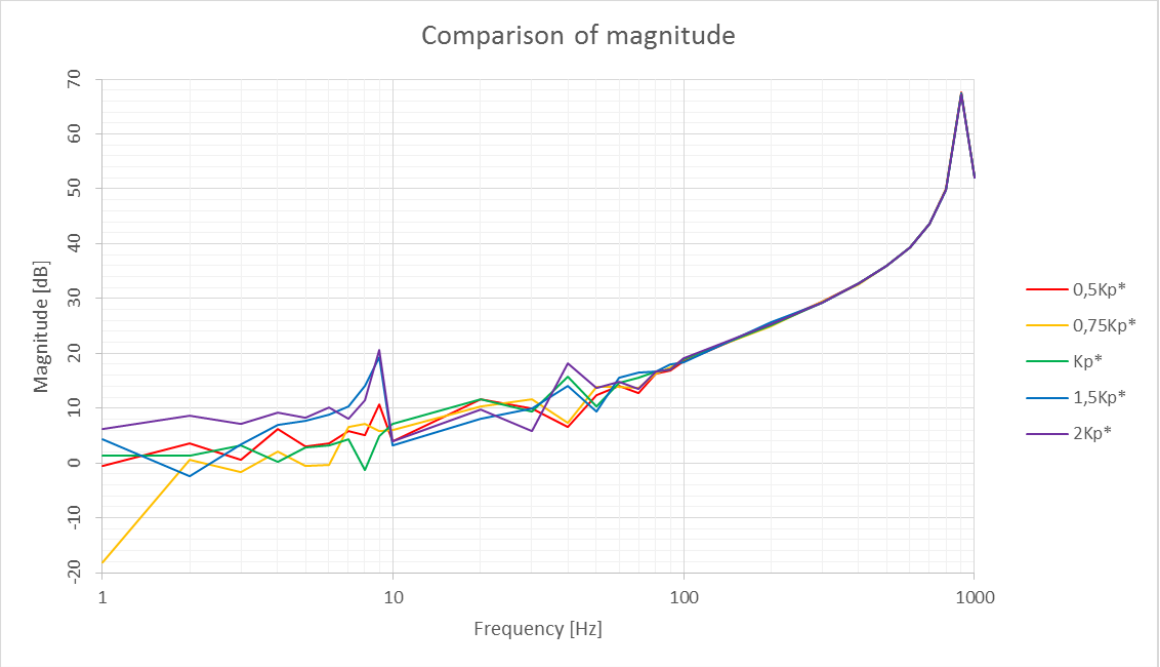

Figure 6.23: Influence on impedance magnitude from current regulator proportional gain

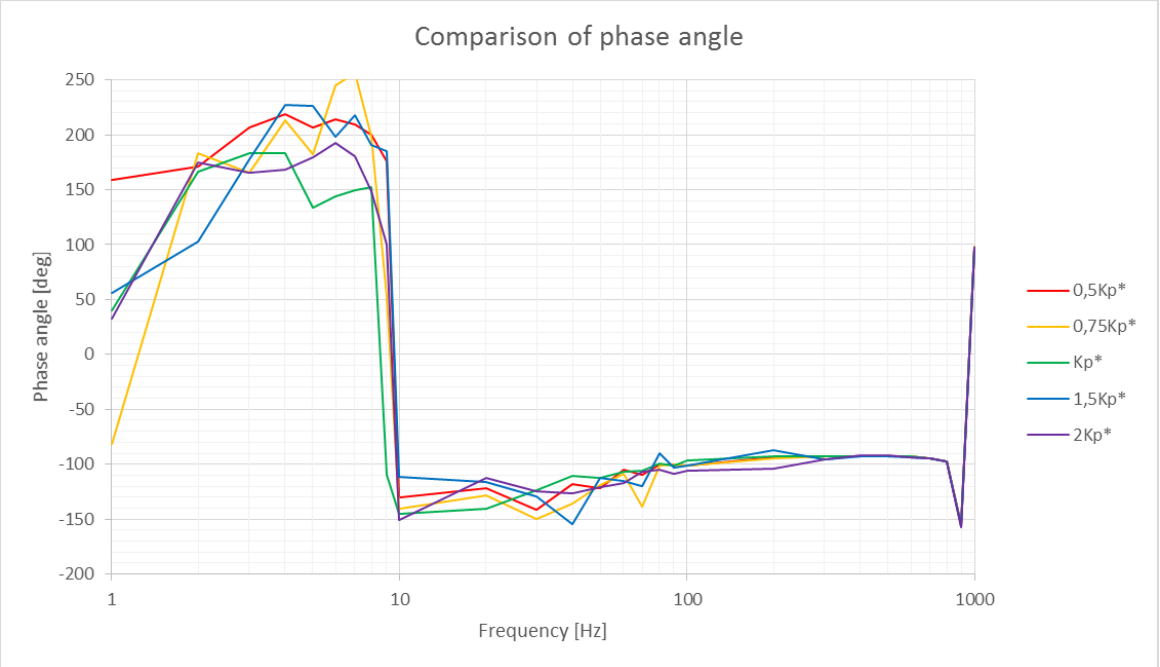

Figure 6.24: Influence on impedance phase angle from current regulator proportional gain

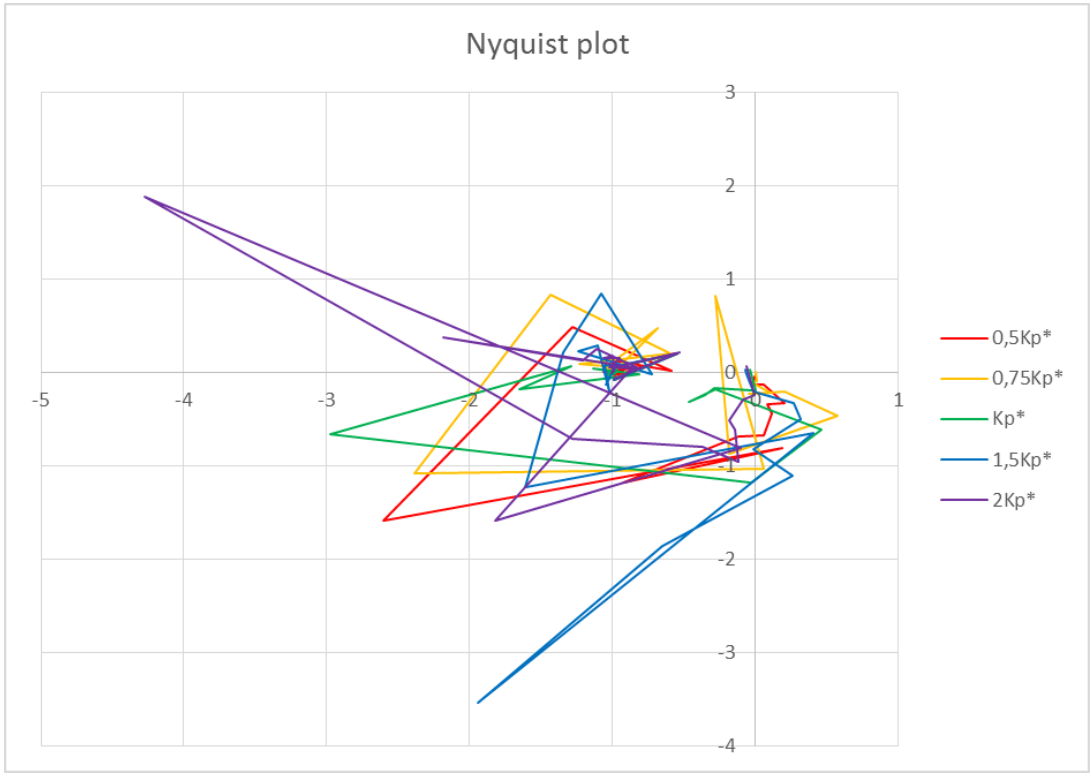

Figure 6.25: Influence on Nyquist plot from current regulator proportional gain

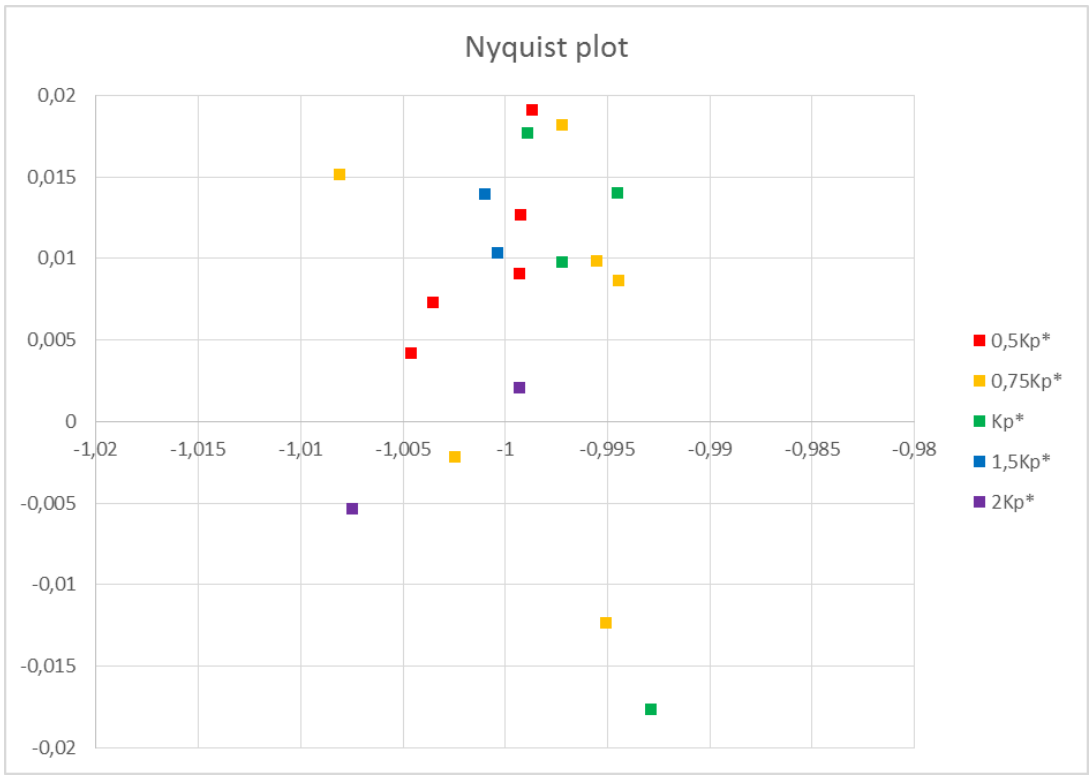

Figure 6.26: Influence on Nyquist plot from current regulator proportional gain, highlighted around the instability point

6.3.4. Current regulator integral time

The current regulator integral time's influence on the impedance magnitude and phase angle can be seen in Figure 6.27 and Figure 6.28, respectively. The observations are quite similar to the ones seen on earlier simulation results, with differences in the curves up to 100 Hz.

A few observations stand out, particularly for $1{,}5 \cdot T_i^*$ where both magnitude and phase angle show a significant drop at 6 Hz. It is however uncertain if this is due to a resonance point or caused by noise.

In Figure 6.29 the Nyquist plot for different values of integral time is presented, while a magnified area around the instability point can be seen in Figure 6.30.

In this case, none of the tried parameter values seem to stand out as clearly instable. The integral time that is most likely cause instability, according to the Nyquist plot, is $1{,}5 \cdot T_i^*$. For $0{,}5 \cdot T_i^*$, the markers are placed further away from the instability point than the reference markers, which may indicate a slightly more stable parameter value for the system.

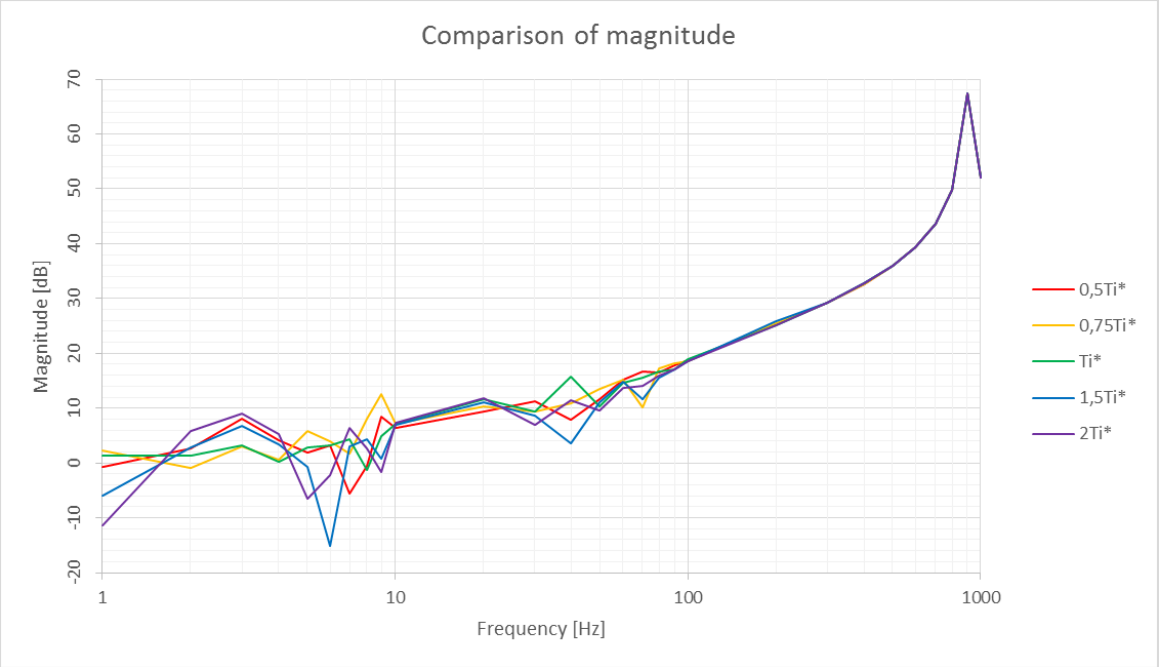

Figure 6.27: Influence on impedance magnitude from current regulator integral time

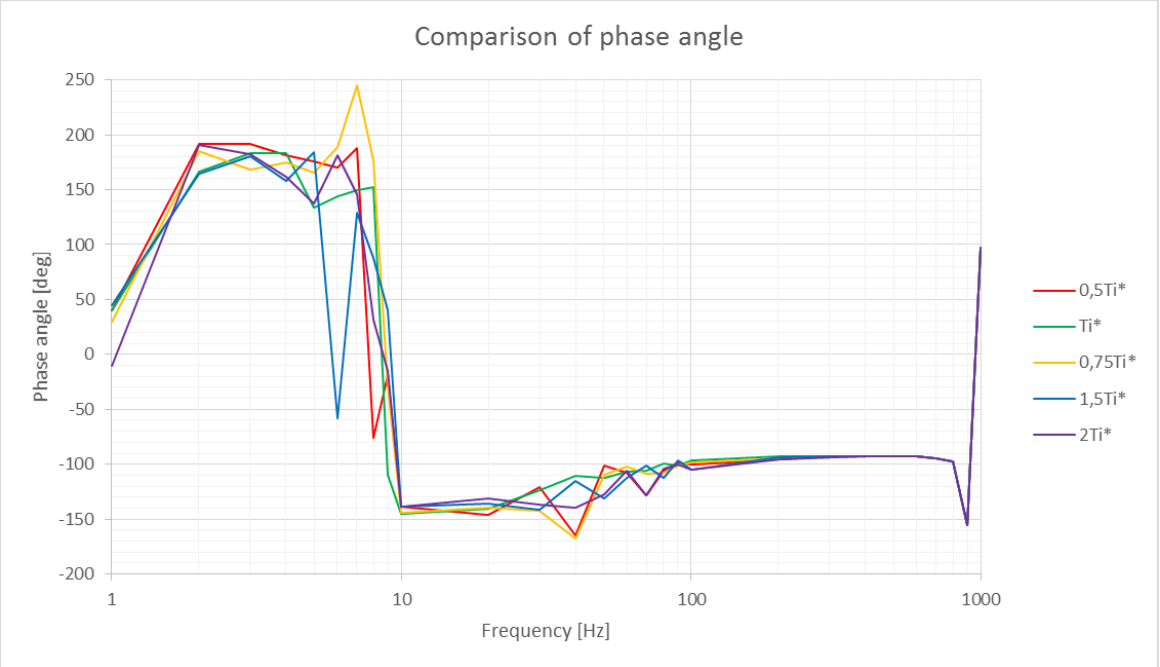

Figure 6.28: Influence on impedance phase angle from current regulator integral time

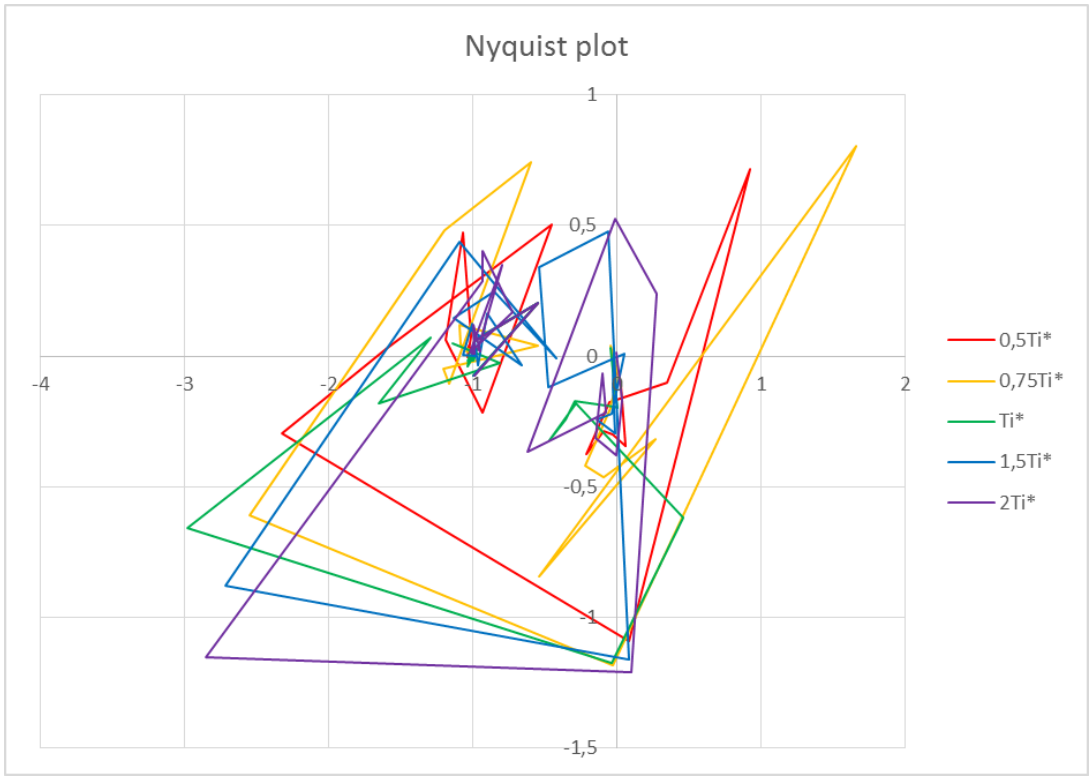

Figure 6.29: Influence on Nyquist plot from current regulator integral time

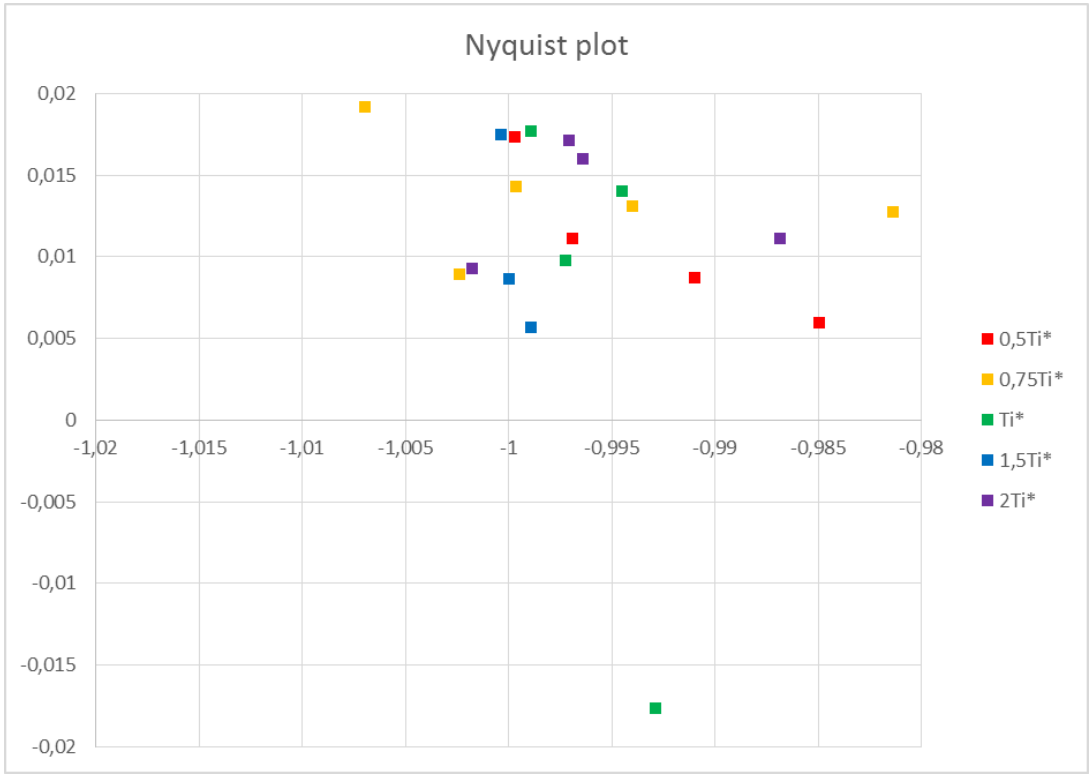

Figure 6.30: Influence on Nyquist plot from current regulator integral time, highlighted around the instability point

6.4. Sensitivity results for inverter

In this section the influence on stability from the inverter's control system will be examined. The control system in the inverter contains only a current regulator, and therefore holds fewer parameters to adjust.

6.4.1. Current regulator proportional gain

The first parameter to investigate is the proportional gain, and the impedance magnitude difference caused by the gain parameter is presented in Figure 6.31. It is interesting to observe that the different values for the gain do not seem to influence the impedance magnitude at all. The five curves follow each other in the whole frequency range, and no differences between the curves can be seen. If the results are due to weaknesses with the voltage injection method, or if the regulator gain is really not affecting the impedance is unclear at this point.

The phase angle, presented in Figure 6.32, shows similar characteristics as the magnitude. All curves are stacked upon each other, and the differences between them are small. To ensure correctness of the bode plots, more simulation with other regulator parameters could be performed.

In Figure 6.33 the Nyquist plot for this case is presented. It is possible to see differences in the curves on lower frequencies, although they are quite small. As the frequency increases the differences decreases, and for high frequencies all curves follow each other.

This is also pointed out in Figure 6.34, where the instability point is highlighted. For all the simulated values of gain, the markers around the instability point falls in the exactly same spots. Thus, there will be no significant difference in stability conditions for the different gain parameters.

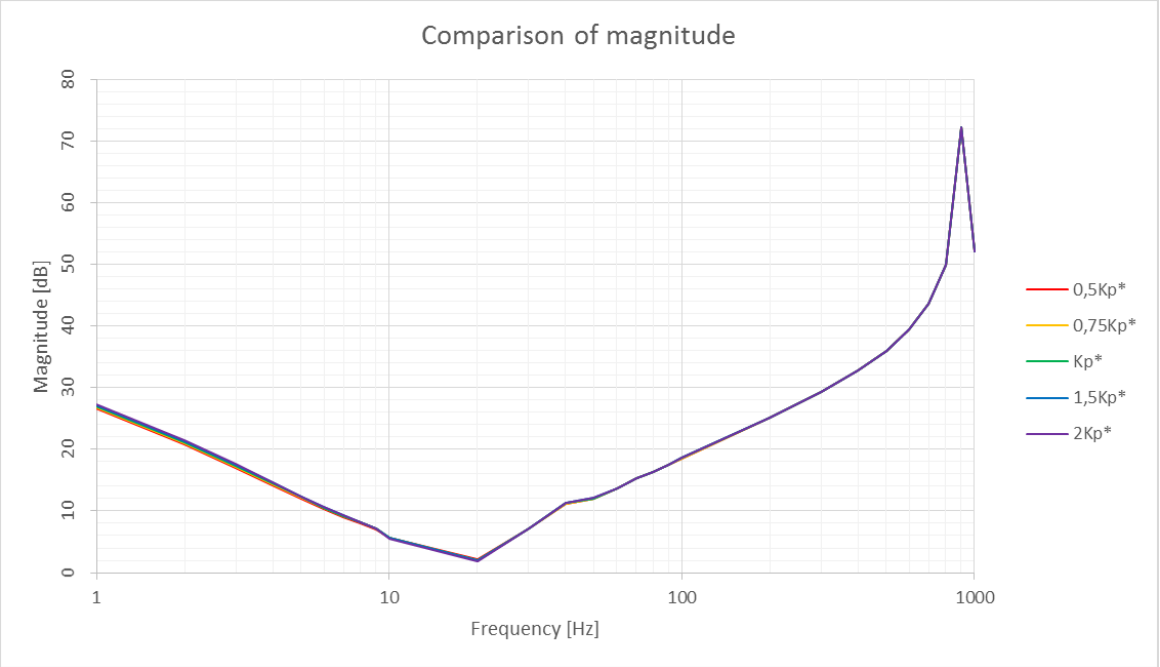

Figure 6.31: Influence on impedance magnitude from current regulator proportional gain

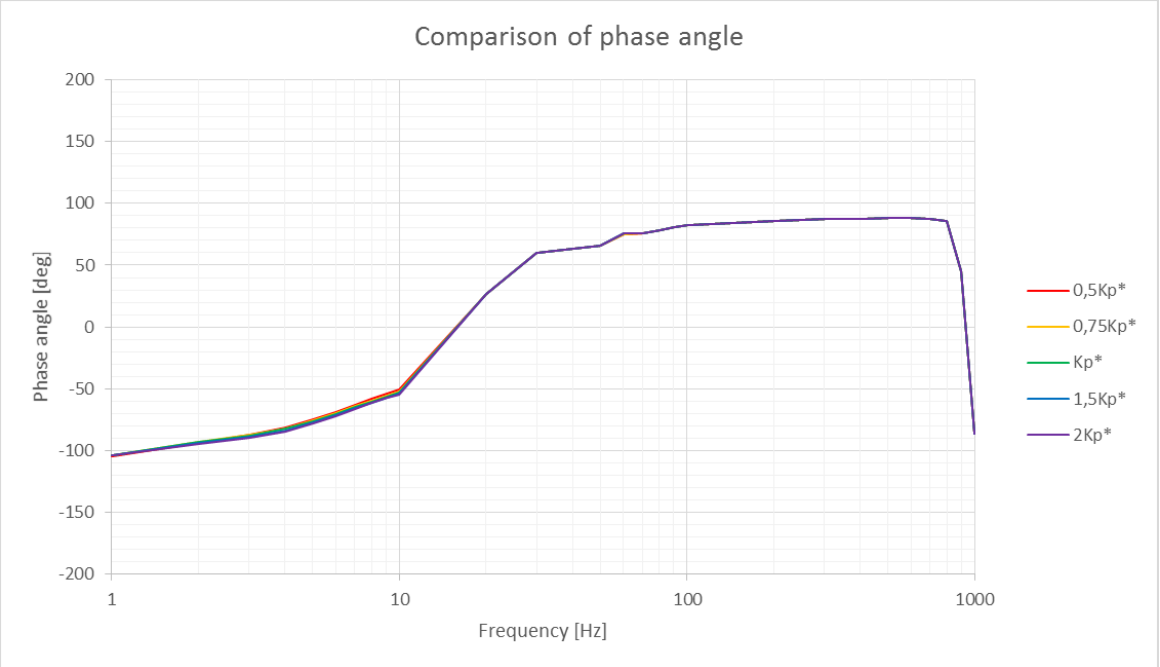

Figure 6.32: Influence on impedance phase angle from current regulator proportional gain

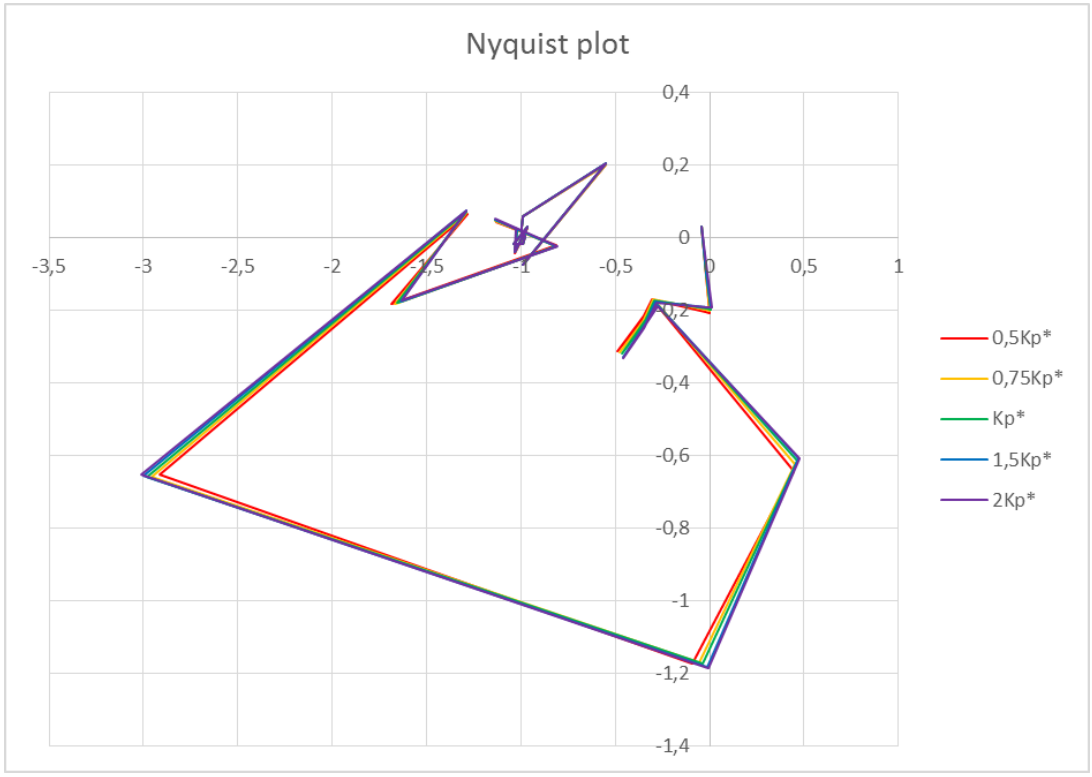

Figure 6.33: Influence on Nyquist plot from current regulator proportional gain

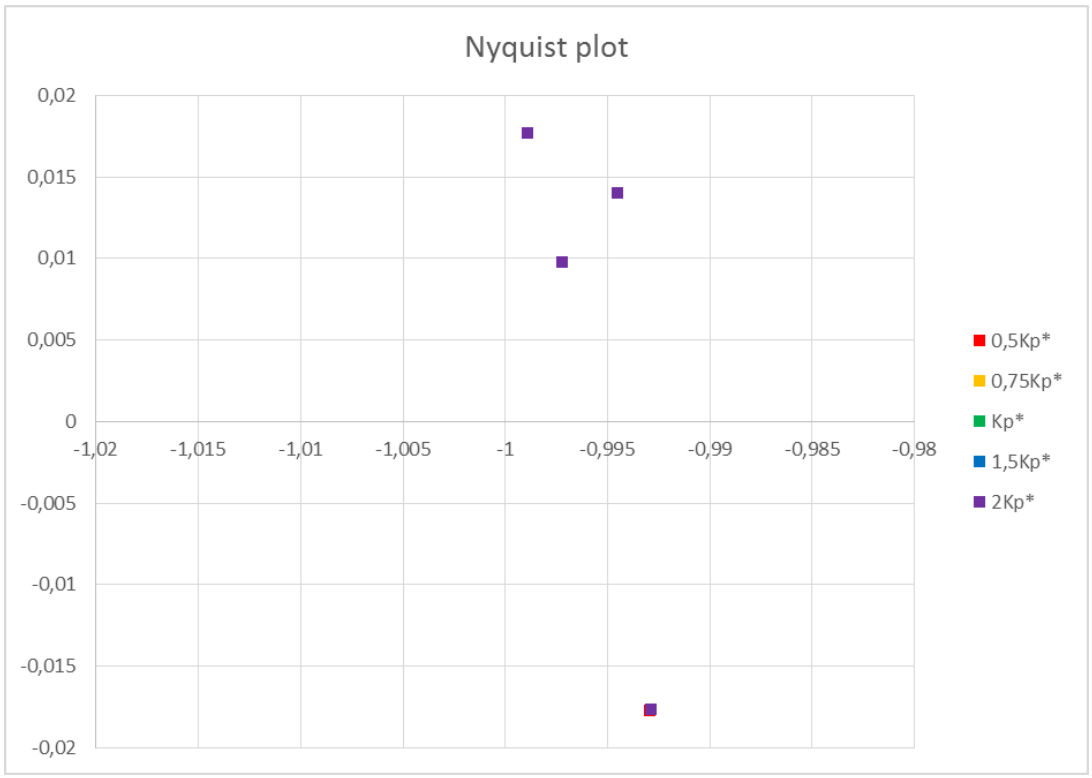

Figure 6.34: Influence on Nyquist plot from current regulator proportional gain, highlighted around the instability point

6.4.2. Current regulator integral time

The last simulations to be performed are related to the current controller's integral time in the inverter. As seen in Figure 6.35 and Figure 6.36, where the harmonic impedance is presented, the impedance is to a small extent under the influence of integral time. Only at the bottommost frequencies can any differences be spotted.

Also the Nyquist plots, presented in Figure 6.37 and Figure 6.38, show an almost absent influence by integral time. The same results were seen in the simulation results regarding the proportional gain for the inverter. This may indicate either that the method involving voltage injection is unsuitable for such analysis, or that the impedance is actually not affected by the PI regulator in the inverter's control system.

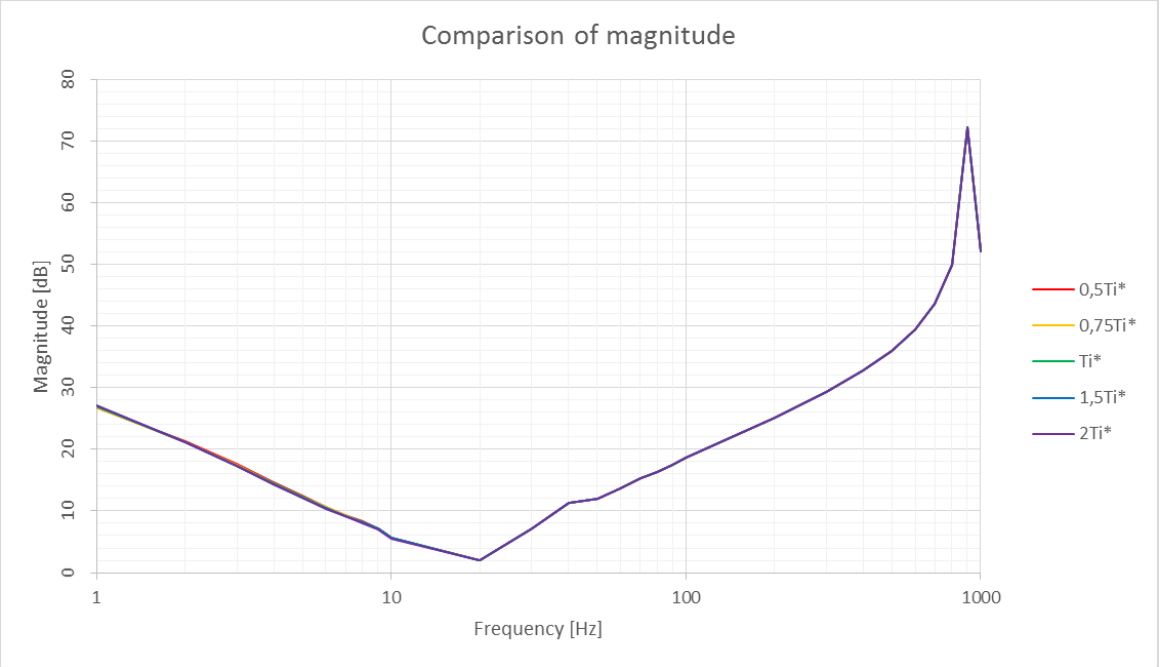

Figure 6.35: Influence on impedance magnitude from current regulator integral time

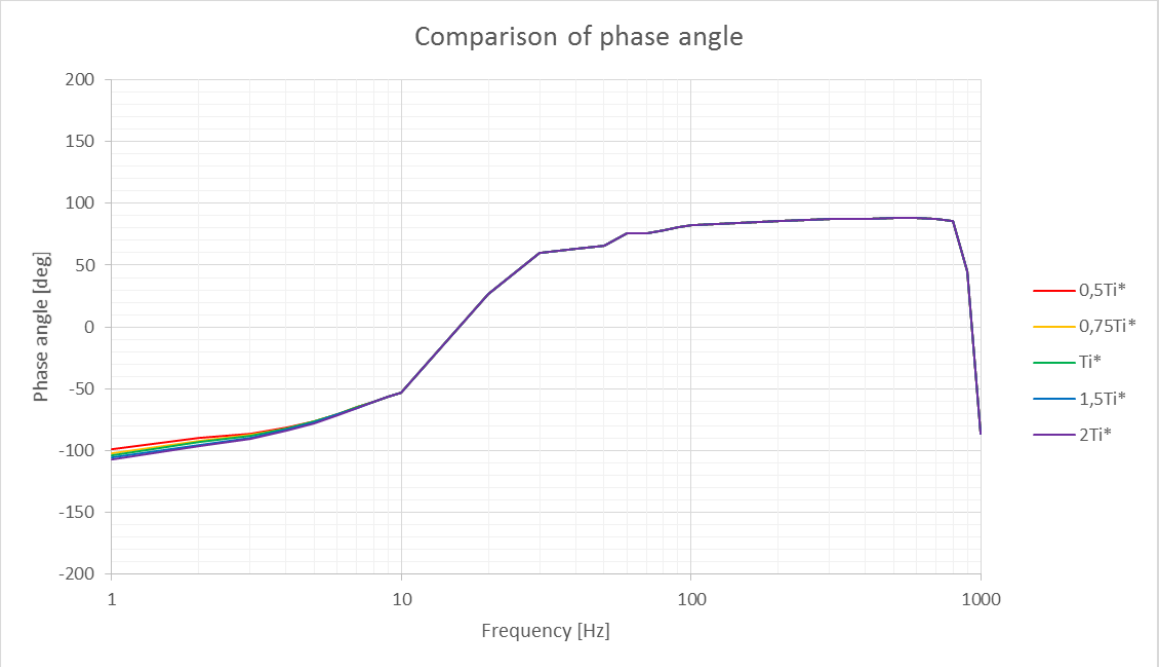

Figure 6.36: Influence on impedance phase angle from current regulator integral time

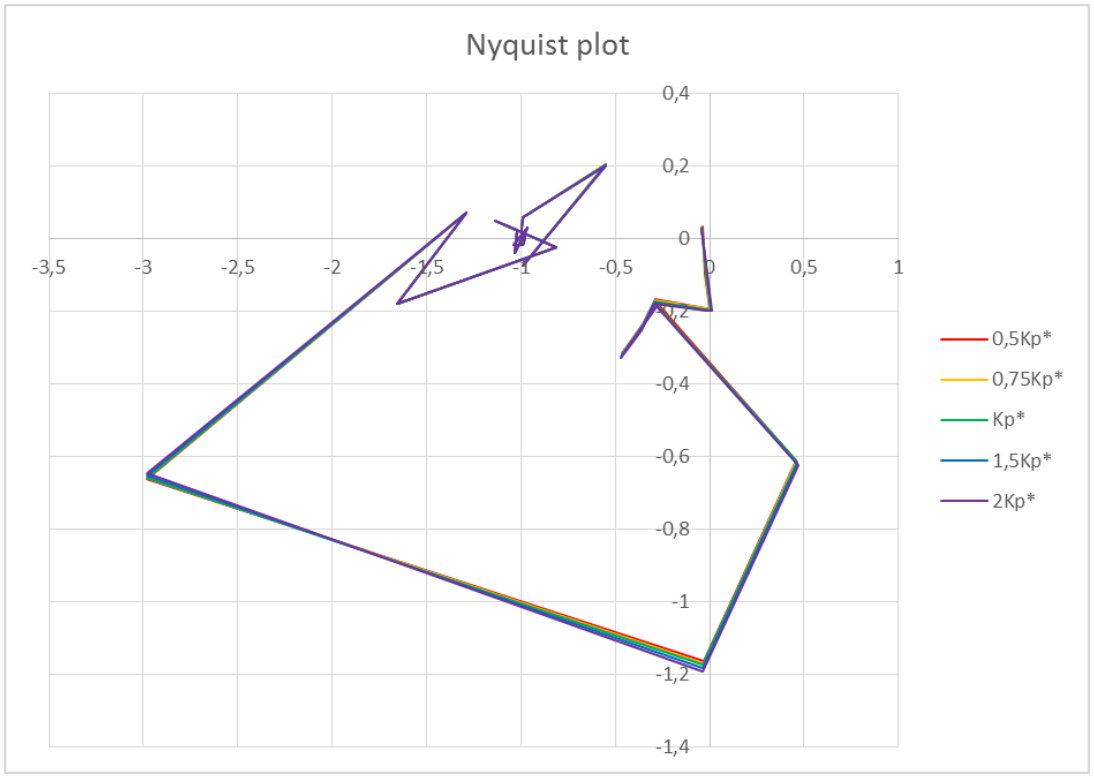

Figure 6.37: Influence on Nyquist plot from current regulator integral time

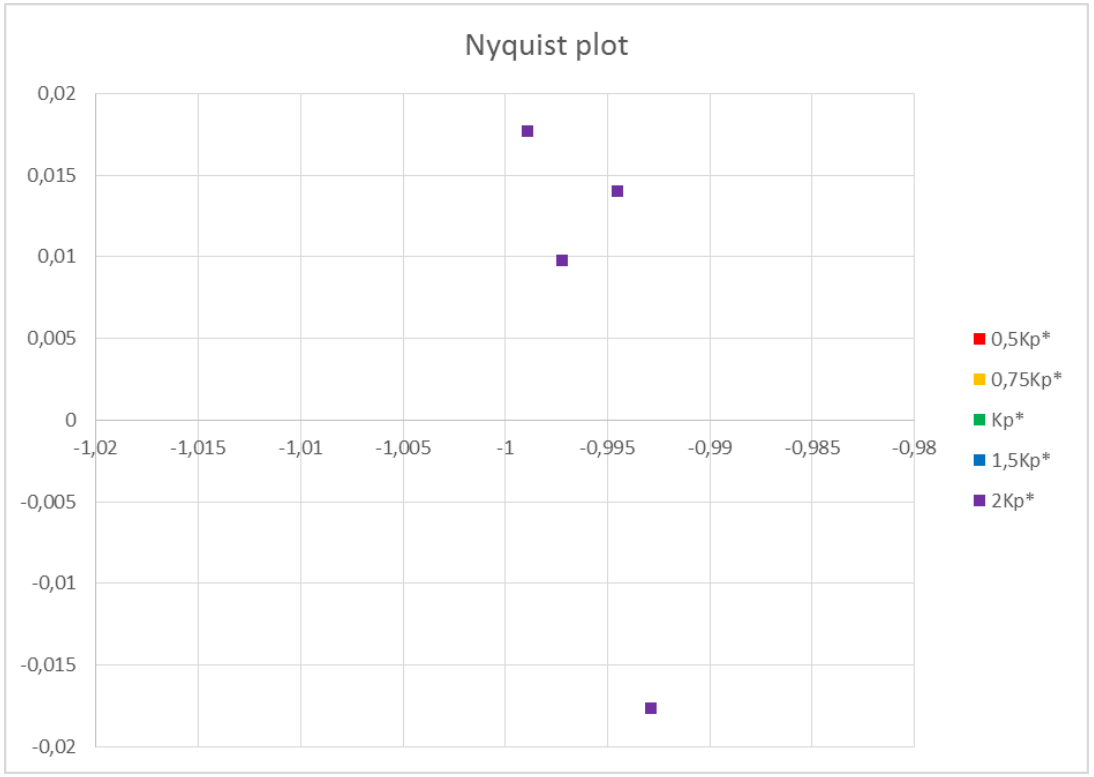

Figure 6.38: Influence on Nyquist plot from current regulator integral time, highlighted around the instability point

Chapter 7 Discussion

7.1. The method

In this report, a method for determining the stability in a HVDC system is explained and applied. This method turns out to be a powerful tool for performing sensitivity analysis of the control system, but applications for other parts of the power system should not be excluded.

As the concept is to perform sensitivity analysis, where a series of experiments are performed by adjusting a parameter value, the most stable setting can be determined by graphical interpretation in terms of a Nyquist plot. This tool can then be applied to every component or parameter in a HVDC system to find values that give the most stable conditions.

The proposed method involves obtaining the harmonic impedance in a system by using frequency response analysis. The approach of the method has been to inject either voltage or current into the system, measure the system's response to the injections, and calculate the impedance at the frequency of the injected signal. By running several experiments in a series, where the frequency of the injected signal increases for each run, the harmonic impedance has been obtained for a desired frequency range.

In this work, the tool is utilized to carry out stability investigations in a HVDC system based on the latest generation of converter technology. A model of such a system has been developed in MATLAB/Simulink, which constitutes the basis for all simulations. As the MMCs uses a very sophisticated control system to ensure correct operation, using analytical expressions to obtain the harmonic impedance of this system would have been a demanding task. By using the proposed method, the harmonic impedance can be obtained for large and complex systems by doing dynamical experiments, which is rather convenient. However, for very large and complicated models, the simulations can take several hours to perform.

As the Nyquist stability criterion was to be used for stability interpretations, the HVDC system had to be partitioned into two subsystems. It was decided to split the model in the middle of the DC line, as this created two nearly identical subsystems, where the only difference is the operation of the converters. For finding the harmonic impedance of each subsystem, two different techniques have been used.

A model of the source subsystem has been created, where the load is replaced by a DC current source. For finding the harmonic impedance, a perturbation current source was placed in parallel with the DC current source. The perturbation signals were then injected at the same time as the DC current source was producing the load current. During this operation, no active power was actually transmitted into the load subsystem, but the current flow was the same as during normal operation. The rectifier was now controlling the DC voltage, which was measured and used to calculate the impedance. To ensure accuracy during the calculation

process, DFT was used to extract the correct frequency components from both the current and voltage signals.

For the load subsystem model, the source was replaced by a DC voltage source with a perturbation voltage source in series. The inverter was in this situation controlling the DC current, and the procedure for calculating the impedance was the same as mentioned above.

The resulting impedance obtained from the proposed method is actually the one seen from the middle of the DC line and outwards to the AC grids on each side. The fact that the DC line is composed of two poles makes the method very easy and convenient to use, as each subsystem is represented as only one impedance. It would be difficult to imagine the impedance seen the other way, from the AC grid towards the middle of the DC link. One problem will be the three-phase representation of the AC side, which would cause three impedances to be taken into consideration for each subsystem. Another problem would be how to represent the DC link at the midsection, where the two subsystems meet. Also applications of this method to a pure three-phase system would have been more complicated, because of the increased amount of impedances to take into consideration

7.2. Harmonic impedance

Preliminary simulations have been run to ensure the most credible results for harmonic impedance. Both simulation time length and injected signal amplitude have been investigated. These parameters were first tested for the source subsystem, which showed large influence of both simulation parameters. It is still unclear why these parameters are affecting the impedance, and more work is required for better answers. The parameters giving the most likely result, with least variation and spontaneity, was chosen. These values are 1,0 second of simulation time and an injected perturbation current amplitude of 20 % of the DC current. The load subsystem, where voltage injection is used, showed no influence of injected perturbation voltage amplitude.

Ragarding the source subsystem, the different regulator parameter values clearly affected the harmonic impedance. The influence is most significant on lower frequencies, and above 300 Hz the control system shows very little influence on harmonic impedance. This means that the converter is only significant at low frequencies, while the passive components in the system dominate as the frequency increases. The harmonic impedance magnitude of both source and load subsystem is the same at high frequency, this comes as no surprise as the two subsystems are symmetrical except from the control systems.

Voltage injection, used for finding the load subsystem impedance, has caused a lot of thinking as the bode plots show almost no influence from the control system. In the inverter's control system only a current regulator is implemented, and while this regulator shows great significance on the impedance in the rectifier, the load subsystem impedance shows no difference when adjusting the parameters for this regulator. As the load subsystem impedance has shown no affection by either injected perturbation voltage amplitude or control system parameters, it might be the method that is not functioning correctly. However, as the obtained

impedance magnitude above 100 Hz was the same as the one obtained for current injection, the results are assumed to be correct at high frequencies.

More work should be carried out to solve the uncertainty with voltage and current injection. It would have been a great advantage to compare the harmonic impedance obtained from simulations with the analytically correct harmonic impedance. To ensure accurate sensitivity analysis results based on interpretation of the Nyquist plot, veritable results for harmonic impedance are crucial.

An interesting and important discovery is the frequency range where the converters are able to affect the impedance. This frequency range is found to be up to 100 Hz, and in some cases up to 300 Hz. Above these frequencies the converters will have very little significance, and mainly the passive power system components are determining the impedance.

7.3. Sensitivity analysis

The Nyquist stability criterion is applied to determine the stability conditions in the system. By running several simulations in series, where the regulator parameter values are changed for each run, the Nyquist plots indicate how the stability conditions in the system have changed.

For the initial state the system is actually quite vulnerable, as the ratio between source and load impedance is close to -1 at several frequencies. In general, a system is or can be instable if the coordinates (-1,0) is encircled in the Nyquist plot. Regarding this system, it is easier to see that the curve is actually aiming for the instability point as the frequency increases. If a signal is present on a frequency represented at the exact coordinates of the instability point, either current or voltage will in theory approach infinity.

It was chosen to plot all the curves obtained from each regulator in the same Nyquist plot to visualize the differences. This, however, made the plot difficult to read as the curves had very different ways towards the instability point. The plot then became quite chaotic, and did not show any marginal increase or decrease in stability conditions. In addition to the full Nyquist plots, a section of the plot, around the instability point, was magnified and the lines were removed. In this way the main concern of the plot is highlighted, and only markers representing the ration between source and load impedance is present. This is also a common strategy for sensitivity analysis, where several experiments are done in a series and the different results are plotted in a scatter plot.

In general, the proportional gain seems to have a larger influence on the Nyquist plots than the integral time. However, only five different values for each parameter has been simulated, and more simulations with smaller parameter value steps could give a clearer picture of the change in stability.

Concerning the rectifier's control system, the changes in proportional gain for both regulators seem to increase the probability for instability to occur. This also applies for the integral time, where the reference values seem to have markers furthest away from the instability point, but the differences seen in the Nyquist plots are smaller when the integral time is adjusted.

The sensitivity analysis performed for the inverter suffer from the very small differences found in the harmonic impedance when adjusting the regulator settings. At low frequencies it is actually possible to see differences between the curves in the Nyquist plot, which was not easily spotted in the bode plots. However, when the frequency increases the differences fade out, and around the instability point it is not possible to observe any differences. In the meantime one can say that the current regulator in the inverter is affecting the harmonic impedance, thus also stability in the system, but to a very small extent. The step change in the parameter values that was done during the simulations was clearly not enough to influence the occurrence of the Nyquist plot around the instability point.

A conclusion that can be drawn with a high degree of accuracy is that there do not exist a tuning for the control systems that do not lead to instability concerns according to the Nyquist plots. The converters have been found to be significant only at frequencies below 300 Hz, and the Nyquist plots show representation of values close to the instability point above this frequency. To avoid any probability of instability to occur, it is desirable to have no frequencies represented inside a circle with a radius of 0,5 placed at the instability point. Therefore, in order to guarantee stable operating conditions, the design of the power system itself must be changed.

Conclusion

The method described in this report for performing analysis of the stability in a HVDC system proves to be a powerful tool for sensitivity analysis.

The results from current injection show that the harmonic impedance for the source subsystem is clearly affected by different settings for the regulators in the control system. The influence on the impedance is most significant at low frequencies, and above 100 Hz the different regulator parameter values give almost the same results. Preliminary simulations revealed that the current injection to a large extent was sensitive for changes in the simulation parameters. Both simulation time length and current injection amplitude proved to have influence on the resulting impedance. This influence occurred for frequencies mainly below 300 Hz, and additional work is needed to explain this unexpected dependency. In general, the method seems to have good accuracy on high frequency, while results on low frequencies may contain errors.

Results from voltage injection show almost no influence from the inverter's control system. Although several simulations have been carried out, with different settings for the regulators, the harmonic impedance end up as approximately the same. If it is the method itself that gives wrong results, or if the control system is actually not affecting the impedance needs further investigations to find out. An interesting observation is that the impedance magnitude for both source and load subsystem are found to be the same at frequencies above 100 Hz. Both injection methods can therefore be assumed to be accurate at high frequencies.

The frequency range where the converters are able to influence the impedance, and thereby also the stability, has been found. Above 300 Hz the converters have no significant influence on the impedance, and the passive components are dominating. The converters will therefore only be able to affect the impedance and stability conditions below this frequency.

It was discovered that instability is likely to occur for the HVDC system in the initial state, as the curve in the Nyquist plot approaches the instability point at frequencies above 100 Hz. This means that large oscillations in voltage and current can occur if perturbations with the correct frequency are present. As many values close to the instability point represent frequencies that exceed the frequency range where the converters are significant, the power system itself must be redesigned to guarantee stable operating conditions.

Regarding frequencies inside the converters' significant range, the sensitivity analysis for the rectifier shows that the initial tuning of the control system is actually the most stable of those that are simulated. By changing the regulator parameters values in any direction, the Nyquist plots indicate increased probability of instability to occur. For the inverter, which proved to be almost immune to changes in the regulator parameter values, no changes concerning stability conditions were observed during the sensitivity analysis.

For the proposed method to be applied as a tool in stability analysis for a real system, the uncertainty regarding the resulting harmonic impedance obtained from voltage and current injection should be sorted out. As the frequency response analysis does not give results guaranteed as veritable, any further sensitivity analysis of the obtained data will take place with low credibility.

Further Work

The most important topic to further investigate is the accuracy for both current and voltage injection at low frequencies. Particularly the influence caused by simulation time length and injection current amplitude should be explained, as these are parameters that ideally should not have any affection on the results. Regarding voltage injection, more investigations should be done to account for the non-existent influence by the control system.

To be able to compare and recognize the obtained results from the frequency response analysis, an analytical expression for the harmonic impedance can be elaborated. This will probably be a quite challenging task if contributions from both the load current control system and the differential current control systems are to be considered.

When the accuracy for the frequency response analysis is clarified, the differential current control system should be tuned so that satisfactory simulations can be performed. The approach of the sensitivity analysis can be the same as for the load current control system, by adjusting one regulator parameter at a time.

References

[1] P. Kundur. “Power System Stability and Control”. McGraw-Hill, Inc., 1994.

[2] ABB. North-East Agra. Available November 2012 at: http://www.abb.com/industries/ap/db0003db004333/9716a8ac9879236bc125785200694f18.aspx.

[3] ABB. “HVDC Light Training, Generation 4 Basics”. Ludvika, September 2011.

[4] B. Jacobson, P. Karlsson, G. Asplund, L. Harnefors and T. Jonsson. “VSC-HVDC Transmission with Cascaded Two-Level Converters”. CIGRE B4-110, 2010.

[5] Working Group B4.48. “Components Testing of VSC Systems for HVDC Applications”. CIGRE, 2011.

[6] K. Friedrich. “Modern HVDC PLUS Application of VSC in Modular Multilevel Converter Topology”. IEEE International Symposium on Industrial Electronics, 2010.

[7] M. Molinas. Lectures in ELK-23 Power Electronics in Future Power Systems. Norwegian University of Science and Technology, Trondheim, 2012.

[8] ABB. HVDC Light. Available November 2012 at: http://www.abb.com/industries/us/9AAC30300394.aspx.

[9] N. Mohan, T. M. Undeland and W. P. Robbins. “Power Electronics – Converters, Applications and Design”. Third Edition. John Wiley & Sons, Inc., 2003.

[10] ABB. “HVDC Light G4 Valves – SK4, Voltage and Thermal Design”. Ludvika, September 2011.

[11] Z. Yang et al. “Harmonic Impedance Measurement for an Islanded Microgrid Using Current Injection”. IEEE 7th Power Electronics and Motion Control Conference – ECCE Asia. 2012.

[12] National Instruments. Available February 2013 at: http://www.ni.com/cms/images/devzone/tut/6-bode_plot_with_gain.png

[13] E. Kreyszig. “Advanced Engineering Mathematics”. 9th edition. John Wiley & Sons, Inc., 2006.

[14] M. Céspedes and J. Sun. “Renewable Energy Systems Instability Involving Grid-Parallel Inverters”. IEEE, 2009.

[15] Gamry Instruments. “Basics of Electrochemical Impedance Spectroscopy”. 2010.

[16] National Instruments. Available February 2013 at: http://www.ni.com/cms/images/devzone/tut/3-gain_and_phase_margin_graph.png.

[17] J. G. Balchen, T. Andresen and B. A. Foss. “Reguleringsteknikk”. Norwegian University of Science and Technology, department of Engineering Cybernetics, January 2003.

[18] J. Machowski, J. W. Bialek and J. R. Bumby. “Power System Dynamics – Stability and Control”. Second Edition. John Wiley & Sons, Ltd., 2008.

[19] T. Midtsund. "Control of Power Electronic Converters in Distributed Power Generation Systems". Master thesis at Norwegian University of Science and Technology, department of Electric Power Engineering, Trondheim, 2010.

[20] T. Kalitjuka. “Control of Voltage Source Converters for Power System Applications”. Master thesis at Norwegian University of Science and Technology, department of Electric Power Engineering, Trondheim, 2011.

[21] Manitoba HVDC Research Centre. "Multi-terminal HVDC VSC PSCAD Model Components and Systems to Support the 3- and 5 terminal Studies in Sweden and Norway", Rev: 4. Canada, May 2011.

[22] STRI. Report R11-730 "Multi-terminal HVDC modelling and simulation". Ludvika, May 2011.

[23] L. Xu and S. Li. “Analysis of HVDC Light Control using Conventional Decoupled Vector Control Technology”. IEEE, 2010.

[24] G. Bergna, E. Berne, P. Egrot, P. Lefranc, A. Arzandé, J. C. Vannier and M. Molinas. “An Energy-Based Controller for HVDC Modular Multilevel Converter in Decoupled Double Synchronous Reference Frame for Voltage Oscillation Reduction”. IEEE Transaction on Industrial Electronica, Vol. 60, No. 6, June 2013.

[25] G. Bergna, A. Garcés, E. Berne, P. Egrot, A. Arzandé, J. C. Vannier and M. Molinas. “A Generalized Power Control Approach in ABC Frame for Modular Multilevel Converter HVDC Links based on Mathematical Optimization”.

[26] G. Bergna, J. A. Suul, A. Garcés, E. Berne, P. Egrot, A. Arzandé, J. C. Vannier and M. Molinas. “Improving the Dynamics of Lagrange-based MMC Controllers by means of Adaptive Filters for Single-Phase Voltage, Power and Energy Estimation”.

[27] J. Sun. “Impedance-Based Stability Criterion for Grid-Connected Inverters”. IEEE Transaction on Power Electronics, Vol. 26, No. 11, November 2011.

[28] F. Wang, J. L. Duarte and M. A. M. Hendrix. “Pliant Active and Reactive Power Control for Grid-Integrated Converters Under Unbalanced Voltage Dips”. IEEE Transaction on Power Electronics, Vol. 26, No. 5, May 2011.

[29] P. Rodriguez, A. V. Timbus, R. Teodorescu, M. Liserre and F. Blaabjerg. “Flexible Active Power Control of Distributed Power Generation Systems During Grid Faults”. IEEE Transaction on Industrial Electronics, Vol. 54, No. 5, October 2007.

[30] S. Bødal. “Stability Analysis of a High Voltage Direct Current System Based on Modular Multilevel Converters”. Specialization project at Norwegian University of Science and Technology, department of Electric Power Engineering, Trondheim, 2012.

Appendices

Appendix A

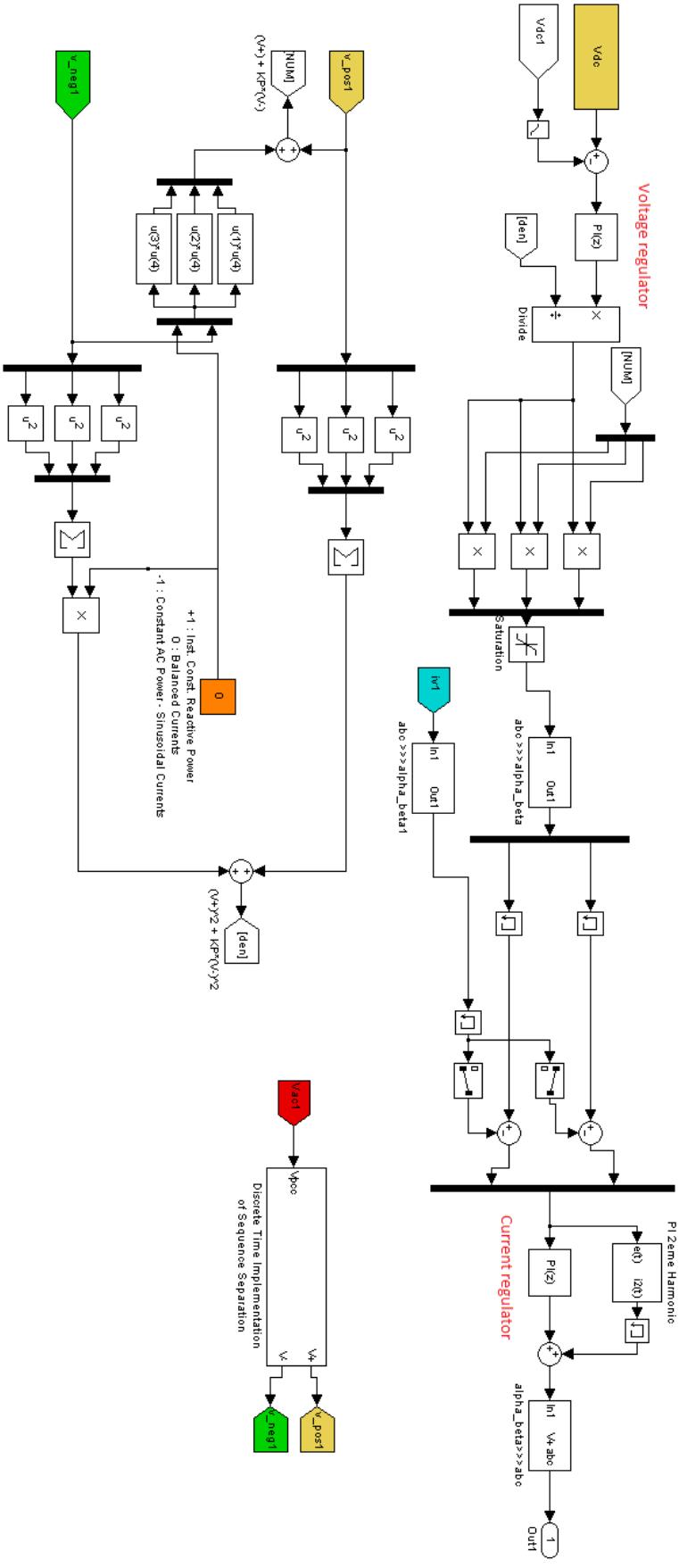
Vdc1
Vdc
Voltage regulator
[den]
PI(z)
Divide
[NUM]
Saturation
In1
Out1
abc >>> alpha_beta
alpha_beta >>> abc
Current regulator
PI 2eme Harmonic
e(t)
i2(t)
Vabc
Vdc
Discrete Time Implementation of Sequence Separation
Vac1
V+
V-
v_neg1
v_pos1
v_Neg1
v_Pos1
u^2
u(3)*u(4)
u(2)*u(4)
u(1)*u(4)
+1 : Inst. Const. Reactive Power
0 : Balanced Currents
-1 : Constant AC Power - Sinusoidal Currents
0
(V+)^2 + KP*(V-)^2

Appendix B

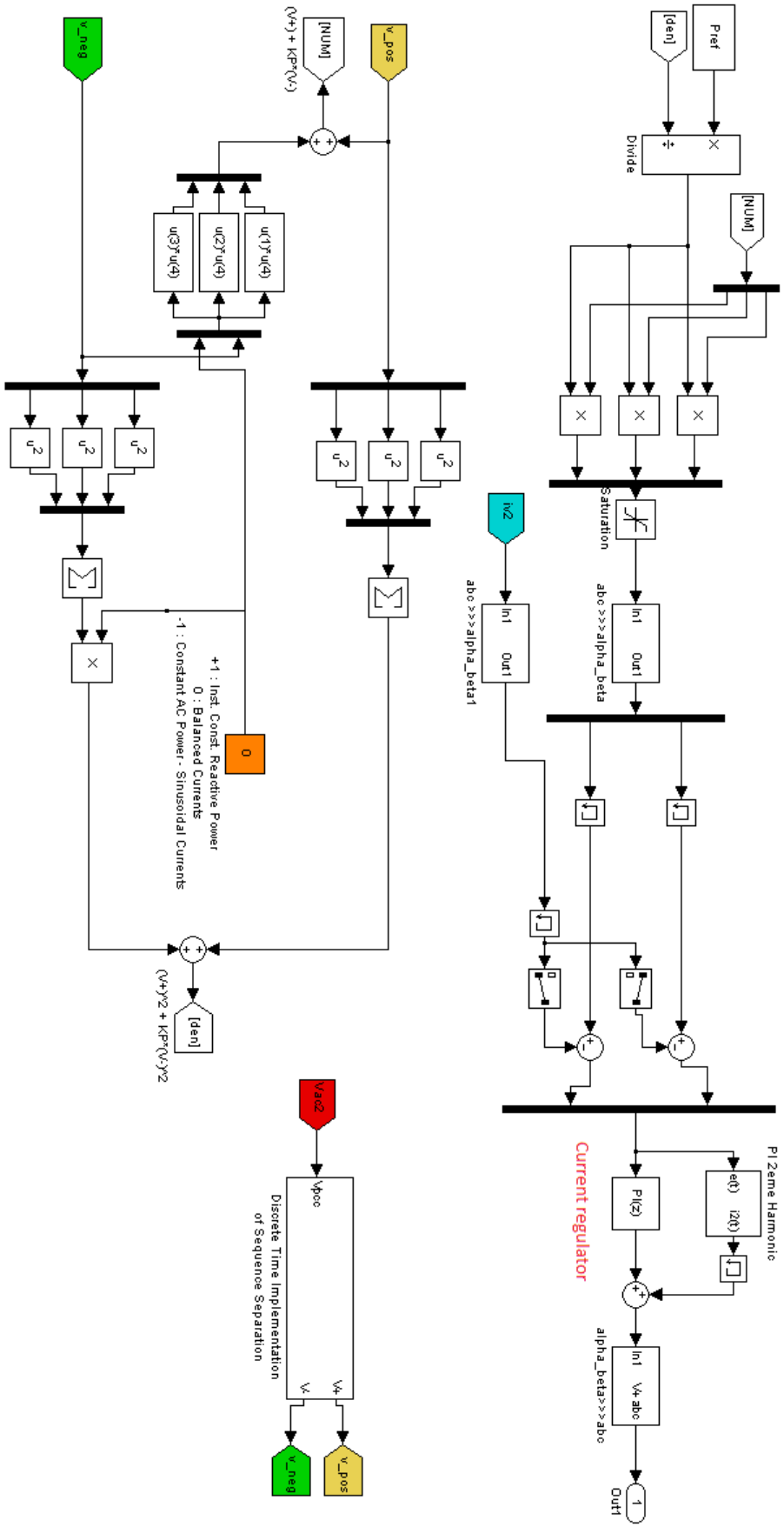
[den]
Pref
Divide
[NUM]
Saturation
iv2
abc >>>alpha_beta1
In1
Out1
abc >>>alpha_beta
alpha_beta>>>abc
Current regulator
PI(z)
e(t)
i2(t)
PI 2eme Harmonic
1
Out1
v_neg
v_pos
(V+) + KP*(V-)
u(1)*u(4)
u(2)*u(4)
u(3)*u(4)
c2
0
+1 : Inst. Const. Reactive Power
0 : Balanced Currents
-1 : Constant AC Power - Sinusoidal Currents
(V+)*2 + KP*(V-)*2
Vabc2
Vpcc
Discrete Time Implementation
of Sequence Separation
V-
V+

Appendix C

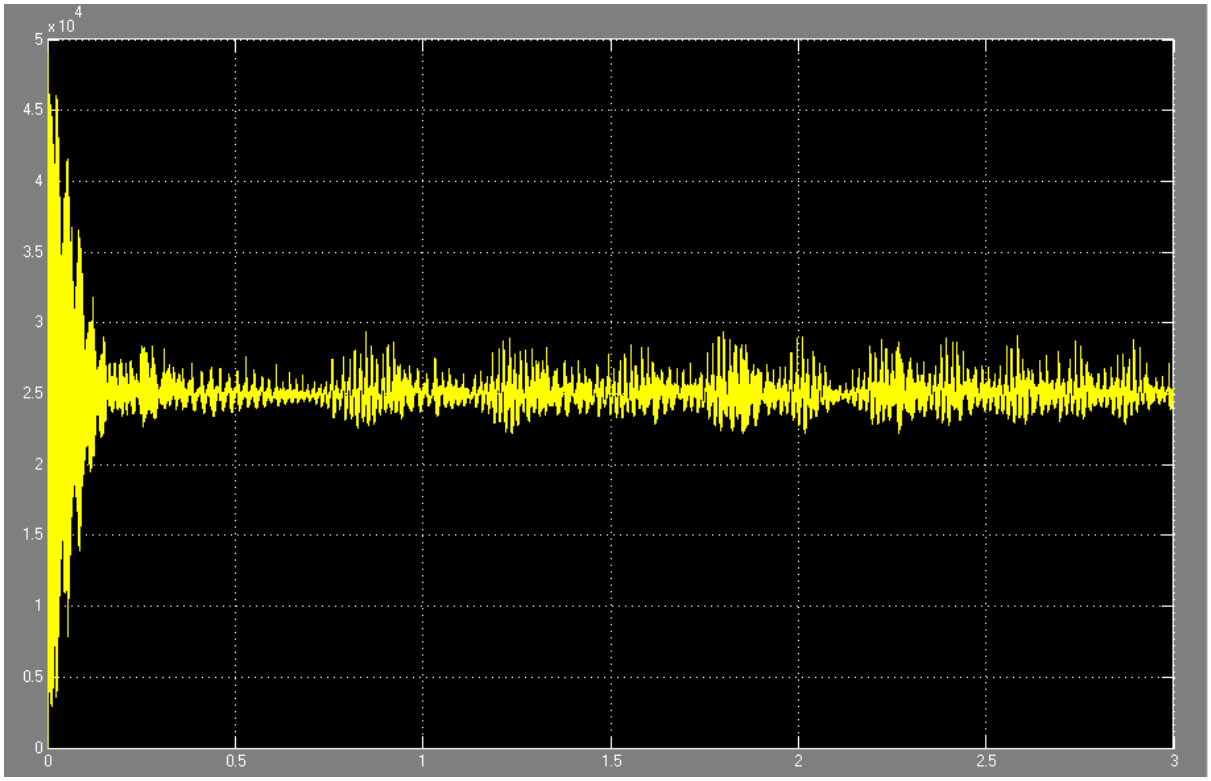

Figure C.1: DC voltage waveform

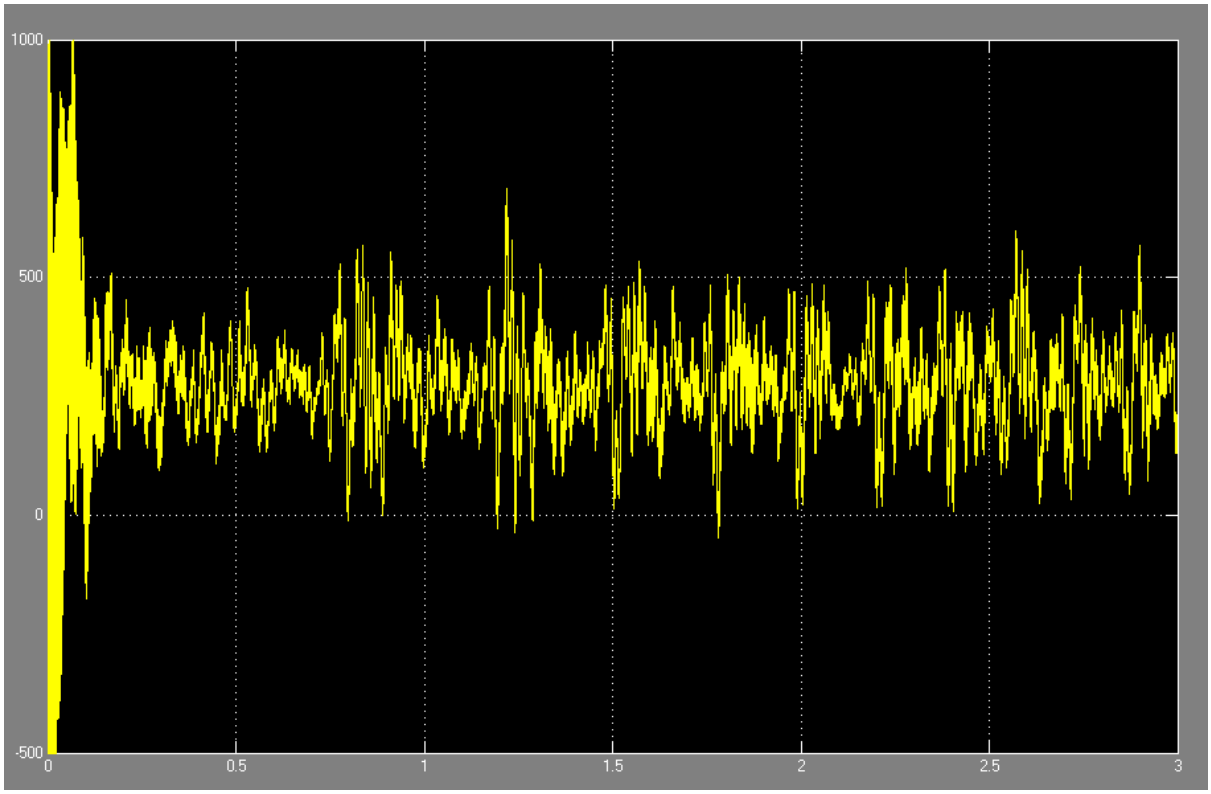

Figure C.2: DC current waveform